

# Lawrence Berkeley National Laboratory

## LBL Publications

### Title

Advances and challenges in electrochemical CO<sub>2</sub> reduction processes: an engineering and design perspective looking beyond new catalyst materials

### Permalink

<https://escholarship.org/uc/item/3tv0j7vr>

### Journal

Journal of Materials Chemistry A, 8(4)

### ISSN

2050-7488

### Authors

Garg, Sahil

Li, Mengran

Weber, Adam Z

et al.

### Publication Date

2020-01-28

### DOI

10.1039/c9ta13298h

### Copyright Information

This work is made available under the terms of a Creative Commons Attribution-NonCommercial-NoDerivatives License, available at

<https://creativecommons.org/licenses/by-nc-nd/4.0/>

Peer reviewed

## **Advances and challenges in electrochemical CO<sub>2</sub> reduction processes: an engineering and design perspective looking beyond new catalyst materials**

Sahil Garg<sup>1</sup>, Mengran Li<sup>1,\*</sup>, Adam Z. Weber<sup>2</sup>, Lei Ge<sup>1,3</sup>, Liye Li<sup>4</sup>, Victor Rudolph<sup>1</sup>, Geoff Wang<sup>1</sup>, Thomas E. Rufford<sup>1,\*</sup>

1. *School of Chemical Engineering, The University of Queensland, St Lucia 4072, Australia*

2. *Joint Center for Artificial Photosynthesis, Lawrence Berkeley National Laboratory, 1 Cyclotron Rd, Berkeley CA 94720 USA*

3. *Center for Future Materials, University of Southern Queensland, Springfield 4300, Australia*

4. *HBIS Group Technology Research Institute, Shijiazhuang, 050023, China*

\* **Corresponding Authors:** Mengran Li and Thomas E. Rufford -

### **Abstract**

Electrochemical CO<sub>2</sub> reduction (CO<sub>2</sub>R) is one of several promising strategies to mitigate CO<sub>2</sub> emissions. Electrochemical processes operate at mild conditions, can be tuned to selective products, allow modular design, and provide opportunities to integrate renewable electricity with CO<sub>2</sub> reduction in carbon-intensive manufacturing industries such as iron and steel making. In recent years, significant advances have been achieved in the development of highly efficient and selective electrocatalysts for CO<sub>2</sub>R. However, to realize fully the potential benefits of new electrocatalysts in low cost, large scale CO<sub>2</sub>R electrolyzers requires advances in design and engineering of the CO<sub>2</sub>R process. In this review, we examine the state-of-the-art in electrochemical CO<sub>2</sub>R technologies, and highlight how the efficiency of CO<sub>2</sub>R processes can be improved through (i) electrolyzer configuration, (ii) electrode structure, (iii) electrolyte selection, (iv) pH control, and (v) the electrolyzer's operating pressure and temperature. Although a comprehensive review of catalytic materials is beyond this review's scope, we illustrate how other engineering and design decisions may also influence CO<sub>2</sub>R reaction pathways because of effects on mass transfer rates, the electrode surface chemistry, interactions with intermediate reaction species, and rates of charge transfer.

## 1 Introduction

Utilization of CO<sub>2</sub> from industrial waste gases is considered a complementary route to other CO<sub>2</sub> emission reduction strategies such as renewable energy sources, CO<sub>2</sub> capture and storage (CCS), and other low carbon emission technologies.<sup>1</sup> The main pathways to utilize CO<sub>2</sub> include reuse of CO<sub>2</sub> without conversion (e.g. enhanced oil recovery, supercritical CO<sub>2</sub>)<sup>2,3</sup> or to convert the CO<sub>2</sub> to a valuable fuel, energy storage vector, or chemical feedstock. Among CO<sub>2</sub> conversion technologies such as biochemical, photosynthetic, thermo-catalytic, and photocatalytic processes,<sup>4-7</sup> electrochemical CO<sub>2</sub> reduction (CO<sub>2</sub>R) is one of the most promising CO<sub>2</sub> utilization strategies because of the mild electrolyzer operating conditions, opportunities to tune the process towards desired products, the potential to use industrial or municipal wastewaters as electrolytes, and modular reactor designs.<sup>8</sup> In addition, CO<sub>2</sub>R technologies could be integrated with renewable electricity generation from solar or wind<sup>9-11</sup> (as shown in **Figure 1**) to reduce carbon footprints in carbon intensive manufacturing industries such as ammonia production or iron and steel production through CO recycling,<sup>12</sup> for example.

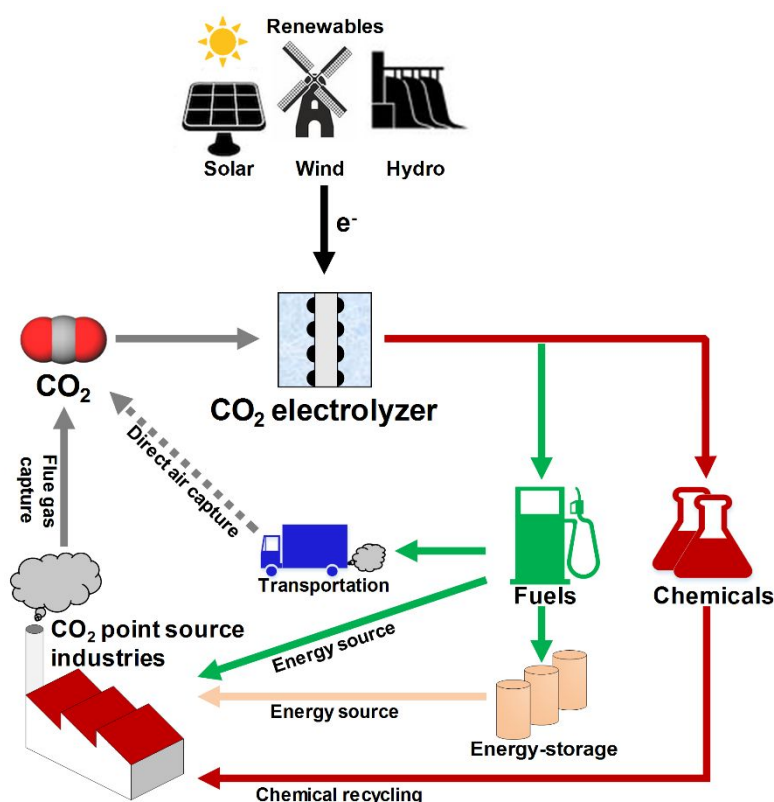


**Figure 1.** Closing the carbon cycle. CO<sub>2</sub> electrolyzer utilizing renewable energy can convert the captured CO<sub>2</sub> into chemicals or fuels for direct usage or energy storage.

**Table 1** shows several organisations report electrochemical CO<sub>2</sub>R technologies to operate at pilot-scale with current densities in the range  $j = 100 - 200 \text{ mA} \cdot \text{cm}^{-2}$ . These technologies could lead to commercially viable processes to convert CO<sub>2</sub> to CO,<sup>13</sup> light hydrocarbons including CH<sub>4</sub> and C<sub>2</sub>H<sub>4</sub>,<sup>14</sup> alcohols,<sup>15</sup> and chemical feedstocks like formic acid (HCOOH).<sup>16</sup> However, most of these technologies are currently too costly for practical applications and market penetration. The first challenge to low cost CO<sub>2</sub>R is the high energy requirement to break bonds in the CO<sub>2</sub> molecule.<sup>17</sup> The second challenge is to achieve a high selectivity of CO<sub>2</sub> to desired products to minimize costs and complexity of product separation processes. Achieving high selectivity is difficult because a large number of CO<sub>2</sub>R reactions and the competing hydrogen evolution reaction (HER) all have standard potentials ( $E^0$ ) in a narrow range ( $-0.25 \text{ V}$  to  $0.17 \text{ V}$  vs standard hydrogen electrode (SHE)) as shown in **Figure 2**. The third challenge is to ensure the overall rate of reaction is not limited by rates of CO<sub>2</sub> mass transfer from the gas phase to electrolyte and to active sites on the cathode catalyst. The fourth practical challenge is to maintain stable electrocatalyst performance over extended operating periods because the catalyst can be poisoned by impurities in the electrolytes<sup>18, 19</sup> or CO<sub>2</sub> feed gas (e.g. sulphur compounds), or by products stemming from corrosion of the electrolyzer components.<sup>20-26</sup>

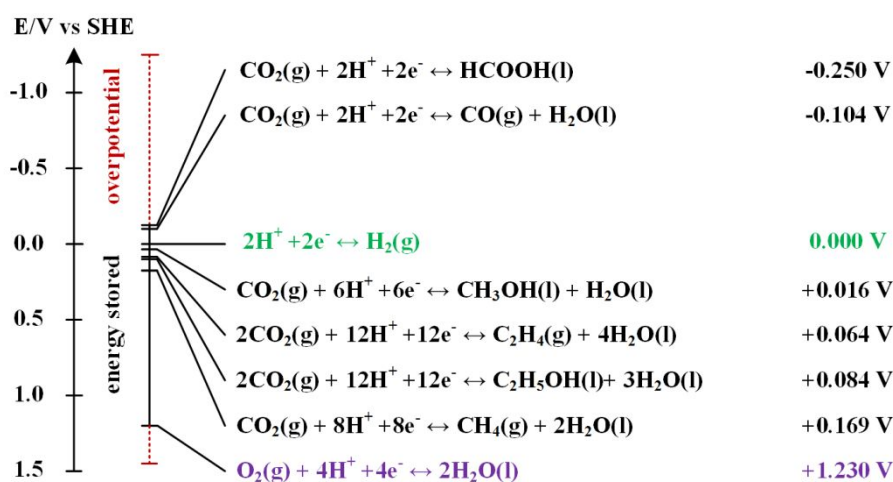


**Figure 2. Standard equilibrium potentials for hydrogen evolution half-cell reaction and several other half-cell reactions to reduce CO<sub>2</sub> into various products at 1 atm and 25 °C. Data presented was taken from Qiao et al.<sup>27</sup> (2014).**

To circumvent these challenges, a significant amount of research effort aims to develop highly efficient, stable, and selective CO<sub>2</sub>R electrocatalysts. Many comprehensive reviews on CO<sub>2</sub>R catalysts are available,<sup>28-38</sup> and these reviews cover advances in transition metals, alloys, metal-organic complexes, metal chalcogenides, metal-nitrogen-carbon materials, and carbon materials. Further review of electrocatalysts is beyond the scope of this article. Instead, we

complement existing catalyst reviews with a critical analysis of engineering factors that affect the performance of CO<sub>2</sub>R electrolyzers. These factors include the reactor configuration, electrode structures, electrolyte selection, and the choice of reaction conditions such as pH, pressure, and temperature. These engineering factors not only predetermine the CO<sub>2</sub>R mass-transport characteristics but can also have significant impacts on the catalytic reaction pathways.<sup>39-41</sup> The review concludes with a discussion of the priorities for future research to understand better the fundamental mechanisms of CO<sub>2</sub>R and improve CO<sub>2</sub>R performance.

**Table 1. Summary of lab-scale or soon to be commercially available electrochemical CO<sub>2</sub> reduction technologies.**

Technology (Location)	Throughput /scale	Reactor configuration	Catalysts	Electrolyte	Target Products	Notes	Reference
Opus-12 (Berkeley, USA)	Lab-scale	Proton exchange membrane (PEM) type electrolyzer	Anode: IrO <sub>2</sub> Cathode: Ag nanoparticles supported on carbon foam <sup>42</sup>	Water	CO and O <sub>2</sub>	Announced plans to develop renewable electricity operated CO <sub>2</sub> R to ethylene, ethanol.	13
Dioxide Materials (Boca Raton, USA)	Lab-scale	Sandwich-type CO <sub>2</sub> electrolyzer where cathode and anode catalysts are painted on either side of the membrane	Anode: IrO <sub>2</sub> or RuO <sub>2</sub> Cathode: Carbon paper coated with silver/ionomer mixture <sup>43</sup>	10mM KHCO <sub>3</sub> as anolyte and humidified CO <sub>2</sub> as catholyte <sup>43</sup>	> 95% selectivity to CO <sup>43</sup>	Report 6 months stable catalyst operation	44
Carbon Electrocatalytic Recycling Toronto (CERT) (Toronto, Canada)	Lab-scale /Pilot-scale cell	Flow cell modified from state-of-the-art fuel cells	Anode: Made from cheap and conventional abundant earth metals Cathode: Nanostructured metals based on copper <sup>45</sup>	7 M KOH <sup>45</sup>	70% selectivity for C <sub>2</sub> H <sub>4</sub> <sup>45</sup>	Uniform selectivity for the initial 150 hours	14
Mantra Energy Alternatives Ltd (Vancouver, Canada)	100 kg/day pilot plant	Fuel-cell type CO <sub>2</sub> electrolyzer	<i>Not disclosed publicly</i>	Water or wastewater	Formate/formic acid	Successfully demonstrated CO <sub>2</sub> RR for greater than 2,500 hours	16
Skyre or Sustainable Innovations (East Hartford, USA)	Pilot plant	<i>Not disclosed publicly</i>	<i>Not disclosed publicly</i>	<i>Not disclosed publicly</i>	Hydrocarbon fuels	-	46
Siemens and Evonik (Germany)	Lab-scale	CO <sub>2</sub> R electrolyzer	Anode: IrO <sub>2</sub> coated titanium Cathode: Silver gas diffusion electrode based on oxygen depolarization cathode (ODC used in industrial chlorine-alkaline electrolysis) <sup>47</sup>	0.1 M K <sub>2</sub> SO <sub>4</sub> /1.5 M KHCO <sub>3</sub> as both anolyte and catholyte <sup>47</sup>	~70% selectivity for CO, then CO fermentation to higher alcohols <sup>47</sup>	Stable CO selectivity for almost 1,200 hours	15

\*The information presented in above table is mostly collected from relevant papers or websites. Some companies have not publicly disclosed any data on CO<sub>2</sub> electrolysis amid high competition.

## 2 Working principles of electrochemical CO<sub>2</sub> reduction

A typical CO<sub>2</sub> electrolyzer (see for example **Figure 3(a)** showing a H-cell type reactor used in research laboratories) consists of a cathode to reduce CO<sub>2</sub> to products such as CO or HCOOH/HCOO<sup>-</sup> and produce hydroxyl ions (OH<sup>-</sup>); an anode to oxidize water via the oxygen evolution reaction (OER) that consumes OH<sup>-</sup> or generates protons (H<sup>+</sup>) and electrons (e<sup>-</sup>); an electrolyte to conduct ions and to dissolve and transport CO<sub>2</sub> to the cathode active sites; an ion-exchange membrane or porous diaphragm to separate the cathode and anode electrodes; and a voltage source with sufficient potential ( $E$ ) to transfer electrons from anode to cathode. In such a system, there are several key steps involved in a CO<sub>2</sub>R process, including (1) mass transfer of CO<sub>2</sub> from the gas phase to the bulk electrolyte, (2) transport of dissolved CO<sub>2</sub> from the bulk electrolyte to cathode/electrolyte interface, (3) absorption of CO<sub>2</sub> at the cathode surface, (4) dissociation of adsorbed CO<sub>2</sub> species into adsorbed intermediates such as \*COOH, \*CO, \*CHO, and \*COH, (5) electron transfer from the cathode catalyst to intermediates, (6) desorption of products from the electrode, and (7) migration of products away from the cathode/electrolyte interface to the bulk gas or liquid phases.<sup>48</sup>

We start our discussion at the electron transfer step (5) to examine the minimum theoretical energy requirement for CO<sub>2</sub>R. The minimum potential required for a CO<sub>2</sub>R reaction is the half-cell standard potential described by  $E^\circ = -\Delta G^\circ/nF$ , where  $\Delta G^\circ$  is the Gibbs free energy at 1 atm and 298 K,  $n$  is the number of moles of electrons transferred in the half-cell reaction, and  $F$  is Faraday constant (96,485 C·mol<sup>-1</sup>). For example, the half-cell reaction CO<sub>2</sub>(g) + 2H<sup>+</sup>(aq.) + 2e<sup>-</sup> → CO(g) + H<sub>2</sub>O(l) with  $\Delta G^\circ = 20.09$  kJmol<sup>-1</sup> has  $E^\circ = -0.104$  V vs SHE.<sup>49</sup> Other half-cell standard potentials at 1 atm and 298 K are shown in **Figure 2**. To drive a sufficient CO<sub>2</sub>R rate, an excess voltage or overpotential to  $E^\circ$  must be applied to overcome the sum ( $R_{total}$ ) of several energy barriers or resistances as described in Equation 1:

$$R_{total} = R_{cathode} + R_{anode} + R_{ions} + R_{membrane} + R_{bubble, cathode} + R_{bubble, anode} + R \quad \text{Eq. (1)}$$

The resistances include (1) the activation barriers or activation overpotentials ( $\eta_s$ )<sup>50</sup> for CO<sub>2</sub>R at cathode ( $R_{cathode}$ ) and OER at the anode ( $R_{anode}$ ); (2) ohmic losses from conduction of ions ( $R_{ions}$ ) in the bulk electrolytes, ion transport across the membrane ( $R_{membrane}$ ); (3) loss of active electrode area from the bubbles formation at the electrodes (e.g.  $R_{bubble, cathode}$  for CO and H<sub>2</sub> at the cathode, and  $R_{bubble, anode}$  for O<sub>2</sub> at the anode);<sup>51, 52</sup> and (4) the sum ( $R$ ) of electrical resistances in other cell components and contact resistances between components.

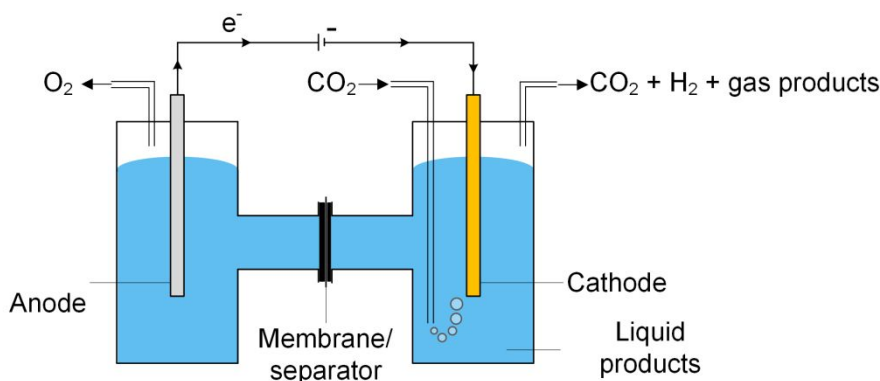


**Figure 3. Schematic of a laboratory electrochemical H-cell (reactor) for CO<sub>2</sub> reduction at the cathode to gas products such as CO and liquid products such as formic acid and methanol with water being oxidized at the anode.**

Because the CO<sub>2</sub>R reaction depletes CO<sub>2</sub> concentrations at the electrode surface, at high current densities the overall reaction rate can be limited by the rates of CO<sub>2</sub> mass-transfer to the electrode surface.<sup>53</sup> In addition according to the Nernst equation, the change in concentration affects the equilibrium potential and this effect can be approximated by the concentration overpotential.<sup>49</sup> In large scale industrial electrolyzers operating at high temperature concentration overpotential becomes important because at higher temperatures the activation overpotential is lower and the improved electrolyte conductivity leads to smaller ohmic losses.<sup>54</sup> Therefore, now that we have established the minimum energy requirements for CO<sub>2</sub>R, we will look next at the steps involved in transferring CO<sub>2</sub> from the gas phase to the electrode surface.

In most CO<sub>2</sub>R electrolyzers, gaseous CO<sub>2</sub> is first dissolved in the liquid electrolyte, then transferred through the liquid to the cathode-electrolyte interface. This process is driven by CO<sub>2</sub> concentration gradients as illustrated in **Figure 4a**, and the rate of CO<sub>2</sub> transfer depends on the interfacial contact area, film and overall mass transfer coefficients, and the overall concentration driving force. The concentration gradients in the system are dependent on the solubility of CO<sub>2</sub> in the electrolyte and the selected operating pressures and temperature of the electrolyzer cell. However, prediction of these gradients is complex during CO<sub>2</sub>R because acid/base reactions (for example CO<sub>2</sub> consumption by OH<sup>-</sup>) in the electrolyte can lead to non-linear deviation of the concentration away from Fick's Law behavior,<sup>55</sup> which reduces the concentrations of CO<sub>2</sub> available to react at the electrode's surface.<sup>56</sup> This effect can be partially controlled with buffering electrolytes such as potassium carbonate (KHCO<sub>3</sub>) to maintain pH at the cathode.<sup>55</sup> The interfacial contact area can be maximized by reducing the size of gas bubbles



injected to the electrolyte<sup>57</sup> or using a 3D-structured electrode such as a gas diffusion electrode (GDE).<sup>58, 59</sup> The magnitudes of CO<sub>2</sub> and CO<sub>2</sub>R product mass transfer coefficients generally increase with temperature, pressure, and the velocities of gas and liquid in the electrolyzer, but also are effected by electrolyte density, viscosity and solubility relationships.

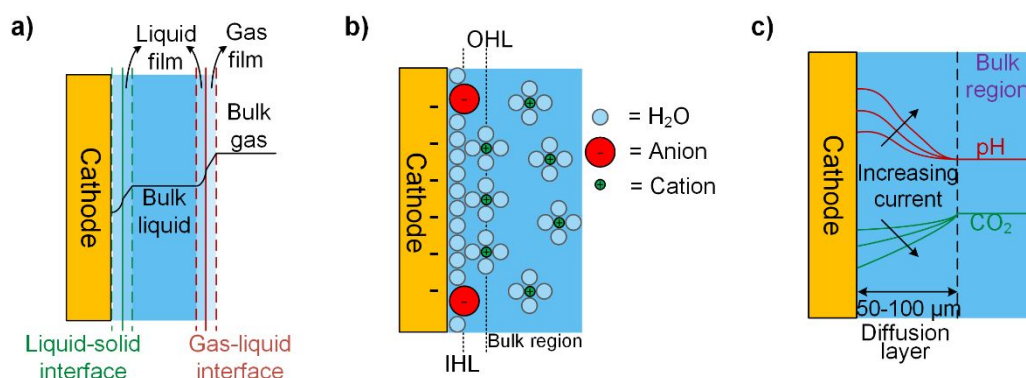


**Figure 4** Schematic illustrations of (a) the concentration profile of CO<sub>2</sub> across gas, liquid, and solid interfaces; (b) the electrochemical double layer with specifically adsorbed anions at the inner Helmholtz layer and solvated cations at outer Helmholtz layer; and (c) changes in CO<sub>2</sub> and pH next to the diffusion layer at increasing current density in a system where CO<sub>2</sub> is supplied from the bulk electrolyte.

Next we examine the cathode-electrolyte interface where CO<sub>2</sub>R occurs in a typical aqueous electrolyzer. Cations in the electrolyte migrate towards the negatively charged cathode surface to form an electrochemical double layer (DL), as shown in **Figure 4b**. This DL is formed by the outer Helmholtz layer (OHL) of fully-solvated cations, and the inner Helmholtz layer (IHL) of less-solvated halide ions or CO<sub>2</sub>-related adsorbed species directly adsorbed at the electrode surface.<sup>49</sup> The presence of this DL can effect CO<sub>2</sub>R through several mechanisms. For example, the local electrical field between the negatively charged cathode and the positively-charged adsorbed cations has been reported to stabilize CO<sub>2</sub>R-related intermediates such as \*CO<sub>2</sub> and \*COOH.<sup>60, 61</sup> On the other hand, in the OHL solvated cations like Li<sup>+</sup>, Na<sup>+</sup>, and K<sup>+</sup> act as a source of protons for the HER and disrupt the local pH within the DL.<sup>62, 63</sup> Another effect relates to interactions between anions and the electrode surface, which have been reported in some cases like I<sup>-</sup> and a Cu surface to be strong enough to allow anion absorption within the IHL.<sup>64</sup> In most cases, anions with a pK<sub>a</sub> close to the local pH may help buffer the pH and adsorbed ions may be directly involved in CO<sub>2</sub>R pathways by affecting the binding strength or adsorption geometry of CO<sub>2</sub>R intermediates such as \*COOH.<sup>65, 66</sup> **Figure 4c** illustrates that the concentrations and rates of consumption of protons, CO<sub>2</sub>, and other species in the DL are directly proportional to the current density and product selectivity during a CO<sub>2</sub>R reaction and

these changes in the local reaction environment could occur even at low currents, and thus limit the overall reaction rate before all available CO<sub>2</sub> becomes depleted at the electrode surface.<sup>53, 67</sup>

This background discussion of the principles of CO<sub>2</sub>R highlights that even though the electrocatalyst determines the underlying reaction kinetics, other factors such as reactor configuration, electrode structure, and conditions including the type of electrolyte, pH, pressure, and temperature can affect the overall rate of CO<sub>2</sub>R reactions.

### 2.1 Figures of merit to describe electrochemical CO<sub>2</sub>R

We briefly describe here the figures of merit commonly used to evaluate and compare electrochemical CO<sub>2</sub>R processes. These are faradaic efficiency, current density, and energy efficiency.

- *Faradaic efficiency (FE)* is the ratio of the amount of charge used to form a product species (e.g. CO) calculated from Faraday's law to the total charge ( $Q$ ) supplied:<sup>68</sup>

$$FE_{\text{product}} = \frac{y \cdot n \cdot F}{Q} \quad \text{Eq. (2)}$$

where  $y$  is the number of moles of the product species formed,  $n$  is the moles of electrons transferred in the half-cell reaction per mole of product, and  $F$  is Faraday's constant.

- *Current density ( $j$  or  $CD$ )* is the total current ( $I$ , in Amps) per unit area of the cathode ( $A$ , m<sup>2</sup> or commonly cm<sup>2</sup>) calculated by Equation 3, and describes the total rate of reaction so is an important input to estimate electrolyzer size and capital cost for a CO<sub>2</sub>R process.<sup>69</sup>

$$j = \frac{I}{A} \quad \text{Eq. (3)}$$

Partial current density ( $j_{\text{product}}$ ) for a specific product can be obtained by:

$$j_{\text{product}} = FE_{\text{product}} \times j \quad \text{Eq. (4)}$$

- *Energy efficiency (EE)* is a measure of net energy consumption toward a specific product expressed in Equation 5 as a ratio of amount of energy used to produce the specific product to the net electrical energy supplied to the system.

$$EE_{\text{product}} = \frac{E^{\circ} \times FE_{\text{product}}}{E^{\circ} + \eta} \quad \text{Eq. (5)}$$

where  $E^0$  is the equilibrium cell potential for the desired product ( $E^0_{\text{cathode}} - E^0_{\text{anode}}$ ), and  $\eta$  is the sum of overpotentials on the cathode and anode.

### 3 Electrolyzer Configurations

The background discussion in Section 2 highlights how, in addition to catalyst materials, the configuration of the electrolyzer impacts the overall efficiency of a CO<sub>2</sub>R process by effecting the limiting rates of CO<sub>2</sub> mass transfer to the catalyst, controlling resistances of cell components, and determining the reaction distribution across electrodes. The two general categories of electrochemical reactors are (i) batch or semi-batch cell and (ii) continuous flow-cell configurations. Batch and semi-batch electrolyzers like the H-cell in Figure 3a are commonly used in laboratory CO<sub>2</sub>R studies with electrodes simply immersed in liquid electrolytes with CO<sub>2</sub> gas bubbled to saturate the catholyte.<sup>70</sup> This configuration is simple, low cost, and allows rapid screening of novel electrocatalysts and electrolytes, but is not practical for treatment of large volumes of CO<sub>2</sub> gases<sup>40, 71</sup> because rates of CO<sub>2</sub> mass transfer to the electrode surface (even if the catholyte is vigorously stirred) are too slow and limit CD to less than 100 mA cm<sup>-2</sup>.<sup>39</sup> In addition, in a semi-batch cell any cations (e.g. K<sup>+</sup>) that pass through the separator accumulate in the catholyte, and this accumulation can degrade the electrode kinetics and CO<sub>2</sub>R selectivity over extended cell operation or result in high ohmic losses due to electro dialysis.<sup>72, 73</sup>

Industrial-scale CO<sub>2</sub>R processes require continuous processes to achieve sufficient reaction rates and be economically viable. **Table 1** presented examples of continuous flow-cell electrolyzers reported for pilot-plant and scale-up studies, and most of these follow scale-up and engineering strategies that were developed for polymer electrolyte (PE) electrolyzers. In this section we will discuss the separator, which is a critical component in all batch cells and continuous flow-cells, and then describe the liquid-fed, vapor-fed, and microfluidic electrolyzers illustrated in **Figure 5**. Our review does not cover flow-field patterns (e.g. straight, parallel, serpentine) that can be manufactured on current collectors to optimize CO<sub>2</sub> and electrolyte contact with the catalyst, and to minimize pressure drop, and to manage heat transfer in the cell.<sup>74</sup> We refer readers interested on flow-field patterns to reviews of PE electrolyzers.<sup>74-76</sup>

## Flow-cell configurations

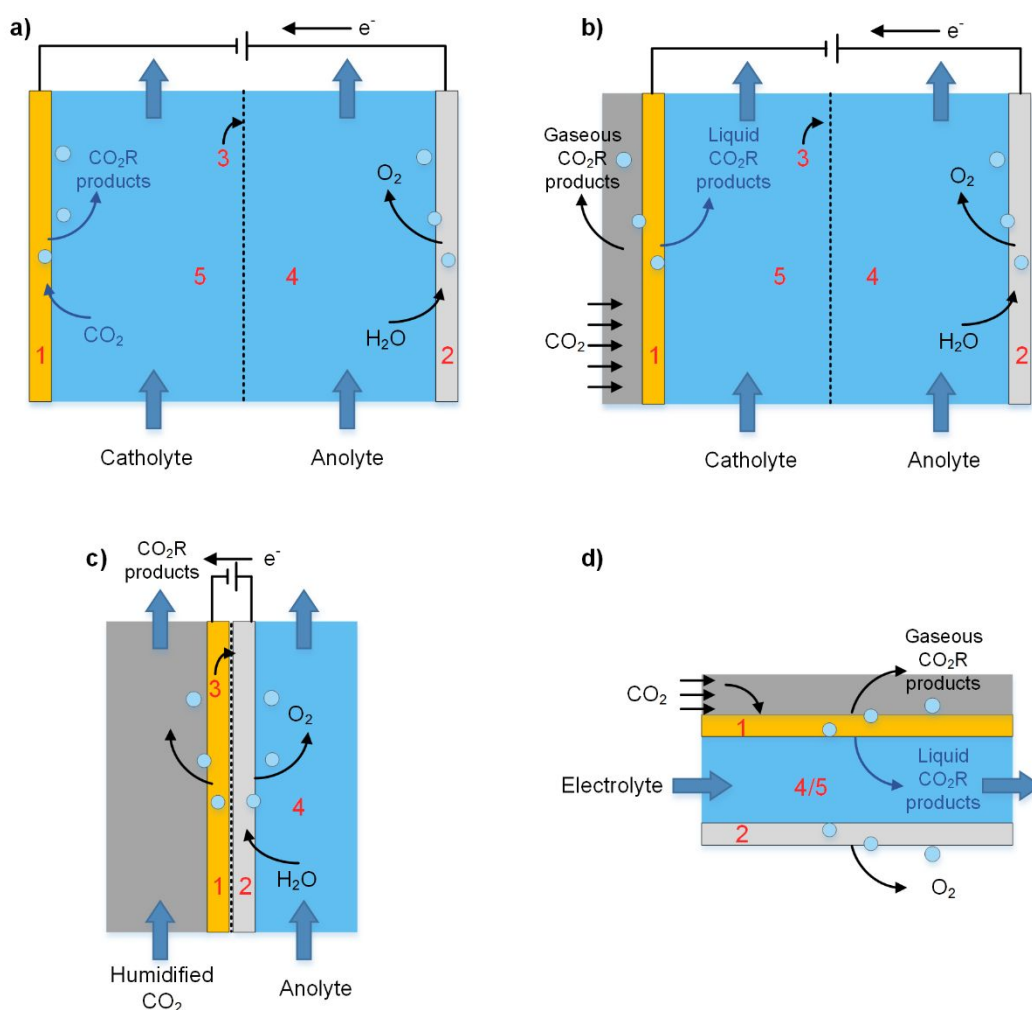


**Figure 5.** Schematic of  $\text{CO}_2$  electrolyzer in flow-cell configurations (a, b) liquid-fed electrolyzer, (c) vapor-fed electrolyzer and (d) microfluidic reactor. The main cell components are labelled as 1. cathode, 2. anode, 3. separator or ion-exchange membrane which could be a cation exchange membrane, anion exchange membrane, or a bipolar membrane, 4. anolyte, and 5. catholyte.

### 3.1 Separator considerations

In a  $\text{CO}_2\text{R}$  electrolyzer the separator between cathode and anode chambers, just like separators in water splitting electrolyzers,<sup>73, 77</sup> is critical to safe and efficient operation of the cell. An effective separator (1) minimizes the risk of a short circuit between electrodes; (2) prevents exchange of reactants and  $\text{CO}_2\text{R}$  products between cell chambers to reduce the risk of forming unsafe gas mixtures (e.g.  $\text{H}_2$  and  $\text{O}_2$ ) and prevent oxidation of products at the anode; (3) maintains desired local conditions in the anode and cathode reactions, (4) provides mechanical

support to withstand any pressure differences between chambers, and (5) must have a good conductivity for certain ions. The two classes of materials that can provide the required selective ion transport and low permeability to other species are porous separators and ion exchange membranes (IEM). Porous separators include plastic mesh (e.g. polyolefin or Netlon) with large pores (0.5 – 12 mm widths) and microporous diaphragms with pore sizes 0.1 – 50  $\mu\text{m}$  (e.g. glass fibres, polytetrafluoroethylene (PTFE)).<sup>77</sup>

Semi-permeable ion exchange membranes selectively transport certain dissolved ions but are not permeable to other ions or non-charged species. Most  $\text{CO}_2\text{R}$  electrolyzers use monopolar IEMs that are either cation exchange membranes (CEM) such as Nafion® or anion exchange membranes (AEM) such as Sustainion®. Bipolar membranes (BPM) with electrocatalyst sandwiched between CEM and AEM layers are also available,<sup>78</sup> and are reported to achieve more stable pH levels between two electrodes at steady state.<sup>79-81</sup> A further advantage of the BPM is that this design may allow lower, cost abundant metals to be used as catalysts instead of precious and noble metals.<sup>82, 83</sup> Further detailed descriptions of IEM working principles and recent advances in IEMs are provided in reviews by Kusoglu and Weber,<sup>84</sup> Kaczur et al.,<sup>85</sup> Luo and Wessling,<sup>86</sup> and Kimberly et al.<sup>87</sup>

The selection of a cation exchange, anion exchange, or bipolar membrane must be considered together with catalyst selection, electrolyte selection, and the targeted  $\text{CO}_2\text{R}$  products. For example, a CEM is commonly used for  $\text{CO}_2\text{R}$  to formate because this IEM blocks formate anions from crossing over to the anode chamber. If the CEM is also proton exchange membrane like Nafion then an acidic anolyte must also be selected to manage proton concentrations,<sup>88</sup> and these decisions limit the choice of OER anode catalysts to expensive precious noble metals such as Ru and Ir. Another consideration for proton exchange membranes is that excess protons will promote HER at the cathode.<sup>89</sup>

Anion exchange membranes can transport anions such as  $\text{HCO}_3^-$ ,  $\text{OH}^-$  and  $\text{CO}_3^{2-}$  ions from alkaline catholytes to the anode chamber.<sup>90</sup> Hori et al.<sup>91</sup> reported a  $\text{FE}_{\text{CO}}$  up to 92% at 20  $\text{mA cm}^{-2}$  which shows the improved performance of AEM-based reactor over CEM. However, there are some important considerations in the use of AEM. For example,  $\text{CO}_3^{2-}$  and  $\text{HCO}_3^-$  transported to the anode chamber are expected to produce  $\text{CO}_2$ , and this reduces the overall efficiency of the  $\text{CO}_2\text{R}$  process. Further, the extended exposure of AEM to alkaline catholytes can lead to blockage of the membrane with less mobile  $\text{HCO}_3^-$  and  $\text{CO}_3^{2-}$  anions, which degrades the AEM's ionic conductivity and increases the membrane's ohmic

resistance.<sup>87, 92-94</sup> In addition, AEM may be susceptible to degradation by excessive OH<sup>-</sup>, especially if the membrane is insufficiently hydrated. A recent report by Sun et al. revealed CO<sub>2</sub>R to methanol and ethanol can also accelerate such degradation.<sup>95</sup>

### 3.2 Continuous liquid-fed electrolyzers

**Figure 5a** depicts a two-chamber liquid-fed electrolyzer in which a CO<sub>2</sub>-saturated catholyte and an anolyte are pumped through the separate cell chambers. In this configuration, the catholyte is saturated with CO<sub>2</sub> outside the electrolyzer which requires additional CO<sub>2</sub> capture process units. A more recent integrated design for a liquid-fed electrolyzer is the three chamber cell shown in **Figure 5b** that uses a gas diffusion electrode to enhance transfer of CO<sub>2</sub> from the gas phase to the electrolyte-cathode interface. We provide further discussion of GDEs in Section 4.

Obviously, one control on the overall mass transfer rates and thus reaction rate in liquid-fed electrolyzers is the flow-rate of the catholyte because it directly effects superficial liquid velocities in the cell.<sup>96-98</sup> For example, Alvarez-Guerra et al.<sup>97</sup> reported that at low current density (CD = 2.5 mA cm<sup>-2</sup>) the overall rate of CO<sub>2</sub>R to formate over a lead-based cathode was insensitive to catholyte flow rates. However, they reported that at higher current densities (12.25 – 22 mA cm<sup>-2</sup>) increasing the catholyte flow-rate from 0.57 mL min<sup>-1</sup> cm<sup>-2</sup> to 1.44 mL min<sup>-1</sup> cm<sup>-2</sup> enhanced formate production because of an improved supply of dissolved CO<sub>2</sub> at the electrode interface for CO<sub>2</sub>R.

Both liquid-fed configurations provide larger active electrode area to electrolyte volume ratios than semi-batch cells, and thus can achieve higher overall reaction rates and lower ohmic losses than batch operation.<sup>99-102</sup> An additional advantage of the high electrode area to electrolyte volume ratio in liquid-fed electrolyzers in laboratory studies is that this allows detection of low concentration products and accurate voltage measurement. For example, Kuhl et al.<sup>99</sup> used a liquid-fed flow-cell electrolyzer like that in **Figure 5a** to detect for the first time acetone, glycolaldehyde, ethylene glycol, glyoxal, and hydroxyacetone as CO<sub>2</sub>R products at low concentrations. The expected H<sub>2</sub>, CH<sub>4</sub>, CO, HCOOH, and C<sub>2</sub>H<sub>4</sub> were also reported by Kuhl et al. Other groups report also sandwich type compression flow-cells for detection of low concentration products in CO<sub>2</sub>R reactions.<sup>57, 63, 101, 103, 104</sup>

**Figure 6a** shows an example of a liquid-fed electrolyzer with a BPM separator that due to the better control of pH imparted by the BPM achieved a more stable cell voltage during a 12 hour

CO<sub>2</sub>R experiment than an electrolyzer with a CEM (**Figure 6b and c**).<sup>71</sup> However, a potential issue with BPMs in liquid-fed electrolyzers is ensuring the rate of water flux across the BPM matches the rate of water dissociation to prevent dry-out of the membrane, which leads to significant increases in ohmic resistance.<sup>105</sup> Another potential issue in liquid-fed electrolyzers is that the ionic conductivity of the BPM depends on the concentration-gradients of salts in the electrolyte<sup>106</sup>, and because a BPM inherently leads to depletion of charge at the CEM/AEM interface this can create significant junction gradients. Therefore, operation of liquid-fed electrolyzers with BPMs requires ion concentrations in both the catholyte and anolyte to be controlled for the reaction kinetics and for the material and thickness of the membrane(s).

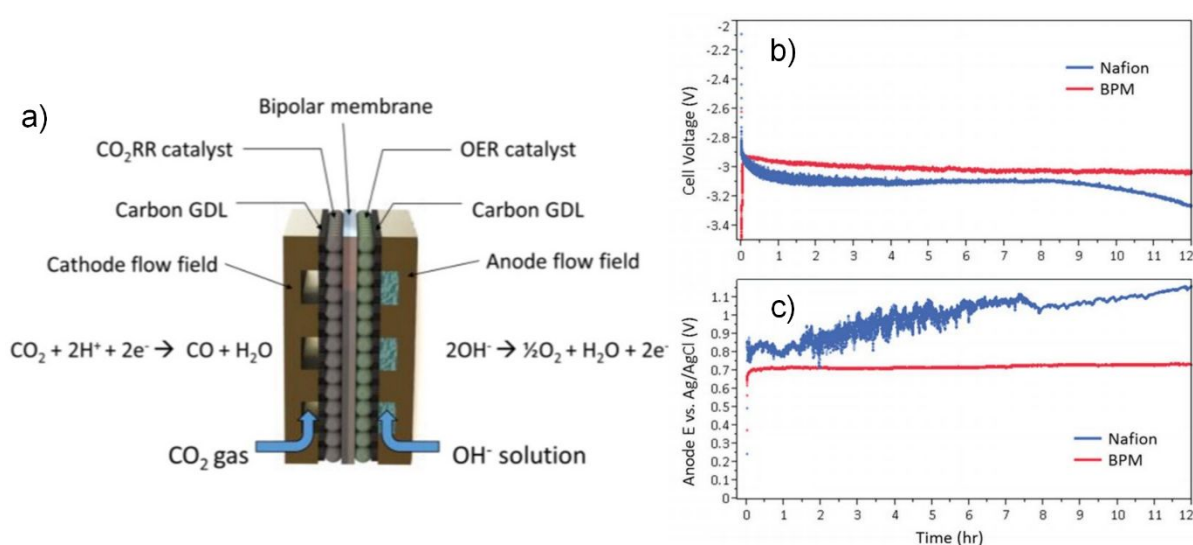


**Figure 6. (a) Schematic diagram of a CO<sub>2</sub> electrolyzer employing a BPM; comparison of (b) overall cell voltage and (c) anode potential vs Ag|AgCl between BPM and nafion membrane. 0.1 M KOH was used as anolyte and 0.5 M KHCO<sub>3</sub> as catholyte. Reprinted with permission from Li et al.<sup>71</sup>, Copyright 2016, American Chemical Society.**

In liquid-fed electrolyzers with a GDE, unstable CO<sub>2</sub>R operation can result from liquid flooding of the GDE. Several researcher groups suggest supplying the CO<sub>2</sub> gas at higher pressures to prevent liquid ingress into the GDE and in this case any gaseous CO<sub>2</sub>R products leave the electrolyzer with the catholyte.<sup>54, 107-109</sup> For example, Haas et al.<sup>47</sup> operated a liquid-fed electrolyzer at 50 mA cm<sup>-2</sup> for more than 1000 h, but report that to achieve this current density they had to sacrifice CO selectivity. Jeanty et al.<sup>110</sup> ran a CO<sub>2</sub> electrolyzer at 150 mA cm<sup>-2</sup> with a CO FE close to 60% for more than 200 h over a 100 cm<sup>2</sup> electrode area. A potential adverse effect of operating with a high gas overpressure across the GDE in a liquid-fed electrolyzer is that the higher partial pressure of CO<sub>2</sub> leads to precipitation from the

bicarbonate/carbonates catholyte which can reduce electrolyte conductivity, block GDE pores or modulate pH. All such effect increase the overall ohmic losses in the cell.

### 3.3 Vapor-fed electrolyzers

**Figure 5c** shows a vapor-fed flow-cell electrolyzer<sup>111</sup> with an IEM coated on one-side with a cathode catalyst and on the other side with an anode catalyst to create a zero-gap cell. In this configuration, the catholyte is supplied via humidified CO<sub>2</sub>-containing gas to maintain membrane hydration during CO<sub>2</sub>R. Compared to liquid-fed electrolyzers, the key advantages of vapor-fed electrolyzers are lower ohmic losses and reduced risk of catalyst poisoning from impurities in the catholyte. In addition because the vapor-fed cell does not require pumps to feed the electrolyzer the equipment and operating costs may be lower than a liquid-fed cell; however, this comparison depends on the cost of the processes required to vaporize catholyte into the CO<sub>2</sub> feed gas. One potential drawback of vapor-fed electrolyzers is liquid CO<sub>2</sub>R products like alcohols can flood back into GDE pores and thereby hinder CO<sub>2</sub> access to the active sites.

Most vapor-fed electrolyzers reported in the literature use a CEM to transport protons from the anode chamber to the cathode for CO<sub>2</sub>R. For example, Lee et al.<sup>112</sup> reported more stable formate production over a tin nanoparticle cathode catalyst in a vapor-fed electrolyzer than a liquid-fed electrolyzer, and they attributed the improved performance to a shorter CO<sub>2</sub> diffusion pathway to the catalyst. However extended CO<sub>2</sub>R operation in CEM vapor-fed electrolyzers is reported to lead to acidification at the cathode, which promotes unwanted HER.<sup>113</sup> In an alternative design, Kutz et al. used AEM like a methylimidazolium-based styrene polymer in a vapor-fed electrolyzers with Ag-based catalyst and reported stable operation for 6 months at CD = 50 mA cm<sup>-2</sup> with a FE<sub>CO</sub> = 90%.<sup>43</sup> Mallouk's laboratory<sup>71</sup> reported a vapor-fed electrolyzer with a BPM separator and ionic liquid catholyte that achieved CDs two times larger than a liquid-fed cell and relatively stable cell voltage close to 3 V during operation at 80 mA cm<sup>-2</sup> for 14 h. However, they did report that the FE<sub>CO</sub> began to degrade after 1 h, which may have been due to de-wetting of the ionic liquid IL from the surface of the catalyst.<sup>71</sup> Salvatore et al.<sup>114</sup> enhanced the stability of this vapor-fed with BPM configuration using a solid support layer of aqueous NaHCO<sub>3</sub> between the Ag-decorated GDE and the BPM, and demonstrated a steady FE<sub>CO</sub> = 65% at 100 mA cm<sup>-2</sup> and 3.4 V for 24 h.<sup>114</sup>



### 3.4 *Microfluidic electrolyzer*

A microfluidic electrolyzer (**Figure 5d**), such as the cells described by Kenis and co-workers,<sup>115, 116</sup> does not use a membrane separator but instead uses a thin (less than 1 mm) electrolyte flow-field channel to separate electrodes. In this configuration gaseous CO<sub>2</sub> diffuses to the electrode-electrolyte interface through a gas diffusion layer (GDL), and crossover of reactants and products is controlled at laminar flow conditions because diffusion of the products is slow. Due to its compact design and high surface area to volume ratio, a microfluidic electrolyzer design could allow fast rates of CO<sub>2</sub> mass transfer to the cathode surface and thus high CDs for CO<sub>2</sub>R.<sup>115, 116</sup> Additionally, microfluidic electrolyzers may provide new opportunities for fundamental studies into the effects of temperature, pH, catalyst deposition methods, electrolyte composition, GDL composition, and channel length on CO<sub>2</sub>R processes and thus help provide new insights for technology improvement.<sup>115, 117</sup>

### 3.5 *Separation of CO<sub>2</sub>R products downstream of the electrolyzer*

Efforts towards improving the selectivity of CO<sub>2</sub>R through catalyst innovations and optimization the electrolysis process are aimed partly at increasing the concentration of products in the electrolyzer effluents so as to the cost of product separation processes.<sup>118, 119</sup> Greenblatt et al.<sup>120</sup> showed just how energy intensive separation of liquid products from a photo-electrochemical CO<sub>2</sub>R could be, with 4.7 to 45 MJ/kg of product required using distillation to recovery products from 10 wt.% to 1 wt.% in the catholyte stream from the electrolyzer.<sup>120</sup> Greenblatt et al. reported more energy efficient technologies such as membranes and solvent extraction could potentially reduce the energy requirements to 0.1 - 8.3 MJ/kg product), but these technologies cannot always compete with distillation in terms of higher throughput and desired purity.<sup>120</sup>

One strategy to avoid separation costs could be direct use of effluent streams from the CO<sub>2</sub>R reactor. For example, potential opportunities could include tuning the CO<sub>2</sub>R performance tuned to produce CO + H<sub>2</sub> mixtures to feed a Fischer-Tropsch process, CH<sub>4</sub> + C<sub>2</sub>H<sub>4</sub> mixtures for synthesis of C<sub>3</sub>H<sub>6</sub>,<sup>121</sup> or alcohol and/or hydrocarbon mixtures for liquid fuels<sup>122, 123</sup>. However, that strategy is likely only viable in a small number of circumstances where the CO<sub>2</sub> source and the potential use of CO<sub>2</sub>R products are closely located and integrated. Therefore, consideration must be made for separation of CO<sub>2</sub>R product streams. One of the challenges with CO<sub>2</sub>R processes compared to many other industrial conversion processes is that the concentration of products, especially liquid products, leaving the electrolyzer are low. For

example, in the conventional formic acid route of hydrolysis of methyl formate produces formic acid + methanol mixtures with more than 10% formic acid that are relatively easy to separate by distillation or liquid/liquid extraction.<sup>124, 125</sup> However, the concentration of formic acid leaving a CO<sub>2</sub>R electrolyzer is typically less than 1 % in a mixture of water and the electrolyte salts. Recovery of the formic acid from this CO<sub>2</sub>R effluent stream requires an acidification process then azeotropic separation to obtain a pure formic acid product. Furthermore, formic acid separation processes are sensitive to pH like acidification and potential inorganic salts separation (e.g. crystallization) so conditions in the electrolyzer may affect downstream process.<sup>126</sup>

Control of the engineering factors described in the article (e.g. reactor design, electrode structure, electrolyte, pH, pressure, and temperature) may ultimately help to design efficient downstream separation processes. For example, the choices of conducting salts, solvents, IEMs, and flow rates can all effect the concentration and types of liquid CO<sub>2</sub>R products that must be recovered from the electrolyte. Yang et al.<sup>127</sup> provide a clear demonstration of the relationships between reactor design and product distribution in their report of electrolyzer with a Sustainion™ AEM to obtain streams with up to 20 wt.% formic acid from the reactor. In summary, the overall reactor design is a key factor that governs the properties of the CO<sub>2</sub>R product streams.

#### 4 Electrode structure

The cathode in a CO<sub>2</sub>R electrolyzer must provide active catalyst sites, facilitate sufficient contact between CO<sub>2</sub>, electrolyte and catalysts, and conduct electrons. **Figure 7** depicts the three types of cathode architectures: (a) planar electrodes (e.g. a metal foil or glassy carbon plate),<sup>128-133</sup> (b) simple porous electrodes (e.g. carbon paper or mesh),<sup>134-138</sup> and (c, d) gas-diffusion electrodes (GDEs).<sup>139-141</sup> Most CO<sub>2</sub>R electrocatalyst screening and fundamental catalysis studies<sup>30, 31, 47, 142-144</sup> use planar electrodes or simple porous electrodes because these types are relatively simple to construct and immerse in a CO<sub>2</sub> saturated electrolyte (for example, in an electrochemical cell like that shown in **Figure 3a**).

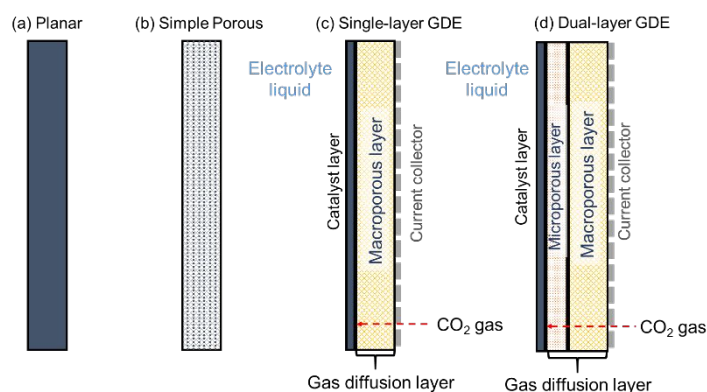


**Figure 7. Schematic diagrams of (a) planar electrode, (b) simple porous electrode, (c) single-layer gas diffusion electrode (GDE), and (d) dual-layer GDE.**

The planar electrode is useful to screen catalyst materials in a laboratory scale because of its relatively simple geometry that rules out impacts induced by complex factors such as structures of the electrodes. In addition, placement of a reference electrode is straightforward, thereby enabling single electrode overpotential measurements. However, the CO<sub>2</sub>R half-cell reaction rates achieved with a planar electrode or porous electrode are often limited by the rate of CO<sub>2</sub> transfer across the hydrodynamic layer from the bulk electrolyte to the electrode surface especially at a high CD.<sup>58</sup> In such systems, mass-transfer rates could be improved by operating the electrolyzer at high pressure, low temperature, or selecting organic electrolytes to increase the solubility of CO<sub>2</sub> in the electrolyte. But those options add costs and complexity to the CO<sub>2</sub>R process.

For high CD electrolyzers, one prefers the application of the last three electrode types (**Figure 7b to d**) that are 3D-structured catalytically-active materials or electron conducting material with coverage of catalysts. A 3D-structure increases the active electrode area and decreases the transport resistance of gaseous and liquid reactants and products. Increasing the active electrode area reduces overall cell voltage and increase the rate of charge and mass-transport. Fast charge and reactant transport also accelerate the electrode kinetics. However, challenge arises in understanding the property-performance relationship and optimisation of the 3D-structure for efficient CO<sub>2</sub>R conversion. This results from the complexity of the 3D-structured electrodes that involves multiphase flow in the pores, interactions at interfaces and multiscale kinetics at the catalysts. Though this area still remains underexplored in CO<sub>2</sub>R application, a lot can be drawn from the studies in other electrochemical conversion applications such as PEM fuel cells and redox flow batteries. Recently, Shojaeefard et al.,<sup>145</sup> Weber et al.,<sup>146</sup> and Fadzillah et al.<sup>147</sup> reviewed the electrode microstructure restructuring and pore-scale simulations. Moreover, Lai et al.<sup>148</sup> and Walsh et al.<sup>149</sup> reviewed the design and fabrication of

general 3D-structured electrodes, including the 3D-electrode architecture and decoration of catalysts.

Overall, the ultimate goal of developing 3D-structured electrode is to minimise the various cell resistances due to electron and ion transport, multiphase flow (e.g. bubble), transport-related, and electrochemical reaction. The ohmic resistance of 3D-structured electrode is mainly influenced by both the 3D-skeleton and the interfacial conductivity. The 3D-electrode structure is a composite made of conductive matrix (carbon or metals) and less-conductive binders (e.g. PTFE or ionomers) and/or pores containing electrolyte or gas, thus requiring multiple percolations pathways for reactant molecules, ions and electrons.<sup>150-152</sup> Simply put, increasing porosity decreases the overall conductivity of the matrix and therefore increases the overall ohmic resistance. The interfacial conductivity, governed by the interfacial contacts and heterogeneous phases, contributes more to the ohmic resistance. This is valid especially for a pure metal matrix as prepared through sintering, where sintering temperature, interfacial contact and sizes of metal particles and pore formers are important factors to consider.<sup>151</sup> 3D-structured electrodes decorated with heterogeneous catalyst materials also have extensive interfaces between the conductive backbone and less conductive catalysts, thus facing an increase of ohmic resistance. Therefore, the size and shapes of the catalysts and pore structures of the matrix also matter for the overall electrical conductivity of the structure.<sup>153</sup> Compared with the ohmic resistance, the resistance related to transport is more critical, particularly for mass-transport-controlled CO<sub>2</sub>R electrolysis.<sup>111</sup> In a 3D-porous electrode, transport of liquid and/or gas reactants and products is dominated by either molecular or Knudsen diffusion, depending on the pore size and electrode structures. Similarly, wettability and pore size dominate the intrinsic saturation/capillary-pressure relationship that is critical for optimal multiphase performance.<sup>146</sup>

The electrochemical reaction resistance is related to the electrode kinetics. In addition to the catalyst materials (where compositions, surface orientations, morphology, and sizes are important factors) that directly affect the kinetics, catalyst support, multiphase flows within the electrode and local environments are all crucial for CO<sub>2</sub>R surface reaction rate and selectivity. For the effects of catalyst support, one could refer to a recent review published by Li, MacFarlane, and Zhang,<sup>30</sup> as well as herein. However, there are still gaps remaining, especially regarding the exact interfacial structure of the catalysts (especially with ionomer),<sup>146</sup> and how these structures affect the electrode kinetics. Answering these questions is essential to guide where and how to deposit catalysts in the electrode structure. It is also important to note that

an optimal balance has to be achieved among these resistances. For example, oxide-derived catalysts are active for CO<sub>2</sub>R<sup>154, 155</sup> but may not be very electrically conductive, leading to a decrease of electrode kinetic resistance but an increase of ohmic resistance. In the case where liquid products are targeted products, a high reaction rate consumes quickly the CO<sub>2</sub> gas and lowers the local gas pressure, which may lead to local flooding that blocks gas transport and in turn degrades CO<sub>2</sub>R selectivity. Such a balance appears more crucial in the GDEs that include the transport of gases in the electrode structure. Because recent works have demonstrated a superior CO<sub>2</sub>R performance of GDEs compared to planar and simple porous electrodes, in the following subsections we mainly focus the review of recent GDE development for CO<sub>2</sub>R.

#### 4.1 Gas diffusion electrodes

GDEs offer an alternative approach to improve mass-transfer and overall CO<sub>2</sub>R rates.<sup>156, 157</sup> The key difference between a GDE and a simple porous electrode is that in a GDE, the CO<sub>2</sub> gas diffuses through a gas-diffusion layer (GDL) to the electrode-electrolyte interface inside the catalyst layer (CL). This type of GDE electrolysis has been reported to achieve reaction rates up to an order of magnitude faster than porous electrodes that require CO<sub>2</sub> transfer from the bulk electrolyte to the electrode surface.<sup>58</sup> A typical GDE, as shown in **Figure 8**, consists of a GDL, a CL, and a current collector as shown in the two examples in **Figure 7c** and **d**. The porous metal mesh or foam current collector serves to distribute current and maybe engineered with gas flow channels.<sup>142, 158-160</sup> The porous GDL should enable fast transport of gaseous CO<sub>2</sub> to the CL, where the electrochemical reactions occur. A critical property of the GDL is that this layer must be hydrophobic (or more generally, the GDL must be gas wet relative to the wetting with electrolyte) to prevent liquid electrolyte from seeping to the gas flow channel. The GDL can be designed with a single-layer of porous materials (**Figure 7c**) or dual-layers with different porosities and wettabilities (**Figure 7d**). In a single-layer GDL, the hydrophobic macroporous layer might be a metal mesh or metal foam, or a hydrophobically-treated porous carbon such as polytetrafluoroethylene (PTFE) treated carbon paper. A dual layer GDL (**Figure 7d**) includes a macroporous layer and a microporous layer (MPL).<sup>161</sup> The MPL is normally a hydrophobic layer with small pores that is composed of carbon powder and PTFE.<sup>162</sup> The catalyst layer (CL) is commonly prepared by depositing the catalytically active phase, including catalysts and an ionic binder on the GDL or membrane.

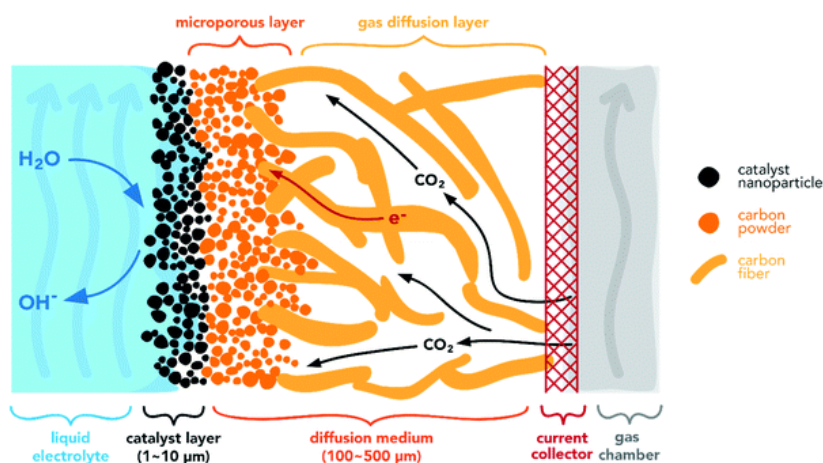


**Figure 8. Schematic diagrams of a gas diffusion electrode.<sup>58</sup>**

In a recent publication, Weng, Bell and Weber predicted with a mathematical model that a Ag-based GDE could potentially achieve a partial CD (PCD) for CO one order of magnitude higher than that achieved with a planar Ag electrode.<sup>58</sup> That study concluded that good GDE performance is achieved by (1) a high density of active sites per geometric electrode area, and (2) a low mass-transfer resistance in the GDE, especially at more negative potentials. The predictions of the Weng, Bell and Weber modelling study are consistent with various experimental studies.<sup>58</sup> For example, Castillo et al. reported that a Sn-based GDE with 1.5 mg Sn cm<sup>-2</sup> achieved a maximum FE of ~ 70 % in producing formate at a current density of 40 mA cm<sup>-2</sup>, which was more efficient than the planar Sn electrode with a maximum formate FE of 67 % at 12 mA cm<sup>-2</sup>.<sup>163</sup> In another example, Hass et al.<sup>47</sup> demonstrated a commercial Ag-based GDE, which was developed by Covestro as an oxygen depolarized electrode (ODE) for chlor-alkali applications, as a cathode in a CO<sub>2</sub> flow cell electrolyzer with stable operation at a CD of 300 mA cm<sup>-2</sup> and CO FE close to 70 % for over 1200 h. A brief summary of other recent reports of GDEs as cathode for CO<sub>2</sub>R is provided in **Table 2**.

**Table 2. A summary of recent works on GDEs as cathode for CO<sub>2</sub>R.**

Catalyst material	Catalyst loading	GDE Configuration	Current Collector	Remarks	Reference
Ag	NA	Dual layer	NA	Oxygen depolarization cathode (from Covestro)	47
Ag	0.8 mg cm <sup>-2</sup>	Dual layer	Carbon	20 wt.% PTFE MPL, 10 wt.% carbon fiber substrate 190 μm	162
Cu	20 nm	Dual layer	Carbon	(20 nm thick catalyst layer)	45
Cu (-350 mesh, 5N purity)/ carbon	NA	Single layer	Cu gauze	Cu mixed with carbon black (CB, hydrophilic) and CB <sub>hydrophobic</sub> as the catalyst layer, Cu / (CB <sub>hydrophilic</sub> + CB <sub>hydrophobic</sub> ) = 1.2	164
Cu	7 mg cm <sup>-2</sup>	Single layer	Cu grid		157
Cu <sub>2</sub> O/ZnO	1 mg cm <sup>-2</sup>	Single layer	Carbon	Air brushed on porous carbon paper	165
In/C	1 ± 0.05 mg cm <sup>-2</sup>	Single layer	Carbon		140
La <sub>1.8</sub> Sr <sub>0.2</sub> CuO <sub>4</sub>	NA	Single layer	Stainless steel mesh	Carbon/Teflon	141
Pt	0.56 mg cm <sup>-2</sup>	Single layer	Stainless steel mesh		159
Pt/CNTs	NA	Dual layer	Carbon	Sigracet 25 BC GDL with imidazolate-based SIM-1	166
Sn	NA	Single layer	Carbon	Sn electrodeposited on carbon fibers	167
Sn	1.5 mg cm <sup>-2</sup>	Single layer	Carbon	Sn on Toray carbon paper	163

<b>Sn</b>	1.9 mg cm <sup>-2</sup>	Dual layer	Carbon	Sn electrodeposited on dual layer GDL	168
<b>Sn</b>	5 mg cm <sup>-2</sup>	Single layer	Carbon	11.1 wt.% PTFE in catalyst layer	169
<b>Sn nanoparticles (10-15 nm)</b>	0.75 mg cm <sup>-2</sup>	Dual layer	Carbon		144
<b>Sn@Cu</b>	NA	Dual layer	Cu mesh	Sn loaded on a Cu mesh through electroless deposition, and subsequently rolled on the GDL	160
<b>Sn</b>	NA	Single layer	Carbon	Sn electrodeposited on carbon fiber paper	170



Although only a relative small number of studies report use of GDEs for CO<sub>2</sub>R,<sup>141, 157, 159, 171</sup> GDEs have been extensively developed and optimized for fuel-cell applications.<sup>161, 172, 173</sup> The knowledge from this field can be leveraged to develop more efficient GDEs for CO<sub>2</sub>R, but the requirements for CO<sub>2</sub>-electrolyte contacts in a CO<sub>2</sub>R electrolyzer are more challenging than in a fuel cell. We describe in the following sections recent advances to optimize GDEs for use as the cathode in a CO<sub>2</sub>R electrolyzer.

## 4.2 Engineering the gas diffusion layer

### 4.2.1 Macroporous layer

As one of the key components of GDE, the GDL normally (1) serves as a mechanical support for the CL, (2) allows an easy diffusion of the gaseous CO<sub>2</sub> and release of gas products such as CO and CH<sub>4</sub> through its pores at the reaction sites, (3) enables electron conduction from the current collector to the CL, and (4) prevents the electrolyte from seeping to the gas channel. The macroporous layer of the GDE can be fabricated by (1) mixing the carbon materials (e.g. acetylene black<sup>142, 164, 174, 175</sup> and carbon fiber) with PTFE<sup>164</sup> or Teflon<sup>174</sup>, (2) hydraulic pressing or rolling<sup>176</sup> the mixture with or without current collector to form the film, and (3) sintering the film at 340 to 380°C. The sintering temperature is slightly above the melting temperature of the hydrophobic agents, so that the agents can bind strongly with the carbon materials. In most cases, however, commercially available carbon papers (e.g. Toray or SGL carbon papers) have been used as the macroporous layer of the studied GDEs.

The thickness and hydrophobicity of the macroporous layer predetermine the mass-transfer resistance of CO<sub>2</sub> in the GDEs, and thus have an impact on the CO<sub>2</sub>R reaction rate. For example, Ikeada et al. compared the CO<sub>2</sub> gas permeability and CO<sub>2</sub>R performance over Ag-based GDEs with carbon-fiber substrates (i.e. macroporous layer) in different thicknesses ranging from 170 to 380 μm.<sup>162</sup> With the reduction of substrate thickness from 370 to 190 μm, they found that the CO<sub>2</sub> gas permeability increases from 69.25 ± 0.69 to 72.42 ± 0.72 mL min<sup>-1</sup>, and that the PCD of CO also improves from ~180 to ~220 mA cm<sup>-2</sup> at -2.05 V vs Ag|AgCl. The enhanced PCD of CO<sub>2</sub>R for thinner substrates is attributed to the improved CO<sub>2</sub> gas permeability. However, a too thin substrate (Toray Carbon Paper 30 with a thickness of 110 μm) leads to electrolyte flooding (i.e. the electrolyte fully occupies the pores) in the GDE during the CO<sub>2</sub>R operation, in essence turning into a simple electrode case. Therefore, an optimal thickness of the microporous layer is essential to ensure a balanced gas permeability and effective electrolyte management in the GDE.

Another key factor is the wettability of the macroporous layer: too high a hydrophobicity may cause poor electronic conduction due to the high amount of non-conductive hydrophobic agents, while too high of a hydrophilicity may limit the diffusion of CO<sub>2</sub> due to flooding propensity and promote unwanted HER.<sup>40, 58</sup> The wettability can be adjusted by controlling the content of hydrophobic agents (e.g. PTFE),<sup>161, 177, 178</sup> and hydrophilic treatments (such as plasma treatments, addition of inorganic oxides or carbon black, etc.).<sup>161, 179, 180</sup> Ikeda et al. observed similar CO<sub>2</sub>R reaction rates for the macroporous layer with PTFE contents between 10 and 30 wt.%, but a degraded performance for the one over 30 wt.%.<sup>164</sup> A recent detailed investigation on Ag-based GDE showed that the macroporous layer with 10 wt.% of PTFE has a higher CO PCD of 224 mA cm<sup>-2</sup> than those with PTFE content of 30wt% (PCD = 190 mA cm<sup>-2</sup>) and 50 wt.% (PCD = 158.41 mA cm<sup>-2</sup>) at -2.05 V vs Ag|AgCl.<sup>162</sup> (**Figure 9a**) The better performance for the GDEs with lower PTFE content in macroporous layer is a consequence of the better electronic conduction than those with higher PTFE content, as evidenced by the observed lower charge-transfer resistance from the electrochemical impedance spectra. (**Figure 9b**) In the studied PTFE range (10 to 50 wt.%), additionally, the authors observed negligible effects of the PTFE content in the macroporous layer on the CO<sub>2</sub> gas permeability and durability of the GDEs.

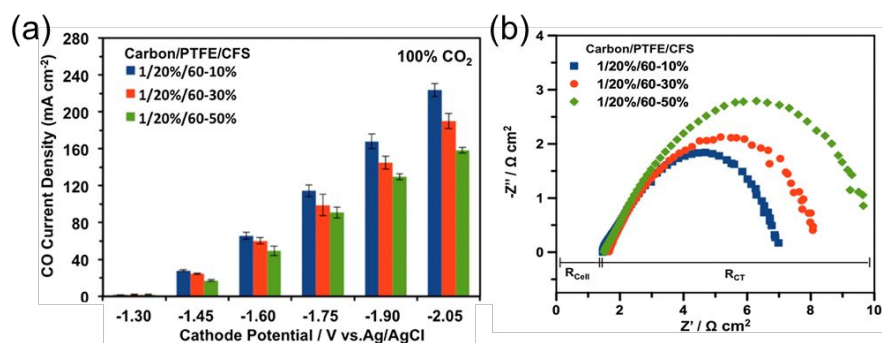


**Figure 9 (a)** A comparison of GDE with 10, 30, and 50 wt.% PTFE in the macroporous layer as a function of potential. **(b)** The Nyquist plot of electrochemical impedance spectra of the corresponding GDEs at -2.0 V vs Ag|AgCl. CFS means the carbon fiber substrate, which is the macroporous layer of the GDE. R<sub>cell</sub> represents the ohmic resistance of the cell, and R<sub>CT</sub> is the polarization resistance related to charge transfer. Reprinted with permission from Kim et al.<sup>162</sup>, Copyright 2016, Elsevier Ltd.

#### 4.2.2 Microporous layer

As compared with the macroporous layer, the MPL is normally a thinner porous layer with smaller pore sizes and volumes, and is sandwiched between the macroporous layer and CL. A comparison of scanning electron micrographs of GDE with or without MPL is shown in **Figure 10b and d**, respectively. The fabrication procedure of MPLs is similar to the processes

to make the macroporous layer. The mixtures of carbon black and hydrophobic agents are casted onto one side of the macroporous layer, followed by sintering treatment to ensure sufficient bonding.<sup>144, 162</sup> One should note that the carbon-based materials normally contains metal residues such as Fe, Co and Ni.<sup>181-183</sup> As the MPL is in direct contact with the catalyst layer, these metal impurities in the carbon materials may promote unwanted HER during the cell operation. Therefore, cleaning the MPL or the whole GDL in highly concentrated acid is highly recommended to minimize the content of metal impurities before deposition of catalyst layer. As shown in the **Table 2**, not all of the GDE-based cathodes for CO<sub>2</sub>R contain MPLs. Research in polymer electrolyte fuel cells have demonstrated that the MPL layer not only plays a key part in maintaining separation between liquid and gas, but also provides the electrode with improved interlayer contact, lower electrode ohmic resistance, higher CL temperatures, and better structural integrity.<sup>161, 184</sup> For the application of CO<sub>2</sub>R, Kenis et al. found that the MPL in the GDE could provide a support for the CL and prevent potential flooding in the macroporous layer.<sup>162</sup> The MPL can also prevent the exposure of the carbon fiber to the electrolyte (**Figure 10a to d**) and thereby suppressing the undesired HER catalyzed by the exposed carbon fibers. As a result, the presence of MPL in the GDE-based cathode contributes to a significantly improved CD as high as  $\sim 220 \text{ mA cm}^{-2}$ , ten-fold higher than the one without MPL at  $-2.2 \text{ V vs Ag|AgCl}$ .<sup>162</sup> (**Figure 10e**)

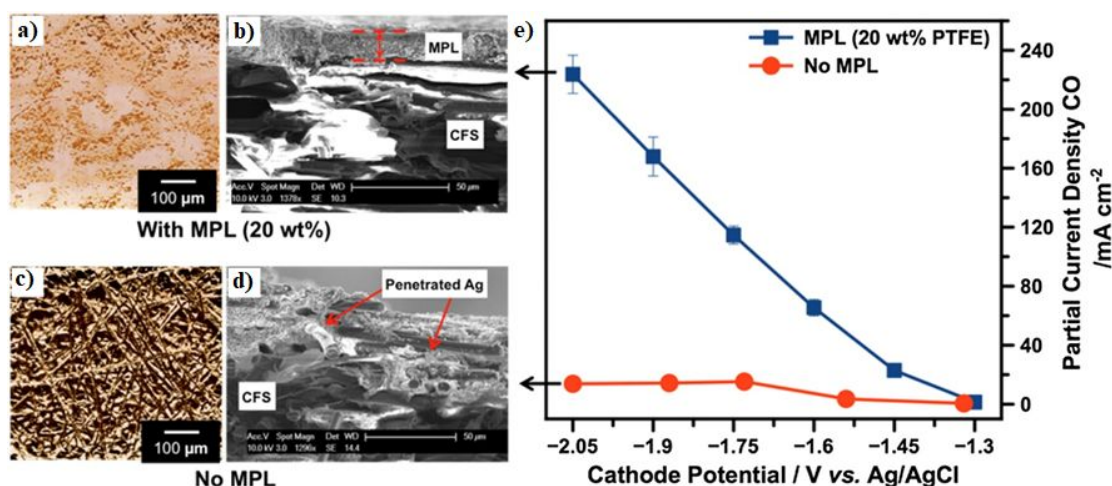


**Figure 10 a, c) Micro-computed tomography and b, d) SEM images of Ag-based GDE with and without the microporous layer. e) A comparison of CO partial CD of Ag-based GDE with and without MPL as a function of potential. Reprinted with permission from Kim et al.<sup>162</sup>, Copyright 2016, Elsevier Ltd.**

Additionally, in the same work, the authors also studied the effects of PTFE content of the MPLs on CO<sub>2</sub>R reaction rate. As shown in **Figure 11a**, the CO PCD increases with PTFE at low PTFE contents  $\leq 20 \text{ wt.}\%$ , but decreases with PTFE at contents  $> 20 \text{ wt.}\%$ .<sup>162</sup> Too little

PTFE content (i.e. 4.5-10 wt.%) in the MPL is insufficient to prevent flooding of the layer by electrolyte and does not provide strong binding between the carbon and catalysts in the CLs, which resulted in the higher HER level and poorer cathode durability. A higher content of PTFE (>20 wt.%) in the MPL degrades the electronic conductivity of the GDE (**Figure 11b**) and also reduces the MPL porosity.<sup>185</sup> Correspondingly, both the resistances of GDE for electron transfer and CO<sub>2</sub> mass transfer become higher, thus leading to a degraded CO<sub>2</sub>R performance.

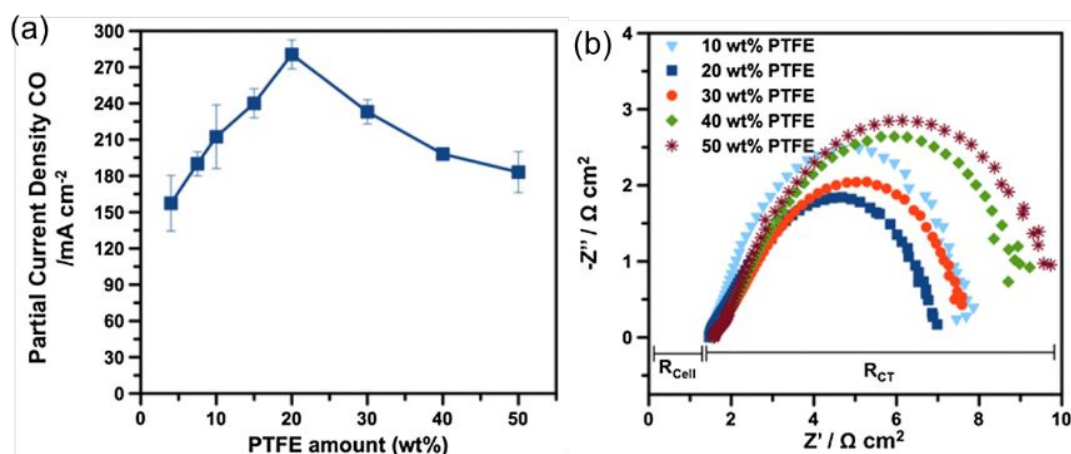


**Figure 11 (a)** A comparison of PCD of CO for Ag-based GDE as a function of PTFE content in the MPLs. **(b)** The Nyquist plot of electrochemical impedance spectra for the corresponding GDEs at cathode potential of  $-2.2$  V vs Ag|AgCl. Reprinted with permission from Kim et al.<sup>162</sup>, Copyright 2016, Elsevier Ltd.

#### 4.2.3 CO<sub>2</sub> adsorption layer

A CO<sub>2</sub> adsorption layer can also be incorporated at the GDL surface facing the CO<sub>2</sub> to further promote the CO<sub>2</sub>R. For example, by covering a substituted imidazolate-based metal-organic framework (SIM-1) on a macroporous layer, Marepally et al. significantly improved the performance over a Pt/carbon nanotube (CNT)-based GDE, with an increased rate of CO<sub>2</sub>R products, including methanol, ethanol, acetone, and isopropanol, by 1.5 times as compared with the counterpart without the adsorption layer.<sup>166</sup> Such remarkable >C1 production improvement, as brought by deliberately concentrating the surface CO<sub>2</sub> through the adsorption layer, highlights the essential roles of electrode design, in addition to the effects from electrocatalysts, in controlling the CO<sub>2</sub>R pathways.

#### 4.3 Optimization of the catalyst layer

The CL is mainly a layer of the electroactive cathode materials normally immobilized on one side of the GDL (typically on the MPL) facing the electrolyte or membrane through various

deposition methods (e.g. electrodeposition,<sup>168</sup> drop casting,<sup>45</sup> thermal evaporation,<sup>45</sup> ionic displacement, or pressing<sup>139</sup>), though the position of the CL can be also extended inside the GDL structure to further increase the electroactive interface boundaries.<sup>186</sup> There are several factors that could contribute to the activity and product distribution of the CO<sub>2</sub> electrolysis, such as the catalyst materials, catalysts loading (i.e. the mass of catalyst per electrode geometric area), ionic binders, and CL deposition methodology.

Immense research efforts have been and continue to be devoted to the study and development of catalyst materials suitable for CO<sub>2</sub>R, and the recent advances in the catalyst development have been extensively reviewed recently.<sup>28, 30, 31, 187, 188</sup> Most of these studies mainly focused on catalysts supported by a planar electrode or simple porous electrode, but not by a GDE, where the CL must deal with complex transport and reaction processes simultaneously and there is an inherent need for porosity.

The processes taking place at the CLs of GDE cathodes are even more complex than those in the GDL, since all of those processes occur as well as the electrochemical reactions and ionic transport. Weng et al. recently discussed in detail regarding the processes involved in the CL of an Ag-based GDE.<sup>58, 189</sup> In addition to local environment change close to the electrode surface in the electrolyte during CO<sub>2</sub>R operation, as discussed in the electrolyte selection and pH effects sections, the CL of the GDE also needs to manage the transport of gas and ions to achieve an optimal cathode performance. Too dry of a CL results in catalytically active sites becoming inactive due to the absence of supporting electrolyte or ionic pathways, but flooded pores increase the mass-transfer resistance of gaseous CO<sub>2</sub>. An ideal CL should facilitate a sufficient contact of liquid electrolyte and gas with the catalysts. Furthermore, the reaction kinetics are intimately connected with the transport phenomena. What also matters is the pore size in the CL. Small hydrophilic pores will be flooded when the liquid/gas pressure difference is low. When the pressure difference between gas and electrolyte increases, the susceptibility to electrolyte flooding of the pores in CL follows the trend: large hydrophilic pores > large hydrophobic pores > small hydrophobic pores.<sup>58</sup>

The amount of catalysts loading in the CL also alters the CD and product distributions. For example, through varying the Sn catalysts loading content ranging from 0 to 15 mg cm<sup>-2</sup>, Kopljar and co-workers found that a higher content of Sn increases the CO<sub>2</sub>R activity as evidenced by the observed higher CD and lower Tafel slope, especially at the higher potential range as shown in **Figure 12a**.<sup>139</sup> Such enhancement could be a result of the increased

concentration of catalytically active sites as imparted by the higher Sn loading. Moreover, the product distribution was also found to be dependent on the catalyst loading: a Sn loading of less than  $5 \text{ mg cm}^{-2}$  could lead to  $\sim 90 \%$  of FE for  $\text{HCOO}^-$  formation,  $< 10 \%$  for CO and  $3 \%$  for  $\text{H}_2$ , and further increase of the loading decreases the selectivity of the  $\text{HCOO}^-$  production but promotes CO and  $\text{H}_2$  evolution (see **Figure 12b**). The authors considered the effects of catalyst loading on product distribution analogous to the effects of cathodic potentials, where a low cathode potential leads to the promotion of CO and  $\text{H}_2$ . Alternatively, we explain such phenomena by two possible reasons. First, a higher Sn loading may hamper the diffusion of  $\text{CO}_2$  to the active regions and therefore lead to the promotion of HER. Second, similar to the effects of interparticle interactions on Cu nano-particles for  $\text{CO}_2\text{R}$  catalysis,<sup>190</sup> a higher catalyst loading could increase the availability of neighboring active sites and therefore promote re-adsorption of  $\text{HCOO}^-$  for further reduction to become CO as the final product.

Sargent et al. recently used Cu-based GDEs with a very thin Cu CL (i.e. 10 or 25 nm thick) as the  $\text{CO}_2\text{R}$  cathode to achieve a higher CD and higher FE for  $\text{C}_2\text{H}_4$  formation than the ones with thicker Cu CLs (i.e. 1000 nm thick and  $\sim 1000 \mu\text{g cm}^{-2}$  CL) at a higher cathodic potential (i.e.  $< -0.54 \text{ V vs RHE}$ ).<sup>45</sup> At lower cathodic potential ( $> -0.4 \text{ V vs RHE}$ ), in contrast, the GDEs with thick CLs exhibited higher CDs than the thin CLs. They explained the higher FE for GDE with the thin Cu CLs by the catalyst-mediated abrupt interface as imparted by the thin layer of Cu, which could accelerate the rate-determining CO dimerization step for  $\text{C}_2\text{H}_4$  formation.<sup>45</sup> It could be thought that the thin layers and high flowrates of electrolyte also did not provide sufficient time for the homogenous acid/base reactions of  $\text{CO}_2$  to occur, thus resulting in higher  $\text{CO}_2$  local concentrations compared to the thicker CLs, where the  $\text{CO}_2$  and electrolyte residence time was higher. The multi-physics model of Ag-GDE developed recently for  $\text{CO}_2\text{R}$  showed that a thinner CL could enhance the mass transfer of the  $\text{CO}_2$  in the GDE, which normally dominates the overall reaction rate at high cathodic potential.<sup>58, 189</sup> Consequently, the negative effect on CD due to the low density of active sites of thin CL could be less significant at high cathodic potential. This mechanism could also partially explain the higher CD of Cu-based GDEs with thin CLs at higher cathodic potentials, as experimentally observed by Sargent et al.<sup>45</sup>

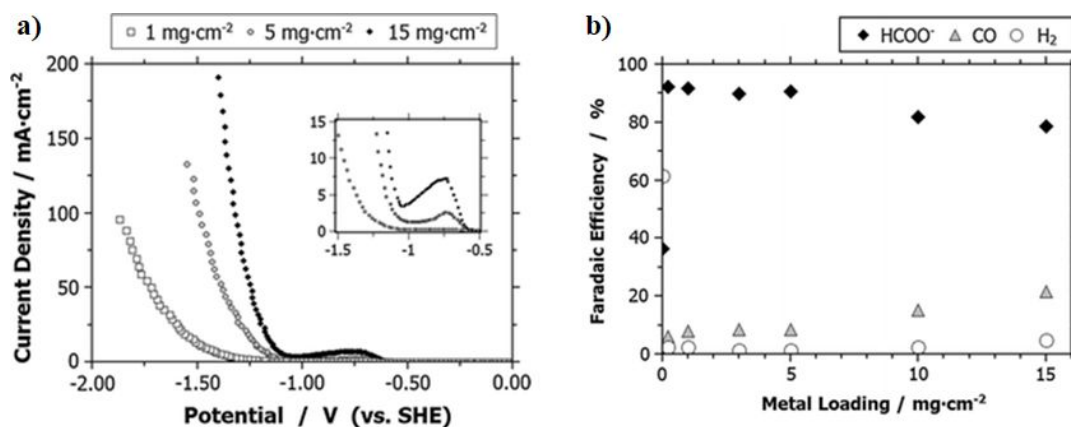


**Figure 12.** a) A comparison of CD for GDEs with various Sn loading as a function of potential. b) The FE for HCOO<sup>-</sup>, CO and H<sub>2</sub> production for GDEs with different Sn loading at 50 mA cm<sup>-2</sup>. All the experiment were conducted in the 0.1 M KHCO<sub>3</sub> aqueous electrolyte. Reprinted with permission from Kopljar et al.<sup>139</sup>, Copyright 2014, Springer Nature.

In addition to the catalyst loading, the ionic binder also influences the cathode performance. Taking Nafion ionomer for example,<sup>84</sup> it not only forms a continuous matrix in the CL that promotes cation conduction, but also has an impact on the microstructure of the CL that governs CO<sub>2</sub> diffusion. For efficient CO<sub>2</sub> electrocatalysis, therefore, an optimal balance needs to be achieved among the pores for CO<sub>2</sub> diffusion, catalyst particles for electron conduction and catalysis, and ionomer for ion conduction.<sup>179</sup> Through constraining the Sn loading, Zhou and co-workers found that the electrode performance is dependent on the content of the Nafion ionomer, and reported an optimal Nafion loading of 20 wt.% in terms of CD and FE.<sup>179</sup> Moreover, the ionomer in the CL can also serve as a co-catalyst promoting the CO<sub>2</sub>R reaction. An example is the incorporation of the imidazole-based ionomers to an Sn-based CL could stabilize the \*CO<sub>2</sub><sup>-</sup> intermediates and therefore enable the electroreduction of CO<sub>2</sub> to HCOOH.<sup>127, 191, 192</sup>

The dispersion of the catalysts in the CL is another crucial factor for the electrode performance towards CO<sub>2</sub>R. Kenis's and coworkers studied the effects of catalyst dispersion by comparing the performance of Ag-based GDEs prepared using hand painting and air-brushing CL deposition methods.<sup>193</sup> They found that the automated air-brushing technique renders a more uniform catalyst distribution and reduced particle agglomeration in the CL, as shown in **Figure 13a to c**, thereby suppressing the HER and promoting the evolution of CO, though the overall CD was not significantly affected by the microstructural difference. They considered such product yield difference to be a result of exposed carbon from MPL that promotes HER, which



is evidenced by the observed high HER PCD for bare GDL (**Figure 13d to e**); a uniformly dispersed CL could reduce such carbon exposure and therefore suppress the unwanted HER.<sup>193</sup>

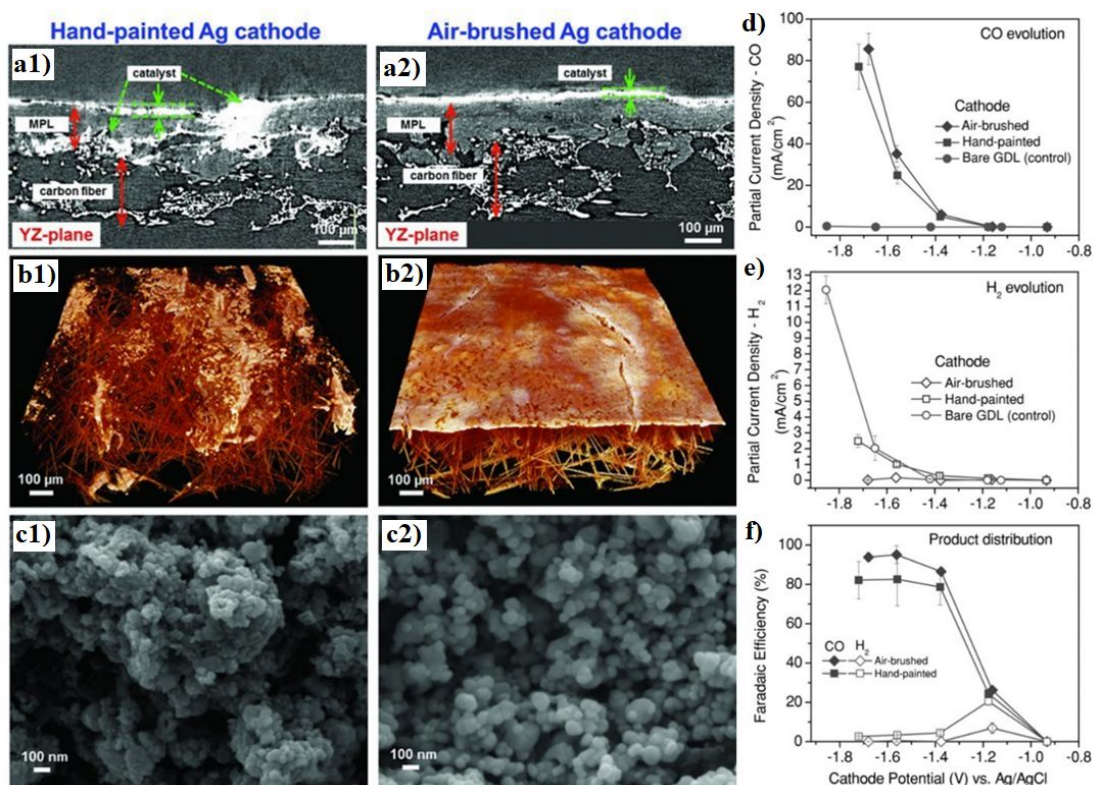


**Figure 13.** a) SEM image of the cross-section b) MicroCT 3D tomographic virtual models and c) SEM topography of the Ag GDEs with hand-painted and air-brushed CLs. A comparison of the partial CD of d) CO and e) H<sub>2</sub> as well as f) product distribution for Ag-based GDEs fabricated through hand painting and air brushing. Reprinted with permission from Jhong et al.<sup>193</sup>, Copyright 2013, John Wiley and Sons.

## 5 Electrolyte selection

The primary function of the electrolyte in a CO<sub>2</sub>R electrolyzer is to conduct ionic charge between electrodes. An electrolyte generally consists of three components: an inert electrolyte or salt, the solvent (e.g. water), and the electroactive species. A good solvent should have (1) a high solubility for the reactant (CO<sub>2</sub>) and desired electrolyte to provide conduction; (2) electrochemically stable; (3) be chemically compatible with the electrode materials including the active catalysts; (4) low viscosity if liquid at the cell operating temperature to ensure good rates of CO<sub>2</sub> mass transfer from the bulk electrolyte solution to the electrode surfaces<sup>194, 195</sup> and (5) easy to handle, storage, and safe. Water is the most common solvent for CO<sub>2</sub>R electrolytes because water satisfies the properties listed above, and can act as both a proton donor and proton acceptor to facilitate production of different electroactive species.



A key requirement of inert electrolytes commonly used in CO<sub>2</sub>R processes is that the electrolyte easily dissociates into cations and anions so as to provide a high ionic conductivity.<sup>196</sup> However, the effect of the electrolyte ions on CO<sub>2</sub>R is far more complex than a simple charge carrier relationship.<sup>197, 198</sup> Even if the ions of inert electrolytes do not participate directly in redox reactions, an inert electrolyte can affect CO<sub>2</sub>R, for example, through interactions of electrolyte ions with radicals and ions produced in the CO<sub>2</sub>R reaction as described by Setterfield-Price and Dryfe.<sup>199</sup>

An operational issue common for all types of electrolytes is that impurities in the electrolyte can poison cathode catalysts. For example, trace metal impurities electrodeposited at the cathode during the CO<sub>2</sub>R process can lead to loss of CO<sub>2</sub>R selectivity with increased relative rates of the HER.<sup>18</sup> Therefore, usually high purity inert electrolytes or electrolyte purification by pre-electrolysis is required. Alternatively, chelating agent such as ethylenediaminetetraacetic acid (EDTA)<sup>19</sup> or a solid-supported iminodiacetate resin (Chelex)<sup>200</sup> could be used to mitigate effects of impurities on CO<sub>2</sub>R.

### 5.1 Aqueous solutions of inorganic salts

The most commonly reported electrolytes for CO<sub>2</sub>R are simple aqueous, inorganic salt solutions such as potassium bicarbonate (KHCO<sub>3</sub>), and some common examples are summarized in **Table 3**. Although CO<sub>2</sub> solubility in aqueous salt solutions<sup>201, 202</sup> may be low as compared to other CO<sub>2</sub> capture solvents such as aqueous amine solutions;<sup>203, 204</sup> aqueous salt solutions are widely available at large scale and low cost; are relatively easy to prepare, handle, and store safely; and exhibit stable ionic conductivity.<sup>154, 205-207</sup> Since the 1950s the natural gas and ammonia industries have captured CO<sub>2</sub> using the Benfield Process with hot solutions (100 – 116 °C) of potassium carbonate (K<sub>2</sub>CO<sub>3</sub>) to capture CO<sub>2</sub> to form KHCO<sub>3</sub>.<sup>208</sup> It's not surprising that given this long industrial history, KHCO<sub>3</sub> solutions have become the most commonly reported aqueous electrolytes for CO<sub>2</sub>R.<sup>196, 209-217</sup> Carbonates are also chemically compatible with most electrode materials (relative to other conducting salts such as sulfides,<sup>218</sup> sulphates,<sup>219</sup> and halides<sup>190, 220, 221</sup>). Importantly, bicarbonate solutions provide capacity to buffer the local pH at the electrode surface during CO<sub>2</sub>R.<sup>56</sup> The KHCO<sub>3</sub> cases described here highlight the complexity of the effects of electrolyte choice in a CO<sub>2</sub> electrolyzer, and to understand these effects more clearly, we discuss separately the roles of cations and anions in aqueous salt electrolytes.

**Table 3. Survey of aqueous solutions of inorganic salts-based electrolytes used for electrochemical CO<sub>2</sub>R with various operating conditions.**

Electrolyte	Catalyst	Major CO <sub>2</sub> R products (Faradaic efficiency, %)	Applied potential (V vs RHE)	Current density (mA cm <sup>-2</sup> )/ mass activity (A g <sup>-1</sup> )	Reactor-type <sup>Ref.</sup>
0.1 M KClO <sub>4</sub>	Cu nanowires	C <sub>2</sub> H <sub>6</sub> (20.3%)	-1.10	-	H-cell <sup>222</sup>
0.1 M K <sub>2</sub> HPO <sub>4</sub>		C <sub>2</sub> H <sub>6</sub> (10%)			
0.1 M KHCO <sub>3</sub>		C <sub>2</sub> H <sub>6</sub> (17.6%)			
0.1 M LiHCO <sub>3</sub>	Cu foil	CH <sub>4</sub> (32.2%), C <sub>2</sub> H <sub>4</sub> (5.2%), C <sub>2</sub> H <sub>5</sub> OH (1.6%), HCOO <sup>-</sup> (4.7%)	-1.45 (vs SHE)	5	H-cell <sup>223</sup>
0.1 M NaHCO <sub>3</sub>		CH <sub>4</sub> (55.1%), C <sub>2</sub> H <sub>4</sub> (12.9%), C <sub>2</sub> H <sub>5</sub> OH (4.2%), HCOO <sup>-</sup> (7%)	-1.45 (vs SHE)		
0.1 M KHCO <sub>3</sub>		CH <sub>4</sub> (32%), C <sub>2</sub> H <sub>4</sub> (30.3%), C <sub>2</sub> H <sub>5</sub> OH (10.9%), HCOO <sup>-</sup> (8.3%)	-1.39 (vs SHE)		
0.1 M CsHCO <sub>3</sub>		CH <sub>4</sub> (16.3%), C <sub>2</sub> H <sub>4</sub> (30.5%), C <sub>2</sub> H <sub>5</sub> OH (2.4%), HCOO <sup>-</sup> (15.8%)	-1.38 (vs SHE)		
1 M NaCl	Ag-GDE	CO (75%)	-1.87 (vs Ag AgCl)	72.7 A g <sup>-1</sup>	Flow-cell <sup>224</sup>
1 M KCl		CO (95.6%)	-1.84 (vs Ag AgCl)		
1 M RbCl		CO (93.6%)	-1.83 (vs Ag AgCl)		
1 M CsCl		CO (87%)	-1.81 (vs Ag AgCl)		
1 M NaBr		CO (60.8%)	-2.33 (vs Ag AgCl)		
1 M KBr		CO (96.6%)	-1.76 (vs Ag AgCl)		
1 M RbBr		CO (95.8%)	-1.80 (vs Ag AgCl)		
1 M CsBr		CO (93.6%)	-1.64 (vs Ag AgCl)		
1 M NaI		CO (80.8%)	-1.81 (vs Ag AgCl)		
1 M KI		CO (96.6%)	-1.64 (vs Ag AgCl)		
1 M RbI		CO (96.5%)	-1.59 (vs Ag AgCl)		
1 M CsI		CO (101.7%)	-1.56 (vs Ag AgCl)		
1 M NaOH		CO (83.0%)	-1.86 (vs Ag AgCl)		
1 M KOH		CO (96.7%)	-1.70 (vs Ag AgCl)		
1 M RbOH		CO (91.6%)	-1.63 (vs Ag AgCl)		
1 M CsOH		CO (89.8%)	-1.60 (vs Ag AgCl)		
3 M KHCO <sub>3</sub>		Ag-GDE*	CO (82.5%)		
3 M KOH	CO (101.5%)		-0.80	234.8	
3 M KCl	CO (73.6%)		-0.81	10.7	
0.1 M LiHCO <sub>3</sub>	Ag foil	CO (59.1%)	-1.0	1.97	H-cell <sup>62</sup>

0.1 M NaHCO <sub>3</sub>		CO (68.4%)		2.75	
0.1 M KHCO <sub>3</sub>		CO (82.9%)		4.06	
0.1 M RbHCO <sub>3</sub>		CO (82.2%)		4.65	
0.1 M CsHCO <sub>3</sub>		CO (80.3%)		5.54	
0.1 M LiHCO <sub>3</sub>	Cu foil	CH <sub>4</sub> (6.2%)		2.40	
0.1 M NaHCO <sub>3</sub>		CH <sub>4</sub> (17.7%), C <sub>2</sub> H <sub>4</sub> (5.5%)		2.57	
0.1 M KHCO <sub>3</sub>		CH <sub>4</sub> (15.3%), C <sub>2</sub> H <sub>4</sub> (10.2%), HCOO <sup>-</sup> (4.7%)		3.03	
0.1 M RbHCO <sub>3</sub>		CH <sub>4</sub> (13.2%), C <sub>2</sub> H <sub>4</sub> (24.4%), C <sub>2</sub> H <sub>5</sub> OH (9.6%)		4.03	
0.1 M CsHCO <sub>3</sub>		CH <sub>4</sub> (9.4%), C <sub>2</sub> H <sub>4</sub> (31.1%), C <sub>2</sub> H <sub>5</sub> OH (11.4%)		4.80	

\*GDE means gas diffusion electrodes

### 5.1.1 Cationic effects

Many studies report that alkali cations effect CD and product distribution of  $\text{CO}_2\text{R}$  in aqueous electrolytes.<sup>223, 224, 226, 227</sup> Several theories have been proposed to explain these observations, including the specific adsorption of cations or DL blocking by cations,<sup>223</sup> the degree of cation hydration,<sup>62</sup> and stabilization of the negatively charged intermediate ( $^*\text{CO}_2^-$ )<sup>224</sup> and related electronic field effects by the cation.<sup>60, 228</sup> For example, as shown in **Figure 14**, Hori et al.<sup>223</sup> observed a higher selectivity for  $\text{C}_2\text{H}_4$  and alcohols over  $\text{CH}_4$  and  $\text{H}_2$  in electrolytes with larger cations using a series of electrolytes with ionic size increasing from  $\text{Li}^+ < \text{Na}^+ < \text{K}^+ < \text{Cs}^+$ ). Hori et al.<sup>223</sup> proposed that such cationic effects arise from the tendency of the cations to specifically adsorb on the electrode surface, which is predominated by the reaction energetics and the hydration capacity of the cation.<sup>224, 229</sup> The hydration capacity is stronger for smaller alkali cations,<sup>230</sup> and therefore a  $\text{Li}^+$  ion binds more strongly with water molecules than a  $\text{Cs}^+$  ion, and the  $\text{Li}^+$  is less likely to adsorb at the cathode surface than  $\text{Cs}^+$ . Larger cations such as  $\text{Cs}^+$  are more readily adsorbed at the electrode surface due to their weaker hydration capacity,<sup>223</sup> which will shift the  $\text{CO}_2$  reduction potential towards the positive direction at the outer Helmholtz layer (OHL). This decreased reduction potential will result in a lower proton concentration at the OHL,<sup>223</sup> as suggested by Frumkin as early as 1959.<sup>231</sup> Also, the repulsion between the adsorbed cations and  $\text{H}^+$  can further reduce proton concentrations at the electrode surface, therefore contributing to a reduced selectivity towards  $\text{CH}_4$  and  $\text{H}_2$  as observed by Hori et al.<sup>223</sup> (**Figure 14**).

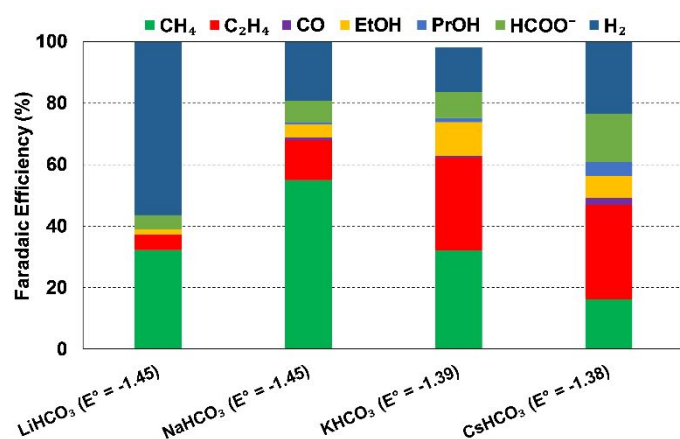


**Figure 14.** Effect of cationic species (different 0.1 M bicarbonate solutions) on FEs of various products at a Cu electrode and at  $5 \text{ mA cm}^{-2}$ ;  $E^0$  values are vs. SHE, reproduced from the data in Akira and Hori (1991).<sup>223</sup>

Thorson et al.<sup>224</sup> proposed that adsorbed cations at the electrode surface could stabilize the intermediate  $^*\text{CO}_2^-$  and thus promote the  $\text{CO}_2\text{R}$ . This theory could explain the observed

enhancement in total CO<sub>2</sub>R efficiencies with cation size from Li<sup>+</sup> to K<sup>+</sup>. (**Figure 14**) Recently, Kim et al.<sup>232</sup> provided further evidence to support this proposed mechanism by observing an efficient CO production over a Au electrode in K<sup>+</sup>-based electrolyte (K<sup>+</sup> is prone to adsorb at the Au electrode) than in a Na<sup>+</sup>-based one. Further DFT calculations reported by Liu et al.<sup>233</sup> revealed that higher electron-density of adsorbed K<sup>+</sup> close to the carbon atom could facilitate in the stabilization of intermediates such as \*COOH and \*CO.

However, there remains some debate around the conclusions of Thorson et al. For example, Mills et al.<sup>234</sup> and Strmcnik et al.<sup>235</sup> argued that the specific adsorption of cations seems impossible under the operating conditions for CO<sub>2</sub>R (usually for potentials larger than  $-1.4$  V vs a normal hydrogen electrode (NHE, potential defined at 1 M H<sup>+</sup> concentration and 1 atm pressure). Bell and co-workers proposed that the observed cationic effect originates from the hydrolysis of the solvated cations close to the cathode surface.<sup>62</sup> At the cathode surface, pK<sub>a</sub> of hydrolysis decreases significantly due to an increasing electrostatic force between the water molecules in the hydration sphere of cation and negatively charged cathode. These interactions can further polarize O-H bonds of water molecules, and consequently facilitate water dissociation to increase the local proton concentration as illustrated in **Figure 15a**. This effect decreases the local pH, which permits an increase of dissolved CO<sub>2</sub> concentration locally that can approach the CO<sub>2</sub> concentration in the bulk electrolyte (**Figure 15b and c**). The net effect reported by Singh et al.<sup>62</sup> was that switching from Li<sup>+</sup> to Cs<sup>+</sup> in an aqueous electrolyte suppressed HER and significantly promoted CO<sub>2</sub>R over Ag cathodes (**Figure 15d**) or Cu cathodes (**Figure 15e**).

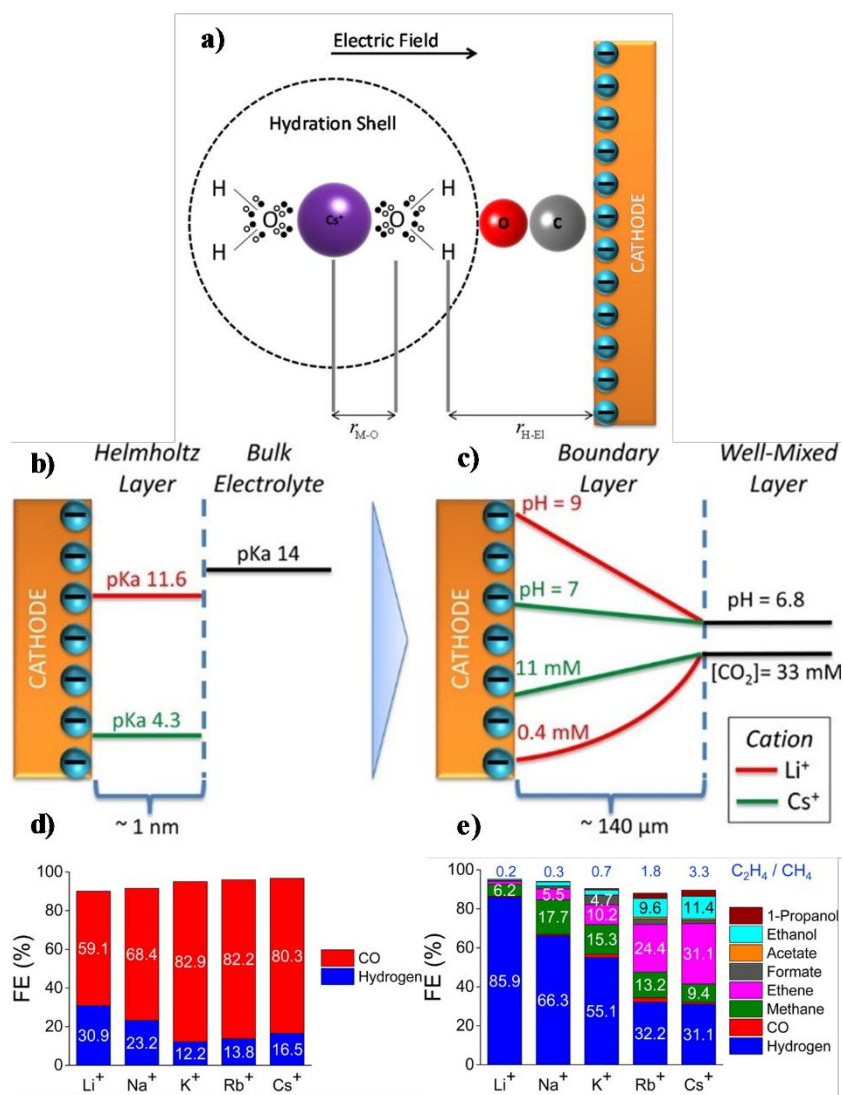


**Figure 15.** a) Interaction of hydrated cation with the negatively charged cathode surface. The additional electrostatic force between the H atom of the  $\text{H}_2\text{O}$  in the primary hydration shell and the cathode causes a decrease in the  $\text{pK}_a$  of hydrolysis; b)  $\text{pK}_a$  of hydrolysis of hydrated  $\text{Li}^+$  and  $\text{Cs}^+$  inside the Helmholtz layer and in the bulk electrolyte; c) concentration of  $\text{CO}_2$  and pH distribution in the boundary layer; d, e) FE of different products over Ag and Cu electrodes respectively at  $-1.0 \text{ V}$  vs RHE. The electrolyte was saturated and the concentration was kept at  $0.1 \text{ M XHCO}_3$  ( $\text{X} = \text{Li}, \text{Na}, \text{K}, \text{Rb},$  and  $\text{Cs}$ ). Reprinted (adapted) with permission from Singh et al.<sup>62</sup>, Copyright 2016, American Chemical Society.

Note that these interpretations of the effects of cation hydrolysis only explain experimental observations at potentials less than  $-1.1 \text{ V}$  vs RHE. The phenomenon of hydrolysis of solvated cations is only applicable when (1) the pH of the electrolyte is close to 7; and (2) the  $\text{pK}_a$  for cation hydrolysis is close to local pH at the electrode; and (3) the reactant concentration is pH dependent.<sup>62</sup> The hydrolysis of the solvated cations close to the cathode surface does not adequately explain the same cationic effects in CO reduction,<sup>223</sup> because the CO concentration is not pH dependent. Koper et al.<sup>236</sup> used density functional theory (DFT) calculations to predict

the effect of cations on CO reduction to C<sub>2</sub>H<sub>2</sub> at pH close to 13, and found that cations could stabilize intermediates, especially dimers \*OCCO and \*OCCOH, via interactions of oxygen atoms in these intermediates.<sup>236</sup> Moreover, the shift in average reaction energies (for Li<sup>+</sup>, Na<sup>+</sup>, and Cs<sup>+</sup>) of CO to C<sub>1</sub> products is close to that reported by Nørskov and co-workers,<sup>60, 61</sup> who showed that the cation-induced local electric effect could alter the free-energy landscape of CO<sub>2</sub>R to CO by stabilizing the key reaction intermediates.<sup>236</sup>

Bell along with other JCAP researchers<sup>63</sup> conducted experimental measurements and DFT calculations at low cell potentials, and reported electrostatic interactions between the hydrated cations located at the OHL and the adsorbed reaction intermediates that have high dipole moments (such as \*CO, \*CO<sub>2</sub>, \*OCCO) at the cathode surface. Such electrostatic interactions lower the energy required for \*CO<sub>2</sub> adsorption (an intermediate for HCOO<sup>-</sup>) and for C-C dimerization to form \*OCCHO or \*OCCO (which are the key intermediates for C<sub>2</sub>H<sub>4</sub> and C<sub>2</sub>H<sub>5</sub>OH, respectively).<sup>63</sup> As a consequence, the PCD for H<sub>2</sub> and CH<sub>4</sub> formation are uninfluenced by the cation size, while the PCD for HCOO<sup>-</sup>, C<sub>2</sub>H<sub>4</sub>, and C<sub>2</sub>H<sub>5</sub>OH enhanced with cation size.

In future research, the investigation of monovalent cations for CO<sub>2</sub>R should be expanded to multivalent cations. Schizodimou and Kyriacou<sup>237</sup> showed that rates of CO<sub>2</sub>R can be accelerated by increasing the size of cations and the surface charge of cations. They demonstrated that the CO<sub>2</sub>R rate is almost two-fold higher in electrolyte containing La<sup>3+</sup> than in electrolytes containing Na<sup>+</sup> at similar operating conditions.

### 5.1.2 Anionic effects

Two principle explanations are described to explain the impact of anions in an electrolyte on CO<sub>2</sub>R<sup>229, 238-241</sup>: pH and buffering effects, and specific adsorption of anions at the cathode surface.<sup>225</sup> Hori et al.<sup>238, 241</sup> studied the effects of pH and reported that the production ratio of C<sub>2</sub>H<sub>4</sub>/CH<sub>4</sub> varies significantly for different anions in electrolyte: the C<sub>2</sub>H<sub>4</sub> / CH<sub>4</sub> ratio is higher for K<sub>2</sub>SO<sub>4</sub> (4.16) and KCl (3.74) than for KHCO<sub>3</sub> (1.02) and K<sub>2</sub>HPO<sub>4</sub> (0.11), (**Figure 16**). This result was attributed to the inadequate neutralization capacity of the non-buffering K<sub>2</sub>SO<sub>4</sub> and KCl, which leads to an increase in local pH, promotes higher hydrocarbons and suppresses CH<sub>4</sub>.<sup>238, 241</sup> Another interesting feature is the promotion of the HER upon increasing the concentration of the K<sub>2</sub>HPO<sub>4</sub> from 0.1 to 0.5 M. This result was attributed to the low pH value at the electrode/electrolyte interface as the concentration of the buffer increases.<sup>229, 238</sup> Through varying the anion types of the electrolyte with or without buffering (e.g. perchlorate, sulfate,

bicarbonate, borate and phosphate), Bell and co-workers<sup>240</sup> found that all the studied anions have negligible effects on evolving pH-independent products, such as CO, HCOO<sup>-</sup>, C<sub>2</sub>H<sub>4</sub> and C<sub>2</sub>H<sub>5</sub>OH,<sup>242-244</sup> but significantly influence the CDs of H<sub>2</sub> and CH<sub>4</sub>, which are highly dependent on pH. In comparison with buffering electrolytes (i.e. HPO<sub>4</sub><sup>2-</sup> and HCO<sub>3</sub><sup>-</sup>), the non-buffering electrolytes with ClO<sub>4</sub><sup>-</sup> and SO<sub>4</sub><sup>2-</sup> as anions demonstrated a higher local pH and significantly lower CDs in producing pH-dependent H<sub>2</sub> and CH<sub>4</sub>.<sup>240</sup> We discuss the effects of pH on CO<sub>2</sub>R in more detail in Section 6 of this review.

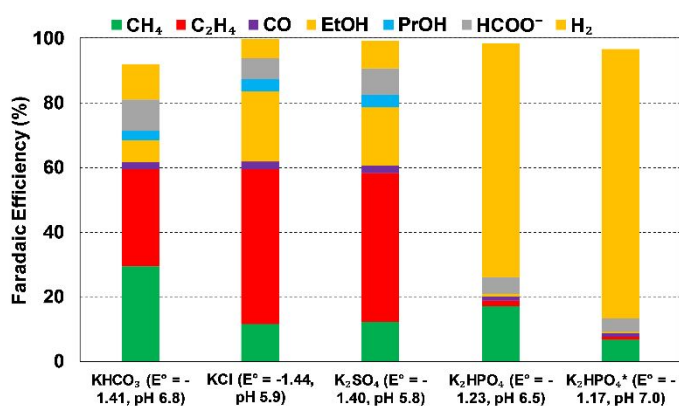


**Figure 16. Effect of anionic species (different 0.1 M bicarbonate solutions) on FEs of various products at a Cu electrode and at 5 mA cm<sup>-2</sup>; E° values are vs. SHE; \*refer to 0.5 M, reproduced from the data in Hori et al.<sup>238</sup> (1989).**

The specific adsorption of anions on cathode can also alter the CO<sub>2</sub>R activity and selectivity.<sup>190, 225, 245, 246</sup> In particular, the adsorption of halide ions on the electrode surface can alter the electronic structure of the catalysts, and thereby influence the interactions between the electrode surface and intermediates.<sup>190</sup> For example, Varela et al. showed that Br<sup>-</sup> and Cl<sup>-</sup> enhanced CO formation, but I<sup>-</sup> facilitated formation of CH<sub>4</sub> instead of CO.<sup>190</sup> Moreover, specifically adsorbed halide anions can suppress proton adsorption and thus prefer CO<sub>2</sub>R to HER for a Cu-metal electrode.<sup>246</sup> This can be attributed to the presence of covalent interaction between the halides and Cu electrodes, which facilitates the transfer of electrons from Cu-surface to CO<sub>2</sub>.<sup>246</sup> In addition, several studies have reported the changes of morphology of a catalyst's surface in the presence of halide anions, especially via oxidation-reduction cycles to promote C<sub>2+</sub> products over copper catalysts.<sup>66, 68, 247-249</sup> However, it still remains unclear which anion factor influences CO<sub>2</sub>R reaction the most.



## 5.2 Organic solvent electrolytes

Some typical examples of organic solvent electrolytes used for CO<sub>2</sub>R are shown in **Table 4** with dimethyl sulfoxide (DMSO), dimethylformamide (DMF), propylene carbonate (PC), and acetonitrile (ACN)<sup>250, 251</sup> the most commonly reported organic solvents used in CO<sub>2</sub>R. The solubility of CO<sub>2</sub> in organic solvents could be much higher than in water (as presented in **Figure 17**). As a result of their higher CO<sub>2</sub> solubility and absence of proton, organic solvents can achieve higher CD and better product distribution for CO<sub>2</sub>R than in aqueous electrolytes.<sup>27, 197, 198, 229</sup> Vassilev et al.<sup>252</sup> reported that DMSO, DMF, PC, and ACN assist in dimerization of \*CO<sub>2</sub> with adsorbed CO<sub>2</sub> molecules to form oxalate (C<sub>2</sub>O<sub>4</sub><sup>2-</sup>) over Pb, In, Sn, and Hg cathodes, which tend to produce HCOO<sup>-</sup>/HCOOH in aqueous electrolytes.<sup>229</sup> Moreover, the overpotential required to convert CO<sub>2</sub> into products is lower than that in aqueous solution, making the process energy-efficient.<sup>253</sup> Mixed electrolytes containing both organic solvents and water are reported, which allows tuning of proton concentrations.<sup>254</sup> Hori et al.<sup>254</sup> found that upon increasing the concentration of water in ACN, CO<sub>2</sub>R favors the formation of formic acid rather than oxalic acid.

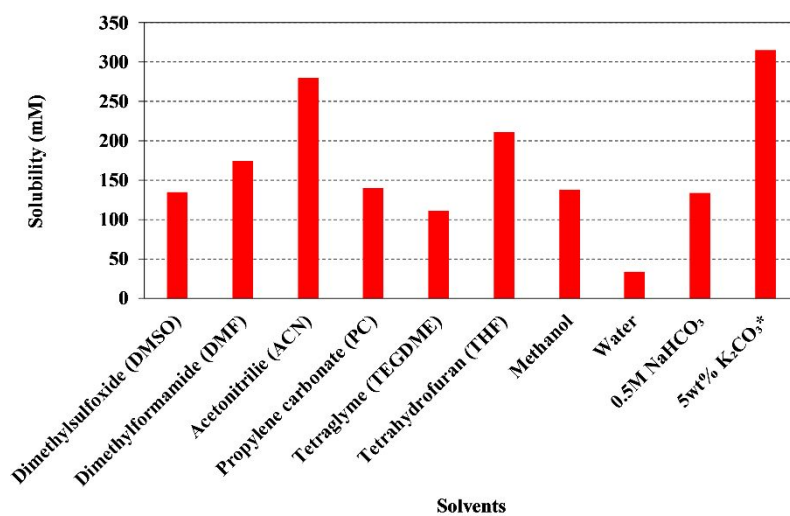


**Figure 17.** The solubility of CO<sub>2</sub> in various organic solvents at 298 K and 1 atm.<sup>255-258</sup>  
 \*Note: CO<sub>2</sub> solubility in 5 wt.% K<sub>2</sub>CO<sub>3</sub> was calculated from the CO<sub>2</sub> loading data (0.830 mol CO<sub>2</sub>/mol K<sub>2</sub>CO<sub>3</sub>)<sup>257</sup> and since it includes both chemical and physical CO<sub>2</sub> solubility, therefore, 5 wt.% K<sub>2</sub>CO<sub>3</sub> has higher CO<sub>2</sub> solubility than organic solvents. Moreover, 5 wt.% K<sub>2</sub>CO<sub>3</sub> has higher CO<sub>2</sub> loading than 30 wt.% aqueous monoethanolamine solution, which is 0.540 (mol CO<sub>2</sub>/mol amine) at 298 K and 2.80 kPa (P<sub>CO<sub>2</sub></sub>).<sup>259</sup>

Although organic solvents offer higher CO<sub>2</sub> solubility than aqueous electrolytes, some critical disadvantages of organic solvent electrolytes are their high cost, their volatility and flammability, and possible toxicity. As the organic solvents are not typically consumed in the CO<sub>2</sub>R reaction it could be possible to recycle solvents to reduce the operational costs of

CO<sub>2</sub>R.<sup>198</sup> However, recycling of organic solvents from the electrolyzer liquid product may be complicated and costly due to the volatility and toxicity of the solvent and potential miscibility with the desired products.<sup>260</sup>

**Table 4. Survey of organic solvent electrolytes used for electrochemical CO<sub>2</sub>R with various operating conditions.**

Electrolyte	Catalyst	Major CO <sub>2</sub> R products (Faradaic efficiency, %)	Applied potential (V vs RHE)	Current density (mA cm <sup>-2</sup> )	Reactor-type <sup>Ref.</sup>
0.1 M TBAP/PC	Au foil	CO (91.8%)	-3.02 (vs Fc/Fc <sup>+</sup> )	2.8	H-cell <sup>260</sup>
0.1 M TEAP/PC	Pb foil	H <sub>2</sub> C <sub>2</sub> O <sub>4</sub> (73.3%)	-2.4 (vs SHE)	-	H-cell <sup>250</sup>
0.1 M TEAP/PC	In foil	CO (85.3%)			
DMF	Pb foil	CO (n.a.)	-	-	H-cell <sup>251</sup>
0.5 M LiCl/Methanol	Cu foil <sup>a</sup>	CO (~ 65%), CH <sub>4</sub> (20%)	-2.8 (vs SHE)	15	H-cell <sup>261</sup>
0.08M CsOH/Methanol	Cu foil	CH <sub>4</sub> (8.3%), C <sub>2</sub> H <sub>4</sub> (23.7%)	-4.0 (vs Ag AgCl)	-	H-cell <sup>262</sup>
0.08M Benzalkonium/Methanol	Cu foil <sup>b</sup>	CO (~7%), CH <sub>4</sub> (42.5%), C <sub>2</sub> H <sub>4</sub> (2.1%)	-2.0 (vs SCE)	-	H-cell <sup>263</sup>

<sup>a</sup>at high pressure (10 atm); <sup>b</sup>at low temperature (-30 °C); PC – Propylene carbonate; TBAP – Tetrabutylammonium perchlorate; TEAP – tetraethylammonium perchlorate; DMF – Dimethylformamide; LiCl – Lithium chloride; CsOH – Cesium hydroxide

### 5.3 Ionic liquids

Ionic liquids (IL) have been proposed as alternatives to aqueous amines for CO<sub>2</sub> capture process<sup>264</sup> because ILs exhibit high CO<sub>2</sub> solubility<sup>265</sup> and high selectivity for CO<sub>2</sub> over other gases such as N<sub>2</sub>, O<sub>2</sub>, and CH<sub>4</sub>.<sup>266</sup> Ionic liquids also exhibit other desirable properties for CO<sub>2</sub>R electrolytes such as excellent thermal stability,<sup>267, 268</sup> stability across a wide electrochemical potential window,<sup>268, 269</sup> high ionic conductivity,<sup>268</sup> and low vapor pressure.<sup>268, 270</sup> In addition, some ILs can form a complex with the intermediates during CO<sub>2</sub>R and thus lower the energy barrier of the reaction.<sup>191</sup> **Table 5** provides a summary of some ILs reported as CO<sub>2</sub>R electrolytes. The most extensively studied ILs for use in CO<sub>2</sub>R electrolyzers are two commercially available ILs: 1-ethyl-3-methylimidazolium tetrafluoroborate ([EMIM][BF<sub>4</sub>]), and 1-butyl-3-methylimidazolium tetrafluoroborate ([BMIM][BF<sub>4</sub>]).<sup>191, 271, 272</sup>

In 2011, Rosen et al.<sup>191</sup> first reported the catalytic effect of an 18 mol% aqueous solution of ([EMIM][BF<sub>4</sub>]) in the CO<sub>2</sub>R to CO over an Ag electrode at low overpotentials to achieve FE<sub>CO</sub> of over 96%. **Figure 18** illustrates Rosen et al.'s<sup>191</sup> hypothesis that an IL cation can stabilize the \*CO<sub>2</sub> intermediate, and therefore substantially lower the energy barrier for the formation of \*CO<sub>2</sub> and its subsequent reduction to CO.<sup>191, 273, 274</sup> Subsequently, the Rosen's team investigated the effect of water on CO<sub>2</sub>R in ([EMIM][BF<sub>4</sub>]) solutions and found that addition of water in the IL enhanced the CO selectivity, with an optimal CO selectivity close to 100% in a solution of 10.5 mol.% IL in water. Such performance enhancement was attributed to a synergistic effect of mass-transfer improvement due to lower the electrolyte's viscosity by dilution with water and an optimal pH (pH around 3.2 at 89.5% water).<sup>274</sup>

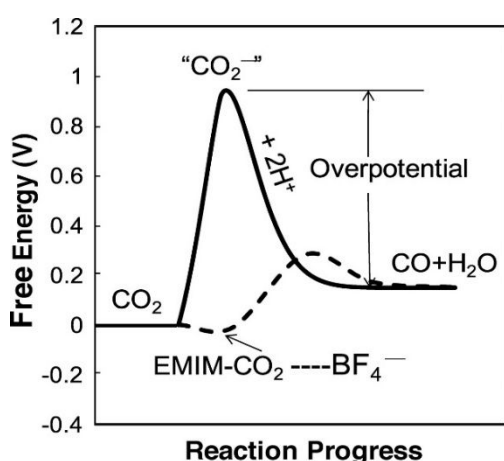


**Figure 18.** A change in free energy of CO<sub>2</sub> to CO in water (solid line) to CO<sub>2</sub> to CO in EMIM-BF<sub>4</sub> (dashed line). Reprinted with permission from Rosen et al.<sup>191</sup>, Copyright 2011, American Association for the Advancement of Science.

Following Rosen et al.'s work,<sup>191</sup> others have attempted to understand the catalytic effect of the ILs in CO<sub>2</sub>R, and although there is still more to understand about the reaction mechanism most reports suggest that the cation is primarily responsible for the observed catalytic effects.<sup>271, 275-278</sup> For example, Rosenthal and co-workers proposed that ILs serve as a proton source by investigating the catalytic performance of the Bi-based catalyst in AN solutions of [BMIM]<sup>+</sup>-based ILs.<sup>279, 280</sup> Deprotonation from the C2 position (refer to **Figure 19**) of the [EMIM]<sup>+</sup> or [BMIM]<sup>+</sup> cation would result in the conversion of CO<sub>2</sub> to CO via the 2e<sup>-</sup>/2H<sup>+</sup> reduction pathway, which has a lower energy barrier.<sup>279, 281 282</sup>

Despite the many promising properties of ILs for CO<sub>2</sub>R electrolytes, the high viscosity of ILs can severely limit the rates of CO<sub>2</sub> diffusion, and thus ILs achieve very low CDs<sup>272</sup> and, as shown in **Table 5**, most CO<sub>2</sub>R studies dilute ILs in aqueous solutions or organic solvents such as AN, DMF, or CH<sub>3</sub>OH to reduce the electrolyte's viscosity.<sup>191, 271, 275, 277</sup> Progress in development and application of ILs has progressed rapidly in the last 30 years to provide a large amount of fundamental understanding of IL properties and physicochemical data, and to lower IL production costs significantly. Thus, ILs are becoming more available and could soon be viable options for use in CO<sub>2</sub>R electrolyzers.

**Table 5. Survey of Ionic liquids (ILs) as electrolytes used for electrochemical CO<sub>2</sub>R with various operating conditions.**

Electrolyte	Catalyst	Major CO <sub>2</sub> R products (Faradaic efficiency, %)	Applied potential (V vs RHE)	Current density (mA cm <sup>-2</sup> )	Reactor-type <sup>Ref.</sup>
18 mol% [EMIM][BF <sub>4</sub> ]/Water	Ag-GDE	CO (~96%)	1.5 to 2.5 V (cell potential)	-	Flow-cell <sup>191</sup>
[EMIM][BF <sub>4</sub> ]	Ag NPs (40-200 nm) onto Sigracet carbon paper (5 mg cm <sup>-2</sup> )	CO (-)	3.25 V (cell potential)	4	Flow-cell
0.02 M [EMIM][BF <sub>4</sub> ]/0.1 M [TBA][PF <sub>6</sub> ]/ACN	Bi electrodeposited onto a glassy carbon electrode	CO (93±7%)	-1.95 (V vs SCE)	~ 3.77	H-cell <sup>279</sup>
0.02 M [BMIM][BF <sub>4</sub> ]/0.1 M [TBA][PF <sub>6</sub> ]/ACN		CO (95±6%)		~ 5.51	
0.02 M [BMIM][PF <sub>6</sub> ]/0.1 M [TBA][PF <sub>6</sub> ]/ACN		CO (90±9%)		~ 4.82	
0.02 M [BMMIM][BF <sub>4</sub> ]/0.1 M [TBA][PF <sub>6</sub> ]/ACN		CO (76±6%)		~ 0.67	
80 wt% [BMIM][Cl]/Water	Ag foil	CO (> 99%)	-1.5 (V vs SCE)	-	H-cell <sup>271</sup>
4 mol% [EMIM][BF <sub>4</sub> ]/Water	Bulk MoS <sub>2</sub>	CO (~ 98%)	-0.764	65	H-cell <sup>275</sup>
0.1 M [EMIM][NTf <sub>2</sub> ]/ACN					
0.02 M [DMPIM][BF <sub>4</sub> ]/0.1 M [TBA][PF <sub>6</sub> ]/ACN	Ag foil	CO (~100%)	-1.48 (V vs Fc/Fc <sup>+</sup> )	4.2	H-cell <sup>282</sup>
0.5 M [EMIM][N(CN <sub>2</sub> )]	Sn NPS/glassy carbon	HCOO <sup>-</sup> (81.9%)	-1.2	~ 4.18	H-cell <sup>283</sup>
0.1 M [TBA][PF <sub>6</sub> ]/ACN	Ag foil	CO (74%)	-2.1 (V vs SCE)	17	H-cell <sup>284</sup>
0.5 M [BMIM][PF <sub>6</sub> ]/0.1 M [TBA][PF <sub>6</sub> ]/ACN		CO (97%)		50	
[BMIM][PF <sub>6</sub> ]	Pb foil	CO (~100%)	-2.2 (V vs Ag Ag <sup>+</sup> )	0.33	H-cell <sup>285</sup>
30 wt% [BMIM][PF <sub>6</sub> ]/ACN		HCOOH (46.3%), CO (40.2%)		2.63	
30 wt% [BMIM][PF <sub>6</sub> ]/5 wt% water/ACN	Pb foil	HCOOH (91.6%)	-2.3 (V vs Ag Ag <sup>+</sup> )	37.6	
30 wt% [BMIM][PF <sub>6</sub> ]/5 wt% water/ACN	Sn foil	HCOOH (92%)		32.1	

[EMIM] – 1-ethyl-3-methylimidazolium; [BMIM] - 1-butyl-3-methylimidazolium; [TBA] – tetrabutylammonium; [BMMIM] - 1-butyl-2,3-dimethylimidazolium; [DMPIM] - 1,3-dimethyl-2-phenyl-imidazolium; [BF<sub>4</sub>] – tetrafluoroborate; [PF<sub>6</sub>] – hexafluorophosphate; [NTf<sub>2</sub>] - bis(trifluoromethylsulfonyl)imide; [CN<sub>2</sub>] – dicyanamide; ACN – acetonitrile.

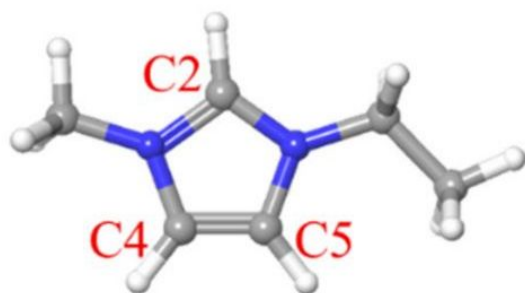


**Figure 19.** Structure of imidazolium cation; white is H<sub>2</sub>, grey is C and blue is N<sub>2</sub>. Reprinted (adapted) with permission from Lau et al.<sup>282</sup>, Copyright 2016, American Chemical Society.

## 6 pH effects

The pH of the electrolyte affects the phase stability of CO<sub>2</sub> in aqueous solutions as illustrated by the Pourbaix diagram in **Figure 20**.<sup>229</sup> The Pourbaix diagram highlights the acid/base homogeneous interactions of CO<sub>2</sub> into different forms, such as carbonic acid (H<sub>2</sub>CO<sub>3</sub>), bicarbonate (HCO<sub>3</sub><sup>-</sup>), carbonate (CO<sub>3</sub><sup>2-</sup>) and methanol (CH<sub>3</sub>OH) in water as a function of pH and potential. Reaction 6 shows that the introduction of CO<sub>2</sub> into an aqueous solution entails a complex series of reversible reactions between CO<sub>2</sub>, water, carboxylic acid, and its deprotonated species. In solutions with a pH up to about 6, CO<sub>2</sub> is in the form of a weak carboxylic acid; at pH between 6 and 10.3, HCO<sub>3</sub><sup>-</sup> anions are formed; and at pH above 10.3 HCO<sub>3</sub><sup>-</sup> deprotonates further to CO<sub>3</sub><sup>2-</sup> (reaction 7). Due to the various reactions and the feed CO<sub>2</sub>, most aqueous solutions are normally in the HCO<sub>3</sub><sup>-</sup> form and around pH 9 unless specific measures are used to counteract them (e.g., high flow rates).<sup>45</sup>

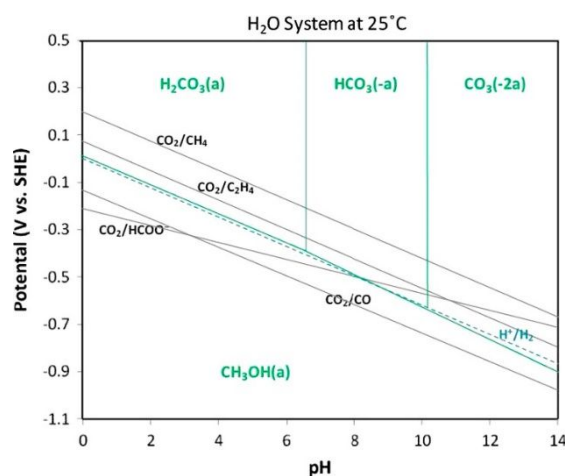
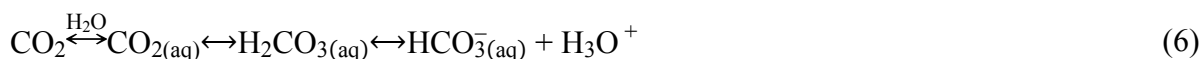


**Figure 20.** Pourbaix diagram for electrochemical CO<sub>2</sub>R at 25 °C. Reprinted with permission from Ganesh,<sup>286</sup> Copyright 2014, Elsevier Ltd.



Note that the local pH near the cathode surface is usually different to that in the bulk electrolyte due to the catalytic reactions generating  $\text{OH}^-$  or consuming  $\text{H}^+$ , and diffusion limitations.<sup>287</sup> Despite the significance of local pH on  $\text{CO}_2\text{R}$  as discussed in Hori's works,<sup>229, 238, 239</sup> only recently has the influence of local pH been re-re-examined.<sup>55, 287-292</sup> Additionally, some electrolytes, such as bicarbonates provide pH buffering effects (see section 5.1.2 for more details).<sup>240</sup>

As the major competing side reaction, HER needs to be minimized for an optimal  $\text{CO}_2\text{R}$  reaction. Therefore, pH is crucial in determining the HER activity, as it characterizes the availability of the protons. Although  $\text{CO}_2\text{R}$  produces  $\text{OH}^-$ , its equilibrium potential is not much influenced by the pH in comparison to HER.<sup>286</sup> A rise in pH moves the equilibrium potential of HER to a more negative value, thus significantly slowing down HER.<sup>293</sup> As shown in **Figure 21**, the equilibrium potential denoted by  $E_{\text{rev}}$  reflects the potential of the HER derived from the Nernst equation. Moreover, the mechanism of HER switches from protons-to- $\text{H}_2$  in acidic media to water-to- $\text{H}_2$  in alkaline media, where the kinetics of latter is significantly slower and does not have a pH dependence, although the concentration is typically much greater.<sup>294-297</sup>

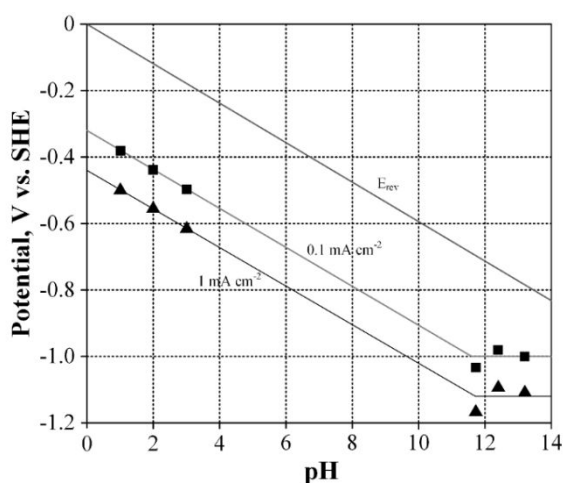


**Figure 21. Hydrogen evolution polarization data at copper (Cu) with varying solution pHs. Reprinted with permission from Gattrell et al.<sup>293</sup>, Copyright 2006, Elsevier Ltd.**

The pH is also an essential factor in determining the products of  $\text{CO}_2\text{R}$ . Taking Cu as an example, an increase of pH shifts the product selectivity from  $\text{H}_2$  and  $\text{CH}_4$  to higher carbon products such as  $\text{C}_2\text{H}_4$ .<sup>45, 238, 241, 298, 299</sup> The HER suppression at higher pH can be easily



described by the reduced availability of  $H^+/H_{ads}$ . However, how pH affects  $CO_2R$  products (i.e.  $CH_4$  preferred at low pH and  $C_2H_4$  at higher pH) is very complex, and is likely related to the multiple proton-coupled-electron steps involved in their various reaction pathways, and the rate-determining steps in those various microkinetics.<sup>294, 298, 300-302</sup> The different onset potentials<sup>238, 299, 303</sup> and Tafel slopes<sup>304-306</sup> for  $CH_4$  and  $C_2H_4$  evolution suggest that they follow different reaction pathways. Hori and co-workers proposed that  $C_2H_4$  evolution is pH independent, while the pathway for  $CH_4$  evolution is pH-dependent, during or prior to the rate-determining step (RDS).<sup>306</sup> By using online electrochemical mass spectrometry (OLEMS), however, Schouten's group found that the onset potential for forming  $CH_4$  and  $C_2H_4$  are both pH-dependent particularly over Cu (111) electrode.<sup>307, 308</sup> Schouten and co-workers proposed two possible reaction pathways for the formation of  $C_2H_4$  as illustrated in **Figure 22a**. One pathway is pH-independent, involving the formation of CO dimer where proton transfer is not the RDS, and preferentially takes place at Cu (100) facets. This pathway has also been theoretically confirmed by Calle-Vallejo and Koper.<sup>309</sup> Another pathway is pH dependent, sharing the same  $^*CHO$  intermediate, which is also critical in evolving  $CH_4$ , and takes place both at Cu (100) and (111) facets. More interestingly, the overpotential for both  $CH_4$  and  $H_2$  evolution is lowered at a very high pH (e.g. pH = 13, see **Figure 22b**).<sup>308, 310</sup> The reduced overpotential of HER at higher pH could be a result of the possible reaction pathway shift from pH dependent (due to proton availability) to pH independent (due to water discharge).<sup>293, 311</sup> Likewise, it could be understood that a similar shift likely takes place during the formation of the  $CH_4$  at higher pH. Based on this understanding, electrolytes with higher pH can favor the formation of higher hydrocarbon products (especially over copper catalysts). Recently, Sargent and co-workers<sup>45</sup> showed that strong alkaline media (7 M KOH) accelerates the kinetics of  $CO_2R$  by lowering the C-C coupling energy barrier over Cu catalyst and could achieve a  $C_2H_4$  FE of ~70% at  $-0.55$  V vs RHE over 150 h of continuous  $CO_2R$  operation. Therefore, more researchers are investigating KOH as electrolyte to further enhance the efficiency and selectivity of  $>C_2$  products.<sup>45, 312</sup>

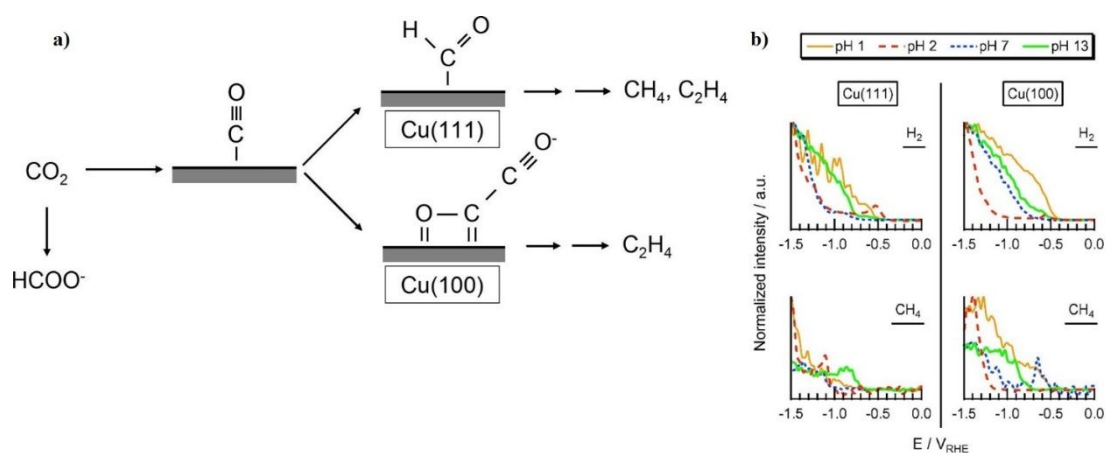


**Figure 22.** a) The proposed reaction mechanism for the reduction of CO<sub>2</sub> on Cu single crystal electrodes and b) the reduction of CO in 0.1 M HClO<sub>4</sub> (pH 1), 0.2 M NaClO<sub>4</sub> (pH: 2 and 7) and 0.1 M NaOH (pH: 13) on Cu (111) left and Cu (100) right. Reprinted with permission from Schouten et al.<sup>308</sup>, Copyright 2014, Elsevier Ltd.

Additionally, it could be understood that a rise in the local pH could be beneficial for >C<sub>2</sub> products; however, with a rise in local pH, the equilibrium of CO<sub>2</sub> and water neutralization reaction shifts more towards bicarbonate formation, which eventually depletes the local CO<sub>2</sub> concentration and thus reduces the CO<sub>2</sub>R selectivity by promoting HER.<sup>62, 290</sup> This conflicting statement really begs a question on whether a high local pH is really desirable or deleterious for the CO<sub>2</sub>R reaction. At higher pH, CO<sub>2</sub> may still exist in low quantity (if ample CO<sub>2</sub> is transported into the solution) due to its limited hydration kinetics.<sup>242, 313</sup> Therefore, an optimal pH may exist for an efficient reaction and sufficient CO<sub>2</sub> supply. Recent modeling studies found a relationship between pH and selectivity of CO<sub>2</sub>R with a maximum CO<sub>2</sub> selectivity over an optimal local pH range of 9 to 10 (especially for C<sub>2</sub> products).<sup>154, 314</sup> Interestingly, at higher pH, the selectivity and activity of >C<sub>2</sub> products reach a maximum and finally start decreasing, whereas, CH<sub>4</sub> evolution starts increasing.<sup>63</sup> A possible reason for this behavior could be the increased coverage of H\* caused by the depletion of CO\* in the limited mass-transport regime. Such adsorbed protons promote CH<sub>4</sub> evolution (by CO hydrogenation) and reduce the chances of CO\* coupling to make >C<sub>2</sub> products.<sup>315, 316</sup>

Furthermore, in a relatively alkaline environment, the Cannizzaro reaction (**Figure 23a**) could take place during CO<sub>2</sub> electrolysis. In a Cannizzaro reaction, an aldehyde can disproportionate to the corresponding carboxylic acid and alcohol.<sup>317</sup> Through investigating the reduction of formaldehyde in various electrolytes, such as perchloric acid (HClO<sub>4</sub>), sodium perchlorate (NaClO<sub>4</sub>), and phosphate buffers, Koper and co-workers observed that the disproportionation reactions are strongly influenced by the electrolyte pH and buffering strength.<sup>317</sup> As OH<sup>-</sup> ions

are essential for the Cannizzaro reaction, HCOOH is easier to form in the HClO<sub>4</sub>-based electrolyte (pH = 3) than the one with pH = 1 (see **Figure 23b**). In phosphate electrolyte with a high buffering capacity and thereby a relatively low local pH, Cannizzaro reaction was significantly hindered, leading to a negligible formation of HCOOH.<sup>317</sup> Therefore, researchers should be careful in distinguishing the products such as acids and alcohols formed from the disproportionation reactions and those formed by direct CO<sub>2</sub>R, especially for the liquid products such as methanol and ethanol, where the corresponding aldehyde is often proposed as a reaction intermediate.<sup>318</sup> This is especially true since interrogation of the just produced products is hard to measure compared to the ones that further react and transport and are detected in the bulk solution or gas flows.

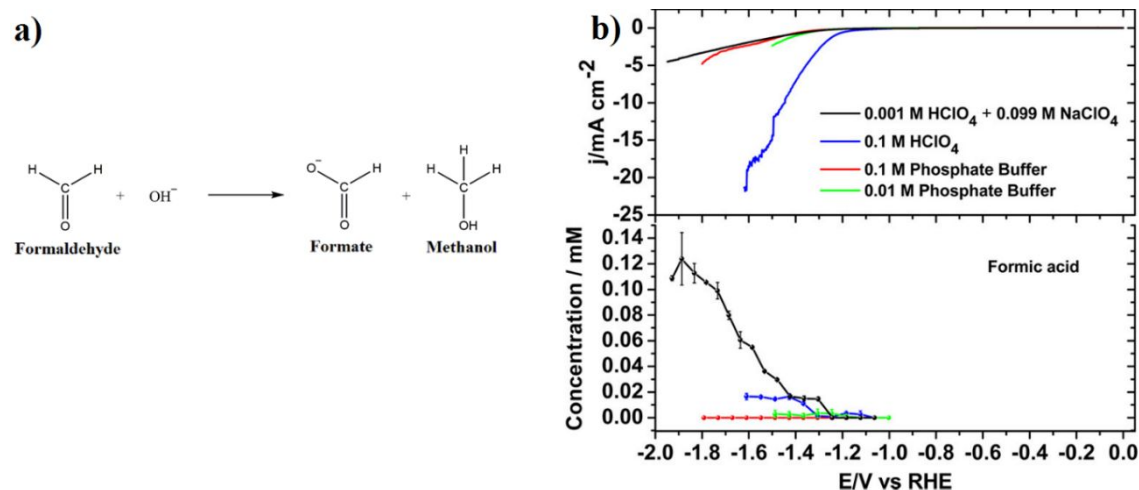


**Figure 23.** a) Cannizzaro disproportionation reactions showing formaldehyde disproportionate to formate and methanol, adapted from Birdja and Koper<sup>317</sup> (2017), b) Formic acid formation during reduction of formaldehyde in perchloric acid (pH: 1 and 3), 0.1 M phosphate buffer pH 6.6, and 0.01 M phosphate buffer pH 6.8. Scan rate: 1 mV s<sup>-1</sup>. Reprinted with permission from Birdja and Koper,<sup>317</sup> Copyright 2017, American Chemical Society.

Enhanced mass transport makes the value of local pH closer to the bulk pH, thus influencing the activity and selectivity of cathodic reactions.<sup>295, 319</sup> Through rotating a Cu cylinder electrode to enhance the mass transfer, Marshall and co-workers found that the CO<sub>2</sub>R activity decreased with the increasing rotation speed, along with a change in product preference from CH<sub>4</sub> to CO, while HER was promoted.<sup>319</sup> Such degradation of CO<sub>2</sub>R is attributed to the formation of graphitic carbon on electrode surface due to low local pH at higher rotation speed, resulting in the deactivation of the active sites for CO<sub>2</sub>R.<sup>319</sup> This evidence is also supported by Mul and co-workers, who presented a pH-dependent pathway for the deactivation of Cu electrode due to carbon formation.<sup>288</sup> In addition, the change in product selectivity from CH<sub>4</sub> to CO at higher

rotation speed could be due to lower coverage of adsorbed \*CO, which is a precursor for CH<sub>4</sub> formation.<sup>319</sup>

## 7 Pressure and temperature effects

### 7.1 Pressure

The partial pressure of CO<sub>2</sub> in the gas fed to the electrolyzer directly impacts the rate of CO<sub>2</sub> mass transfer to the electrode surface due to CO<sub>2</sub>-solvent solubility relationship. For example, at a given temperature CO<sub>2</sub> solubility in aqueous electrolytes and physical organic solvents typically increases linearly with pressure according to Henry's law.<sup>320</sup> Other solvent-electrolytes like amines<sup>321</sup> and ILs<sup>322</sup> exhibit non-linear CO<sub>2</sub> solubility relationships that may reach a plateau at a critical pressure (e.g. around 10 MPa for imidazolium-based ionic liquids<sup>322</sup> and ~ 1 MPa for amines<sup>323</sup>) beyond which further increase of pressure does not improve solubility. Raising the operating pressure increases complexity and cost of electrolyzer construction and operation, so optimization of the pressure must consider costs and the effect of pressure on CO<sub>2</sub>R selectivity.

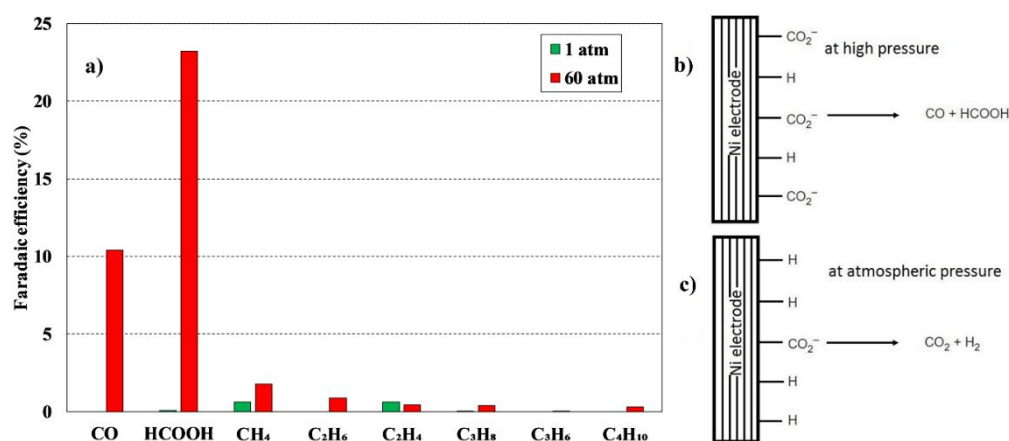
A large number of studies report the effects of pressure on product selectivity and FE of CO<sub>2</sub>R processes.<sup>67, 108, 109, 159, 210, 212, 288, 324-330</sup> Hara et al.<sup>330</sup> reported that on a Cu wire (0.16 cm<sup>2</sup>) in 0.1 M KHCO<sub>3</sub> the CO<sub>2</sub>R products shifted from H<sub>2</sub> at 1 atm to hydrocarbons then to CO and/or HCOOH as the pressure was increased to 30 atm, with PCD<sub>CO</sub> up to 523 mA cm<sup>-2</sup> observed. **Table 6** summarizes a typical example reported by Hori et al.<sup>210</sup> of the effect of CO<sub>2</sub> pressure on product selectivity over different metal electrodes. Hori et al. observed that over group B catalysts, which include Fischer-Tropsch catalysts like Ni, Co and Fe, product selectivity shifted from H<sub>2</sub> at ambient pressures to HCOOH and CO at high pressure.<sup>210</sup> Kudo et al.<sup>331</sup> reported similar shifts from H<sub>2</sub> at low pressures to CO, HCOOH, and hydrocarbons at 60 atm over Ni catalysts as shown in **Figure 24a**. They observed that the hydrocarbons from CO<sub>2</sub>R over Ni followed a Schultz-Flory probability distribution like that obtained by the Fischer-Tropsch reaction, and proposed that like the conventional Fischer-Tropsch process electrochemical CO<sub>2</sub>R at high pressures may involve hydrogenation of metal carbonyl intermediates to facilitate production of carbene groups (-CH<sub>2</sub>-) that polymerize to longer-chain hydrocarbons. In addition, high CO<sub>2</sub> pressure increases the surface coverage of CO<sub>2</sub>R intermediates on the electrode surface, which promotes CO<sub>2</sub>R and suppresses HER as illustrated in **Figure 24b** and **Figure 24c**.<sup>210, 331</sup>

For group C catalysts like Ag and Sn, Hara et al.<sup>210</sup> did not report a major shift in the type of CO<sub>2</sub>R products at higher pressure but the FE towards CO and HCOOH did increase (relative to H<sub>2</sub>), and this was attributed to increased CO<sub>2</sub> solubility at higher pressures. Over Cu catalysts (group D), Hara et al.<sup>210</sup> reported a shift from hydrocarbon production at 1 atm to CO and HCOOH at 30 atm. Jesús-Cardona et al.<sup>326</sup> proposed that at concentrations of CO<sub>2</sub> in the electrolyte at elevated pressure, CO<sub>2</sub> molecules displace may displace at the electrode's surface some of the CO\* that are a key intermediate in the CO<sub>2</sub>R to hydrocarbon pathway.

High-pressure CO<sub>2</sub>R requires balancing the pressure in the anode and cathode chambers to prevent damage to the separator.<sup>98, 212, 262</sup> Ramdin et al.<sup>98</sup> compared the effects of BPM and CEM on CO<sub>2</sub>R to formic acid/formate at high CO<sub>2</sub> pressure, and after the experiment observed delamination of BPM layers. Note that even in electrolyzer operating at near ambient pressures there can be a pressure imbalance across the separator, especially in CO<sub>2</sub>R processes where the anode produces O<sub>2</sub> and the cathode reduces CO<sub>2</sub> to liquid products. This pressure imbalance can deform the separator, so to improve mechanical strength thicker membranes, fabric-reinforced membranes, or additional porous substrates may be require. These approaches may improve strength and durability, but also increase the resistances across the separator.<sup>332</sup>

**Table 6. Effect of pressure on the product distribution of different metal electrodes in an electrochemical CO<sub>2</sub>R process, data was taken from Hara et al.<sup>210</sup> (1995).**

Group	Cathode catalyst	Effect of Pressure	
		Major products at 1 atm	Major products at 30 atm
A	Ti, Nb, Ta, Mo, Mn, and Al	H <sub>2</sub>	H <sub>2</sub>
B	Zr, Cr, W, Fe, Co, Rh, Ir, Ni, Pd, Pt, C and Si	H <sub>2</sub>	CO and HCOOH
C	Ag, Au, Zn, In, Sn, Pb, and Bi	CO and HCOOH	CO and HCOOH
D	Cu	CH <sub>4</sub> and C <sub>2</sub> H <sub>6</sub>	CO and HCOOH

**Figure 24. Electrochemical reduction of CO<sub>2</sub> on Ni electrodes, a) effect of pressure on the FE of various products; reaction mechanism b) at high pressure (60 atm), and c) at atmospheric pressure. Adapted with permission from Kudo et al.<sup>331</sup> Copyright 1993, The Electrochemical Society.**

## 7.2 Temperature

Temperature effects CO<sub>2</sub>R electrolyzer performance because of both CO<sub>2</sub> solubility (i.e. the Van't Hoff equation)<sup>333, 334</sup> and minimum half-cell potentials are temperature dependent, and temperature influences CO<sub>2</sub>R kinetics because of its effect on mass transfer rates, reaction pathways, viscosity and conductivity of electrolytes, and the conductivity of IEM separators. The stability of cell components like membranes, electrodes, and gaskets may also be effected by temperature extremes or by temperature cycles. The range of temperatures reported for electrochemical CO<sub>2</sub>R processes is commonly between 20 - 40°C, although a few studies have explored CO<sub>2</sub>R at temperatures as low as 0°C<sup>209</sup> and up to 125°C.<sup>54</sup> Within this operating range

the temperature dependency of electrical conductivity of cell components like current collectors is unlikely to have a significant effect on CO<sub>2</sub>R electrolyzer performance.

The main CO<sub>2</sub>R reactions and the HER have a positive entropy change so that lower overall thermodynamic cell voltages are required for reactions at higher temperatures. Additionally, lower activation overpotentials are required at higher temperatures than lower temperatures to drive a sufficient overall CO<sub>2</sub>R rate, which can be quantitatively determined through the Butler-Volmer equation.<sup>335</sup> The effect of temperature on overpotential appears to be more significant than the effect on thermodynamic potentials. For example, Dufek et al. reported a significant reduction of cathode potentials from  $-2.19$  V to  $-1.87$  V to achieve  $70$  mA cm<sup>-2</sup> over an Ag-based GDEs when operating temperature was elevated from  $18$  to  $70$  °C, while less than  $0.1$  V decrement in thermodynamic voltage was observed when the temperature was increased from  $25$  to  $125$  °C.<sup>54</sup> Ryu et al.<sup>336</sup> reported a similar trend for CO<sub>2</sub>R over Hg electrodes.

Temperature has a significant effect on hydrodynamic properties (viscosity and density) and concentration gradients (due to solubility relationships) that control rates of CO<sub>2</sub> mass transfer. For example, faster CO<sub>2</sub> mass transfer coefficients from the gas to electrolyte is observed at higher temperatures because diffusivity of CO<sub>2</sub> in gas and liquid phases increases, and the viscosity of the catholyte decreases.<sup>337, 338</sup> But, a reduced solubility at higher temperatures lowers the overall driving force for the mass-transport across the gas/liquid interface. The relative changes in solubility with temperature for CO<sub>2</sub> compared to CO<sub>2</sub>R products such as CH<sub>4</sub> and C<sub>2</sub>H<sub>4</sub> that are sparingly soluble in the catholyte,<sup>339, 340</sup> could be advantageous to promote quick desorption of products from the electrode surface. However, proton transfer rates may also increase at high temperatures and so increasing temperature can potentially promote HER at the cathode.

The enhanced diffusivity and thinner static laminar layer at the electrode exhibited at higher temperatures reduces ohmic resistances in the electrolyte. In GDEs, temperature can also change the phase-change induced flow and result in drier CLs.<sup>189</sup> However, increased temperature means higher water entering into the electrolyzer at same relative humidity and so that can help get to higher CDs, especially if the system is water limited.<sup>189</sup>

Temperature is known to affect the product distribution of the CO<sub>2</sub>R reaction over different catalysts.<sup>341-344</sup> For example, Hori et al.<sup>209</sup> reported a decrease of FE<sub>CH<sub>4</sub></sub> and increase of FE<sub>C<sub>2</sub>H<sub>4</sub></sub> over Cu foil at  $5$  mA cm<sup>-2</sup> when the temperature was raised from  $0$  to  $40$  °C. Ahn et al.<sup>343</sup>

reported a similar trend when increasing the temperature from 2 to 22 °C. A close proximity of \*CO intermediates is important for the formation of C-C bond, meaning that a high \*CO coverage should make it easier for the C<sub>2</sub>H<sub>4</sub> evolution. However, the reported suppression of C<sub>2</sub>H<sub>4</sub> at high temperature, where the coverage of \*CO is low, suggests that \*CO coverage may not play a dominating role at least within the studied range. Alternatively, several recent theoretical studies proposed that \*COH and \*CHO intermediates are crucial to determine whether the product is CH<sub>4</sub> or C<sub>2</sub>H<sub>4</sub>, respectively with a Cu electrode.<sup>318, 345, 346</sup> According to the work reported by Luo et al.,<sup>346</sup> the availability of adsorbed protons is essential to form \*CHO, while the adsorbed H<sub>2</sub>O is important to serve as a shuttle (H<sub>3</sub>O<sup>δ+</sup>) to transfer the proton to the \*CO intermediate to form \*COH. Therefore, one possible explanation of the reported temperature effect is that low temperature can stabilize the formation of (H<sub>3</sub>O<sup>δ+</sup>) proton shuttle, making it easier to form \*COH intermediate, thus facilitating the production of CH<sub>4</sub>. On the other hand, higher temperatures increase the availability of adsorbed protons at the electrode surface, resulting in an easier formation of \*CHO intermediates that promote C<sub>2</sub>H<sub>4</sub>. Moreover, the adsorbed protons could also partially contribute towards promoting HER. When temperature further increased from 22 °C, a degraded FE(C<sub>2</sub>H<sub>4</sub>) over Cu electrode was observed by Ahn et al.<sup>343</sup> This suggests that the aforementioned coverage of \*CO starts to dominate instead of the coverage of adsorbed protons.<sup>343</sup> Interestingly, potential vs RHE showed an opposite trend when comparing the temperature-effect results reported by Hori et al. and Ahn et al. Nevertheless, both studies report similar observations towards FE of CH<sub>4</sub> and C<sub>2</sub>H<sub>4</sub>, suggesting that the potential effect as imparted by the temperature change on the product distribution could be negligible in the studied temperature range.

Considering the effects of the potential on the reactivity and selectivity as mentioned, we recommend the design of experiment to keep the potential vs RHE constant when investigating temperature effects, as this potential is corrected by both temperature and pH. Overall, the temperature has significant impacts on the surface coverage of CO<sub>2</sub>R-related species (\*COOH and \*CO) through affecting their mass-transfer characteristics (e.g. solubility), as well as the coverage of proton-related adsorbates (e.g. H\* and H<sub>3</sub>O<sup>δ+</sup>) that also are important for the formation of key intermediates (e.g. \*CHO and \*COH). Such effects likely contribute the observed temperature-dependent CO<sub>2</sub>R selectivity.

A small increase in temperature can lower the ohmic resistance of the separator.<sup>94, 347</sup> However, too high of a temperature degrades the ionic conductivity and mechanical structure of the membranes. Taking perfluorosulfonic acid (PFSA) polymer-based membrane as an example,



its clusters of the hydrophilic sulfonic-acid group uptake sufficient water and allow protons to move easily in the membrane. In a fuel-cell configuration, a too high temperature ( $> 90\text{ }^{\circ}\text{C}$ ) lowers the water content in the membrane, leading to a decreased ionic conductivity.<sup>348</sup> Common AEMs, such as quaternary ammonia polysulfone, limit the operation to a much lower temperature than CEMs due to chemical stability concerns.<sup>349</sup> The Sustainion® membrane, developed by Dioxide Materials, has an improved ionic conductivity ( $\sim 140\text{ mS cm}^{-1}$  in 1 M KOH aqueous solution at  $80^{\circ}\text{C}$ ) and can stably be operated at temperature up to  $80^{\circ}\text{C}$ .<sup>347</sup> Ceramic based separators such as  $\text{ZrO}_2$  diaphragm can withstand higher operating temperature, but again they also pose other key risks such as product cross-over that lose conversion efficiency of the cells.

## 8 Summary and outlook

We have examined in this review the impact of design and operating decision related to electrolyzer configurations, electrode structure, electrolyte selection, pH, pressure, and temperature affect the reaction conditions at catalyst sites in a  $\text{CO}_2\text{R}$  electrolyzer, and thus impact on the overall efficiency of the process. The key challenges for low cost  $\text{CO}_2\text{R}$  that can be addressed by these factors together with catalyst materials are reducing the required cell voltages, improving selectivity, and lowering product separation costs.

The most promising  $\text{CO}_2\text{R}$  electrolyzers under development are based on designs and understanding translated from polymer electrolyte fuel-cells. Of the types of continuous  $\text{CO}_2\text{R}$  electrolyzers under development, vapor-fed electrolyzers may be the most promising for the large-scale  $\text{CO}_2\text{R}$  processes because this configuration provides opportunity to feed wet  $\text{CO}_2$ -rich flue gas directly to the electrolyzer without  $\text{CO}_2$  capture process units.<sup>350</sup> This technology if coupled with renewable electricity generation could also provide opportunities for passive  $\text{CO}_2$  capture from the atmosphere.<sup>351</sup> Vapor-fed electrolyzers may also reduce risks of catalyst poisoning from trace impurities in liquid electrolytes. For large-area electrodes in industrial scale electrolyzers, achieving uniform current and voltage distribution throughout the electrode surface and managing pressure gradients at the gas-electrolyte interface are critical, thus further work is required to optimize the electrode and flow-field design. In this regard, advanced manufacturing technologies like 3D printing<sup>352</sup> combined with computational modelling may help to optimize electrode and electrolyzer geometries.

There are fundamental aspects of electrolyte interactions in CO<sub>2</sub>R processes that are not fully understood. For example, although the charge carrying capacity of electrolytes is the primary function, researchers have discovered that electrolyte cations contribute in other ways to effect to the availability of protons and to stabilize CO<sub>2</sub>R intermediates. Likewise, electrolyte anions can provide local pH buffering effects due to specific adsorption of anions at the cathode surface. Low CO<sub>2</sub> solubility and competitive HER remain major challenges in inorganic salts-based aqueous electrolytes. Other new solvent-electrolytes such as ionic liquids and deep eutectic solvents may become more attractive if their cost reduces in the future, but to be effective CO<sub>2</sub>R electrolytes the viscosity of these solvents will also need to be managed, for example by mixing with a co-solvent such as water.

While our review has focused on electrochemical CO<sub>2</sub>R at the cathode, we acknowledge that the anode catalyst is also critical and especially because the state-of-the-art Ru and Ir based anode materials are a major contributor to the cost of electrochemical CO<sub>2</sub>R. Therefore, any advances in anode technologies achieved in other applications such as the oxygen evolution reaction in water splitting should help inform development of electrochemical CO<sub>2</sub>R processes. Water purification from treating wastewater through anodic oxidation of organic pollutants could be another approach to be considered for coupling with CO<sub>2</sub>R.<sup>353</sup> Moreover, since the oxidation potential of chloride is similar to that of water, producing chlorine at anode<sup>354, 355</sup> (similar to chlor-alkali cells) without the expense of extra energy could be beneficial for optimizing the overall process.

A final consideration in research needs for CO<sub>2</sub>R relates to experimental methods used to test novel catalysts and electrolytes. Most laboratory studies still use H-type batch setups<sup>40</sup> in which the solubility of CO<sub>2</sub> in electrolyte and gas-liquid mass transfer limits can control the overall rate of CO<sub>2</sub>R reactions, plus the transport of ions across separators in H-type cells can limit applicability of long term stability tests. Lab scale continuous flow-cell electrolyzers offer opportunities to detect minor CO<sub>2</sub>R products<sup>99</sup> and to better control reaction conditions than in H-cells. The cost of flow-cell apparatus is no longer significantly higher than a batch cells, so we expect the trend in reporting continuous CO<sub>2</sub>R measurements in catalyst studies may become more common. Clark et al.<sup>200</sup> have also highlighted the urgent need for standardized protocols, such as those developed for battery testing and fuel cell performance, to benchmark performance of catalyst and electrolyzers for electrochemical CO<sub>2</sub>.

## Acknowledgement

This work was supported by the HBIS Group, China, and Australian Research Council (ARC) Linkage Project No. LP160101729. S. Garg received scholarship support from the University of Queensland Graduate School and the HBIS-UQ Innovation Centre for Sustainable Steel. A.Z. Weber acknowledges support for his effort on this review from the Joint Center for Artificial Photosynthesis, a DOE Energy Innovation Hub, supported through the Office of Science of the U.S. Department of Energy under Award No. DE-SC0004993.

## References

1. H. Naims, *Environ. Sci. Pollut. Res.*, 2016, **23**, 22226-22241.
2. C. Global, *Journal*, 2015.
3. M. M. Halmann, *Chemical Fixation of Carbon Dioxide Methods for Recycling CO<sub>2</sub> into Useful Products*, CRC press, 1993.
4. A. Al-Mamoori, A. Krishnamurthy, A. A. Rowanaghi and F. Rezaei, *Energy Technol.*, 2017, **5**, 834-849.
5. S. Chu and A. Majumdar, *Nature*, 2012, **488**, 294.
6. E. V. Kondratenko, G. Mul, J. Baltrusaitis, G. O. Larrazabal and J. Perez-Ramirez, *Energy Environ. Sci.*, 2013, **6**, 3112-3135.
7. H.-R. M. Jhong, S. Ma and P. J. A. Kenis, *Curr. Opin. Chem. Eng.*, 2013, **2**, 191-199.
8. A. S. Agarwal, Y. Zhai, D. Hill and N. Sridhar, *ChemSusChem*, 2011, **4**, 1301-1310.
9. O. S. Bushuyev, P. De Luna, C. T. Dinh, L. Tao, G. Saur, J. van de Lagemaat, S. O. Kelley and E. H. Sargent, *Joule*, 2018, **2**, 825-832.
10. D. R. Kauffman, J. Thakkar, R. Siva, C. Matranga, P. R. Ohodnicki, C. Zeng and R. Jin, *ACS Appl. Mater. Interfaces*, 2015, **7**, 15626-15632.
11. R. J. Lim, M. Xie, M. A. Sk, J.-M. Lee, A. Fisher, X. Wang and K. H. Lim, *Catal. Today*, 2014, **233**, 169-180.
12. N. Pardo and J. A. Moya, *Energy*, 2013, **54**, 113-128.
13. Opus-12, We have developed a device that recycles CO<sub>2</sub> into chemicals and fuels., <https://www.opus-12.com/technology/>.
14. C. E. R. Toronto, Technology, <https://co2cert.com/technology/>.
15. Evonik, Evonik and siemens to generate high-value specialty chemicals from carbon dioxide and eco-electricity, <https://corporate.evonik.com/en/media/search/pages/news-details.aspx?NewsId=72457>.
16. M. E. Alternatives, 2015.
17. E. Alper and O. Yuksel Orhan, *Petroleum*, 2017, **3**, 109-126.
18. Y. Hori, H. Konishi, T. Futamura, A. Murata, O. Koga, H. Sakurai and K. Oguma, *Electrochim. Acta*, 2005, **50**, 5354-5369.
19. A. Wuttig and Y. Surendranath, *ACS Catal.*, 2015, **5**, 4479-4484.
20. B. Jermann and J. Augustynski, *Electrochim. Acta*, 1994, **39**, 1891-1896.
21. G. Nogami, H. Itagaki and R. Shiratsuchi, *J. Electrochem. Soc.*, 1994, **141**, 1138-1142.
22. J. Yano, T. Morita, K. Shimano, Y. Nagami and S. Yamasaki, *J. Solid State Electrochem.*, 2007, **11**, 554-557.
23. J. Yano and S. Yamasaki, *J. Appl. Electrochem.*, 2008, **38**, 1721.
24. P. Kedzierzawski and J. Augustynski, *J. Electrochem. Soc.*, 1994, **141**, L58-L60.
25. B. Kumar, J. P. Brian, V. Atla, S. Kumari, K. A. Bertram, R. T. White and J. M. Spurgeon, *ACS Catal.*, 2016, **6**, 4739-4745.
26. L. M. Chiacchiarelli, Y. Zhai, G. S. Frankel, A. S. Agarwal and N. Sridhar, *J. Appl. Electrochem.*, 2012, **42**, 21-29.
27. J. Qiao, Y. Liu, F. Hong and J. Zhang, *Chem. Soc. Rev.*, 2014, **43**, 631-675.
28. D. Voiry, H. S. Shin, K. P. Loh and M. Chhowalla, *Nat. Rev. Chem.*, 2018, **2**, 0105.
29. Z. D. Dong, L. J. Long and Q. S. Zhang, *Adv. Mater. (Weinheim, Ger.)*, 2016, **28**, 3423-3452.
30. F. Li, D. R. MacFarlane and J. Zhang, *Nanoscale*, 2018, **10**, 6235-6260.
31. W. Yang, K. Dastafkan, C. Jia and C. Zhao, *Adv. Mater. Technol.*, 2018, **0**, 1700377.
32. Z. Sun, T. Ma, H. Tao, Q. Fan and B. Han, *Chem*, 2017, **3**, 560-587.
33. R. Francke, B. Schille and M. Roemelt, *Chem. Rev. (Washington, DC, U. S.)*, 2018, DOI: 10.1021/acs.chemrev.7b00459.
34. T. Ziqi, P. Chad and C. Liang, *Adv. Theory Simul.*, 2018, **1**, 1800004.
35. C. W. Lee, K. D. Yang, D. H. Nam, J. H. Jang, N. H. Cho, S. W. Im and K. T. Nam, *Adv. Mater. (Weinheim, Ger.)*, 2018, **0**, 1704717.
36. K. A. Grice, *Coord. Chem. Rev.*, 2017, **336**, 78-95.
37. E. E. Benson, C. P. Kubiak, A. J. Sathrum and J. M. Smieja, *Chem. Soc. Rev.*, 2009, **38**, 89-99.
38. N. Kornienko, Y. Zhao, C. S. Kley, C. Zhu, D. Kim, S. Lin, C. J. Chang, O. M. Yaghi and P. Yang, *J. Am. Chem. Soc.*, 2015, **137**, 14129-14135.
39. D. M. Weekes, D. A. Salvatore, A. Reyes, A. Huang and C. P. Berlinguette, *Acc. Chem. Res.*, 2018, **51**, 910-918.
40. B. Endrődi, G. Bencsik, F. Darvas, R. Jones, K. Rajeshwar and C. Janáky, *Progr. Energy Combust. Sci.*, 2017, **62**, 133-154.
41. B. Manuela, F. Jonathan, M. H. A. and V. Francesco, *Energy Technol.*, 2015, **3**, 197-210.
42. S. Ma, J. Liu, K. Sasaki, S. M. Lyth and P. J. A. Kenis, *Energy Technol.*, 2017, **5**, 861-863.
43. R. B. Kutz, Q. Chen, H. Yang, S. D. Sajjad, Z. Liu and I. R. Masel, *Energy Technology*, 2017, **5**, 929-936.
44. D. Materials, CO<sub>2</sub> Electrolyzers, <https://dioxidematerials.com/technology/co2-electrolysis/>.
45. C.-T. Dinh, T. Burdyny, M. G. Kibria, A. Seifitokaldani, C. M. Gabardo, F. P. Garcia de Arquer, A. Kiani, J. P. Edwards, P. De Luna, O. S. Bushuyev, C. Zou, R. Quintero-Bermudez, Y. Pang, D. Sinton and E. H. Sargent, *Science*, 2018, **360**, 783-787.
46. Skyre, Products: CO2RENEW™, <https://www.skyre-inc.com/products/co2renew/>.
47. T. Haas, R. Krause, R. Weber, M. Demler and G. Schmid, *Nat. Catal.*, 2018, **1**, 32-39.

48. J. Qiao, Y. Liu and J. Zhang, *Electrochemical Reduction of Carbon Dioxide: Fundamentals and Technologies*, CRC Press, Boca Raton, 2016.
49. A. J. Bard and L. R. Faulkner, *Electrochemical methods: fundamentals and applications*, Wiley, 1980.
50. K. Scott, in *Sustainable and Green Electrochemical Science and Technology*, 2017, DOI: 10.1002/9781118698075.ch2, pp. 27-85.
51. M. S. Faber, R. Dziedzic, M. A. Lukowski, N. S. Kaiser, Q. Ding and S. Jin, *J. Am. Chem. Soc.*, 2014, **136**, 10053-10061.
52. K. Zeng and D. Zhang, *Progr. Energy Combust. Sci.*, 2010, **36**, 307-326.
53. T. Burdyny and W. A. Smith, *Energy Environ. Sci.*, 2019, **12**, 1442-1453.
54. E. J. Dufek, T. E. Lister and M. E. McIlwain, *J. Appl. Electrochem.*, 2011, **41**, 623-631.
55. H. Hashiba, L.-C. Weng, Y. Chen, H. K. Sato, S. Yotsuhashi, C. Xiang and A. Z. Weber, *J. Phys. Chem. C*, 2018, **122**, 3719-3726.
56. N. Gupta, M. Gattrell and B. MacDougall, *J. Appl. Electrochem.*, 2006, **36**, 161-172.
57. P. Lobaccaro, M. R. Singh, E. L. Clark, Y. Kwon, A. T. Bell and J. W. Ager, *Phys. Chem. Chem. Phys.*, 2016, **18**, 26777-26785.
58. L.-C. Weng, A. T. Bell and A. Z. Weber, *Phys. Chem. Chem. Phys.*, 2018, **20**, 16973-16984.
59. D. Wakerley, S. Lamaison, F. Ozanam, N. Menguy, D. Mercier, P. Marcus, M. Fontecave and V. Mougél, *Nat. Mater.*, 2019, DOI: 10.1038/s41563-019-0445-x.
60. L. D. Chen, M. Urushihara, K. Chan and J. K. Nørskov, *ACS Catal.*, 2016, **6**, 7133-7139.
61. R. B. Sandberg, J. H. Montoya, K. Chan and J. K. Nørskov, *Surf. Sci.*, 2016, **654**, 56-62.
62. M. R. Singh, Y. Kwon, Y. Lum, J. W. Ager and A. T. Bell, *J. Am. Chem. Soc.*, 2016, **138**, 13006-13012.
63. J. Resasco, L. D. Chen, E. Clark, C. Tsai, C. Hahn, T. F. Jaramillo, K. Chan and A. T. Bell, *J. Am. Chem. Soc.*, 2017, **139**, 11277-11287.
64. A. S. Varela, W. Ju, T. Reier and P. Strasser, *ACS Catal.*, 2016, **6**, 2136-2144.
65. M. S. Xie, B. Y. Xia, Y. Li, Y. Yan, Y. Yang, Q. Sun, S. H. Chan, A. Fisher and X. Wang, *Energy Environ. Sci.*, 2016, **9**, 1687-1695.
66. D. Gao, F. Scholten and B. Roldan Cuenya, *ACS Catal.*, 2017, **7**, 5112-5120.
67. M. R. Singh, J. D. Goodpaster, A. Z. Weber, M. Head-Gordon and A. T. Bell, *Proc. Natl. Acad. Sci.*, 2017, **114**, E8812-E8821.
68. C. S. Chen, A. D. Handoko, J. H. Wan, L. Ma, D. Ren and B. S. Yeo, *Catal. Sci. Technol.*, 2015, **5**, 161-168.
69. D. T. Whipple and P. J. A. Kenis, *J. Phys. Chem. Lett.*, 2010, **1**, 3451-3458.
70. C. Delacourt, P. L. Ridgway and J. Newman, *J. Electrochem. Soc.*, 2010, **157**, B1902-B1910.
71. Y. C. Li, D. Zhou, Z. Yan, R. H. Gonçalves, D. A. Salvatore, C. P. Berlinguette and T. E. Mallouk, *ACS Energy Lett.*, 2016, **1**, 1149-1153.
72. M. R. Singh, K. Papadantonakis, C. Xiang and N. S. Lewis, *Energy Environ. Sci.*, 2015, **8**, 2760-2767.
73. C. Xiang, K. M. Papadantonakis and N. S. Lewis, *Mater. Horiz.*, 2016, **3**, 169-173.
74. X. Li and I. Sabir, *Int. J. Hydrogen Energy*, 2005, **30**, 359-371.
75. J. Wang and H. Wang, *Fuel Cells*, 2012, **12**, 989-1003.
76. P. J. Hamilton and B. G. Pollet, *Fuel Cells*, 2010, **10**, 489-509.
77. D. M. F. Santos, C. A. C. Sequeira and J. L. Figueiredo, *Quim. Nova*, 2013, **36**, 1176-1193.
78. F. Harnisch, U. Schröder and F. Scholz, *Environ. Sci. Technol.*, 2008, **42**, 1740-1746.
79. N. M. Vargas-Barbosa, G. M. Geise, M. A. Hickner and T. E. Mallouk, *ChemSusChem*, 2014, **7**, 3017-3020.
80. M. B. McDonald, J. P. Bruce, K. McEleney and M. S. Freund, *ChemSusChem*, 2015, **8**, 2645-2654.
81. J. Luo, D. A. Vermaas, D. Bi, A. Hagfeldt, W. A. Smith and M. Grätzel, *Adv. Energy Mater.*, 2016, **6**, 1600100.
82. M. B. McDonald, S. Ardo, N. S. Lewis and M. S. Freund, *ChemSusChem*, 2014, **7**, 3021-3027.
83. R. S. Reiter, W. White and S. Ardo, *J. Electrochem. Soc.*, 2016, **163**, H3132-H3134.
84. A. Kusoglu and A. Z. Weber, *Chem. Rev. (Washington, DC, U. S.)*, 2017, **117**, 987-1104.
85. J. J. Kaczur, H. Yang, Z. Liu, S. D. Sajjad and R. I. Masel, *Front. Chem.*, 2018, **6**.
86. T. Luo, S. Abdu and M. Wessling, *J. Membr. Sci.*, 2018, **555**, 429-454.
87. K. F. L. Hagesteijn, S. Jiang and B. P. Ladewig, *J. Mater. Sci.*, 2018, **53**, 11131-11150.
88. D. Y. Leung and J. Xuan, *Micro & nano-engineering of fuel cells*, Crc Press, 2015.
89. D. W. Dewulf and A. J. Bard, *Catal. Lett.*, 1988, **1**, 73-79.
90. C. Delacourt, P. L. Ridgway, J. B. Kerr and J. Newman, *J. Electrochem. Soc.*, 2008, **155**, B42-B49.
91. Y. Hori, H. Ito, K. Okano, K. Nagasu and S. Sato, *Electrochim. Acta*, 2003, **48**, 2651-2657.
92. N. Ziv and D. R. Dekel, *Electrochem. Commun.*, 2018, **88**, 109-113.
93. J. R. Varcoe, P. Atanassov, D. R. Dekel, A. M. Herring, M. A. Hickner, P. A. Kohl, A. R. Kucernak, W. E. Mustain, K. Nijmeijer, K. Scott, T. Xu and L. Zhuang, *Energy Environ. Sci.*, 2014, **7**, 3135-3191.
94. K. N. Grew, X. Ren and D. Chu, *Electrochem. Solid-State Lett.*, 2011, **14**, B127-B131.
95. Z. Sun, J. Pan, J. Guo and F. Yan, *Adv. Sci.*, 2018, **5**, 1800065.
96. J. Albo, A. Sáez, J. Solla-Gullón, V. Montiel and A. Irabien, *Appl. Catal. B*, 2015, **176**, 709-717.
97. M. Alvarez-Guerra, S. Quintanilla and A. Irabien, *Chem. Eng. J. (Lausanne)*, 2012, **207**, 278-284.
98. M. Ramdin, A. R. T. Morrison, M. de Groen, R. van Haperen, R. de Kler, L. J. P. van den Broeke, J. P. M. Trusler, W. de Jong and T. J. H. Vlught, *Ind. Eng. Chem. Res.*, 2019, **58**, 1834-1847.
99. K. P. Kuhl, E. R. Cave, D. N. Abram and T. F. Jaramillo, *Energy Environ. Sci.*, 2012, **5**, 7050-7059.
100. T. Hatsukade, K. P. Kuhl, E. R. Cave, D. N. Abram and T. F. Jaramillo, *Phys. Chem. Chem. Phys.*, 2014, **16**, 13814-13819.
101. J. T. Feaster, C. Shi, E. R. Cave, T. Hatsukade, D. N. Abram, K. P. Kuhl, C. Hahn, J. K. Nørskov and T. F. Jaramillo, *ACS Catal.*, 2017, **7**, 4822-4827.
102. E. R. Cave, J. H. Montoya, K. P. Kuhl, D. N. Abram, T. Hatsukade, C. Shi, C. Hahn, J. K. Nørskov and T. F. Jaramillo, *Phys. Chem. Chem. Phys.*, 2017, **19**, 15856-15863.
103. K. Manthiram, B. J. Beberwyck and A. P. Alivisatos, *J. Am. Chem. Soc.*, 2014, **136**, 13319-13325.
104. E. L. Clark, M. R. Singh, Y. Kwon and A. T. Bell, *Anal. Chem.*, 2015, **87**, 8013-8020.
105. J. Balster, D. F. Stamatialis and M. Wessling, *Chem. Eng. Process.*, 2004, **43**, 1115-1127.
106. J. Kamcev, R. Sujanani, E.-S. Jang, N. Yan, N. Moe, D. R. Paul and B. D. Freeman, *J. Membr. Sci.*, 2018, **547**, 123-133.
107. E. J. Dufek, T. E. Lister and M. E. McIlwain, *Electrochem. Solid-State Lett.*, 2012, **15**, B48-B50.
108. E. J. Dufek, T. E. Lister, S. G. Stone and M. E. McIlwain, *J. Electrochem. Soc.*, 2012, **159**, F514-F517.
109. K. Hara and T. Sakata, *Bull. Chem. Soc. Jpn.*, 1997, **70**, 571-576.
110. P. Jeanty, C. Scherer, E. Magori, K. Wiesner-Fleischer, O. Hinrichsen and M. Fleischer, *J. CO2 Util.*, 2018, **24**, 454-462.
111. D. Higgins, C. Hahn, C. Xiang, T. F. Jaramillo and A. Z. Weber, *ACS Energy Lett.*, 2019, **4**, 317-324.
112. W. Lee, Y. E. Kim, M. H. Youn, S. K. Jeong and K. T. Park, *Angew. Chem.*, 2018, **130**, 6999-7003.

113. I. Merino-Garcia, J. Albo and A. Irabien, *Nanotechnology*, 2017, **29**, 014001.
114. D. A. Salvatore, D. M. Weekes, J. He, K. E. Dettelbach, Y. C. Li, T. E. Mallouk and C. P. Berlinguette, *ACS Energy Lett.*, 2018, **3**, 149-154.
115. D. T. Whipple, E. C. Finke and P. J. A. Kenis, *Electrochem. Solid-State Lett.*, 2010, **13**, B109-B111.
116. R. S. Jayashree, S. K. Yoon, F. R. Brushett, P. O. Lopez-Montesinos, D. Natarajan, L. J. Markoski and P. J. A. Kenis, *J. Power Sources*, 2010, **195**, 3569-3578.
117. M. M. Morgan, L. Peter, L. Yanwei and W. A. Joel, *J. Phys. D: Appl. Phys.*, 2017, **50**, 154006.
118. V. Sumit, K. Byoungsu, J. H. R. "Molly", M. Sichao and K. P. J. A., *ChemSusChem*, 2016, **9**, 1972-1979.
119. J. Spurgeon and B. Kumar, *Energy Environ. Sci.*, 2018, DOI: 10.1039/C8EE00097B.
120. J. B. Greenblatt, D. J. Miller, J. W. Ager, F. A. Houle and I. D. Sharp, *Joule*, 2018, **2**, 381-420.
121. J. H. Lunsford, P. Qiu, M. P. Rosynek and Z. Yu, *J. Phys. Chem. B*, 1998, **102**, 167-173.
122. A. Elfasakhany, *Engineering Science and Technology, an International Journal*, 2015, **18**, 713-719.
123. P. Tian, Y. Wei, M. Ye and Z. Liu, *ACS Catal.*, 2015, **5**, 1922-1938.
124. S. Şahin, Ş. S. Bayazit, M. Bilgin and İ. İnci, *J. Chem. Eng. Data*, 2010, **55**, 1519-1522.
125. G. A. Olah, A. Goeppert and G. K. S. Prakash, *J. Org. Chem.*, 2009, **74**, 487-498.
126. H. S. Abdelkader, L. Touhami, B. M. Lakhdar, K. Abdellah, G. Toufik and B. B. Fouzi, presented in part at the International Conference on Environmental, Biomedical and Biotechnology Singapore, 2012.
127. H. Yang, J. J. Kaczur, S. D. Sajjad and R. I. Masel, *J. CO<sub>2</sub> Util.*, 2017, **20**, 208-217.
128. H. S. Jeon, S. Kunze, F. Scholten and B. Roldan Cuenya, *ACS Catal.*, 2018, **8**, 531-535.
129. C. W. Lee, J. S. Hong, K. D. Yang, K. Jin, J. H. Lee, H.-Y. Ahn, H. Seo, N.-E. Sung and K. T. Nam, *ACS Catal.*, 2018, **8**, 931-937.
130. F. Li, L. Chen, M. Xue, T. Williams, Y. Zhang, D. R. MacFarlane and J. Zhang, *Nano Energy*, 2017, **31**, 270-277.
131. Y. Hori, H. Wakebe, T. Tsukamoto and O. Koga, *Electrochim. Acta*, 1994, **39**, 1833-1839.
132. Q. Lu, J. Rosen, Y. Zhou, G. S. Hutchings, Y. C. Kimmel, J. G. Chen and F. Jiao, *Nat. Commun.*, 2014, **5**, 3242.
133. S. Liu, J. Xiao, X. F. Lu, J. Wang, X. Wang and X. W. Lou, *Angew. Chem. Int. Ed.*, 2019, **58**, 8499-8503.
134. M. Rahaman, A. Dutta, A. Zanetti and P. Broekmann, *ACS Catal.*, 2017, **7**, 7946-7956.
135. Q. Li, J. Fu, W. Zhu, Z. Chen, B. Shen, L. Wu, Z. Xi, T. Wang, G. Lu, J.-j. Zhu and S. Sun, *J. Am. Chem. Soc.*, 2017, **139**, 4290-4293.
136. L. Dai, Q. Qin, P. Wang, X. Zhao, C. Hu, P. Liu, R. Qin, M. Chen, D. Ou, C. Xu, S. Mo, B. Wu, G. Fu, P. Zhang and N. Zheng, *Sci. Adv.*, 2017, **3**.
137. P. Su, W. Xu, Y. Qiu, T. Zhang, X. Li and H. Zhang, *ChemSusChem*, 2018, **11**, 848-853.
138. H. Li and C. Oloman, *J. Appl. Electrochem.*, 2005, **35**, 955-965.
139. D. Kopljar, A. Inan, P. Vindayer, N. Wagner and E. Klemm, *J. Appl. Electrochem.*, 2014, **44**, 1107-1116.
140. Z. Bitar, A. Fecant, E. Trela-Baudot, S. Chardon-Noblat and D. Pasquier, *Appl. Catal. B*, 2016, **189**, 172-180.
141. M. Schwartz, R. L. Cook, V. M. Kehoe, R. C. MacDuff, J. Patel and A. F. Sammells, *J. Electrochem. Soc.*, 1993, **140**, 614-618.
142. M. N. Mahmood, D. Masheder and C. J. Harty, *J. Appl. Electrochem.*, 1987, **17**, 1159-1170.
143. G. K. S. Prakash, F. A. Viva and G. A. Olah, *J. Power Sources*, 2013, **223**, 68-73.
144. A. Del Castillo, M. Alvarez-Guerra, J. Solla-Gullón, A. Sáez, V. Montiel and A. Irabien, *J. CO<sub>2</sub> Util.*, 2017, **18**, 222-228.
145. M. H. Shojaeefard, G. R. Molaeimanesh, M. Nazemian and M. R. Moqaddari, *Int. J. Hydrogen Energy*, 2016, **41**, 20276-20293.
146. A. Z. Weber, R. L. Borup, R. M. Darling, P. K. Das, T. J. Dursch, W. Gu, D. Harvey, A. Kusoglu, S. Litster, M. M. Mench, R. Mukundan, J. P. Owejan, J. G. Pharoah, M. Secanell and I. V. Zenyuk, *J. Electrochem. Soc.*, 2014, **161**, F1254-F1299.
147. D. M. Fadzillah, M. I. Rosli, M. Z. M. Talib, S. K. Kamarudin and W. R. W. Daud, *Renewable Sustainable Energy Rev.*, 2017, **77**, 1001-1009.
148. J. Lai, A. Nsabimana, R. Luque and G. Xu, *Joule*, 2018, **2**, 76-93.
149. F. C. Walsh, L. F. Arenas and C. Ponce de León, *J. Chem. Technol. Biotechnol.*, 2018, **93**, 3073-3090.
150. F. Lux, *J. Mater. Sci.*, 1993, **28**, 285-301.
151. L. I. Chernyshev and V. V. Skorokhod, *Powder Metall. Met. Ceram.*, 2003, **42**, 88-93.
152. B. I. Shklovskii and A. L. Éfros, *Phys.-Usp.*, 1975, **18**, 845-862.
153. R. Lipton, *Proc. R. Soc. London, Ser. A*, 1998, **454**, 1371-1382.
154. Y. Lum, B. Yue, P. Lobaccaro, A. T. Bell and J. W. Ager, *J. Phys. Chem. C*, 2017, **121**, 14191-14203.
155. M. Ma, B. J. Trześniowski, J. Xie and W. A. Smith, *Angew. Chem. Int. Ed.*, 2016, **55**, 9748-9752.
156. H. Yano, F. Shirai, M. Nakayama and K. Ogura, *J. Electroanal. Chem.*, 2002, **519**, 93-100.
157. R. L. Cook, R. C. MacDuff and A. F. Sammells, *J. Electrochem. Soc.*, 1990, **137**, 607-608.
158. K. Hara and T. Sakata, *J. Electrochem. Soc.*, 1997, **144**, 539-545.
159. K. Hara, A. Kudo, T. Sakata and M. Watanabe, *J. Electrochem. Soc.*, 1995, **142**, L57-L59.
160. Q. Wang, H. Dong and H. Yu, *J. Power Sources*, 2014, **271**, 278-284.
161. S. Park, J.-W. Lee and B. N. Popov, *Int. J. Hydrogen Energy*, 2012, **37**, 5850-5865.
162. B. Kim, F. Hillman, M. Ariyoshi, S. Fujikawa and P. J. A. Kenis, *J. Power Sources*, 2016, **312**, 192-198.
163. A. Del Castillo, M. Alvarez-Guerra and A. Irabien, *AIChE J.*, 2014, **60**, 3557-3564.
164. S. Ikeda, T. Ito, K. Azuma, K. Ito and H. Noda, *Denki Kagaku*, 1995, **63**, 303-309.
165. J. Albo and A. Irabien, *J. Catal.*, 2016, **343**, 232-239.
166. B. C. Marepally, C. Ampelli, C. Genovese, T. Saboo, S. Perathoner, F. M. Visser, L. Veyre, J. Canivet, E. A. Quadrelli and G. Centi, *ChemSusChem*, 2017, **10**, 4442-4446.
167. E. Irtem, T. Andreu, A. Parra, M. D. Hernández-Alonso, S. García-Rodríguez, J. M. Riesco-García, G. Penelas-Pérez and J. R. Morante, *J. Mater. Chem. A*, 2016, **4**, 13582-13588.
168. Q. Wang, X. Wang, C. Wu, Y. Cheng, Q. Sun, H. Dong and H. Yu, *Sci. Rep.*, 2017, **7**, 13711.
169. Q. Wang, H. Dong, H. Yu and H. Yu, *J. Power Sources*, 2015, **279**, 1-5.
170. S. Guan, A. Agarwal, E. Rode, D. Hill and N. Sridhar, *Advances in Materials Science for Environmental and Energy Technologies II: Ceramic Transactions*, 2013, **241**, 231-243.
171. D. Masheder and K. P. J. Williams, *J. Raman Spectrosc.*, 1987, **18**, 387-390.
172. L. Cindrella, A. M. Kannan, J. F. Lin, K. Saminathan, Y. Ho, C. W. Lin and J. Wertz, *J. Power Sources*, 2009, **194**, 146-160.
173. J. Park, H. Oh, T. Ha, Y. I. Lee and K. Min, *Appl. Energy*, 2015, **155**, 866-880.
174. L. Han, W. Zhou and C. Xiang, *ACS Energy Lett.*, 2018, **3**, 855-860.
175. D. Kopljar, N. Wagner and E. Klemm, *Chem. Eng. Technol.*, 2016, **39**, 2042-2050.
176. Q. Wang, H. Dong and H. Yu, *RSC Adv.*, 2014, **4**, 59970-59976.

177. T. Van Nguyen, A. Aghosseini, X. Wang, V. Yarlagadda, A. Kwong, A. Z. Weber, P. Deevanhxay, S. Tsushima and S. Hirai, *J. Electrochem. Soc.*, 2015, **162**, F1451-F1460.
178. R. Omrani and B. Shabani, *Int. J. Hydrogen Energy*, 2017, **42**, 28515-28536.
179. J. Wu, F. G. Risalvato, S. Ma and X.-D. Zhou, *J. Mater. Chem. A*, 2014, **2**, 1647-1651.
180. A. Li, H. Wang, J. Han and L. Liu, *Front. Chem. Sci. Eng.*, 2012, **6**, 381-388.
181. T.-J. Park, S. Banerjee, T. Hemraj-Benny and S. S. Wong, *J. Mater. Chem.*, 2006, **16**, 141-154.
182. M. Pumera, A. Ambrosi and E. L. K. Chng, *Chem. Sci.*, 2012, **3**, 3347-3355.
183. C. M. Long, M. A. Nascarella and P. A. Valberg, *Environ. Pollut.*, 2013, **181**, 271-286.
184. A. Z. Weber and J. Newman, *J. Electrochem. Soc.*, 2005, **152**, A677-A688.
185. M. Prasanna, H. Y. Ha, E. A. Cho, S. A. Hong and I. H. Oh, *J. Power Sources*, 2004, **131**, 147-154.
186. EP2397578A2, 2016.
187. Y. Wang, J. Liu, Y. Wang, A. M. Al-Enizi and G. Zheng, *Small*, 2017, **13**, 1701809.
188. J. He, N. J. J. Johnson, A. Huang and C. P. Berlinguette, *ChemSusChem*, 2018, **11**, 48-57.
189. L.-C. Weng, A. T. Bell and A. Z. Weber, *Energy Environ. Sci.*, 2019, **12**, 1950-1968.
190. H. Mistry, F. Behafarid, R. Reske, A. S. Varela, P. Strasser and B. Roldan Cuenya, *ACS Catal.*, 2016, **6**, 1075-1080.
191. B. A. Rosen, A. Salehi-Khojin, M. R. Thorson, W. Zhu, D. T. Whipple, P. J. A. Kenis and R. I. Masel, *Science*, 2011, **334**, 643-644.
192. H. Yang, J. J. Kaczur, S. D. Sajjad and R. I. Masel, *ECS Trans.*, 2017, **77**, 1425-1431.
193. H. R. M. Jhong, F. R. Brushett and P. J. A. Kenis, *Adv. Energy Mater.*, 2013, **3**, 589-599.
194. K. Nakata, T. Ozaki, C. Terashima, A. Fujishima and Y. Einaga, *Angew. Chem.*, 2014, **126**, 890-893.
195. P. P. Sharma and X. D. Zhou, *Wiley Interdiscip. Rev.: Energy Environ.*, 2017, **6**, e239.
196. W. Plieth, in *Electrochemistry for Materials Science*, Elsevier, Amsterdam, 2008, DOI: <https://doi.org/10.1016/B978-044452792-9.50003-8>, pp. 1-26.
197. X. Lu, D. Y. C. Leung, H. Wang, M. K. H. Leung and J. Xuan, *ChemElectroChem*, 2014, **1**, 836-849.
198. J.-P. Jones, G. K. S. Prakash and G. A. Olah, *Isr. J. Chem.*, 2014, **54**, 1451-1466.
199. B. M. Setterfield-Price and R. A. W. Dryfe, *J. Electroanal. Chem.*, 2014, **730**, 48-58.
200. E. L. Clark, J. Resasco, A. Landers, J. Lin, L.-T. Chung, A. Walton, C. Hahn, T. F. Jaramillo and A. T. Bell, *ACS Catal.*, 2018, **8**, 6560-6570.
201. Á. Pérez-Salado Kamps, E. Meyer, B. Rumpf and G. Maurer, *J. Chem. Eng. Data*, 2007, **52**, 817-832.
202. Y. Liu, M. Hou, G. Yang and B. Han, *J. Supercrit. Fluids*, 2011, **56**, 125-129.
203. D. Tong, J. P. M. Trusler, G. C. Maitland, J. Gibbins and P. S. Fennell, *Int. J. Greenhouse Gas Control*, 2012, **6**, 37-47.
204. M. Wagner, I. von Harbou, J. Kim, I. Ermatchkova, G. Maurer and H. Hasse, *J. Chem. Eng. Data*, 2013, **58**, 883-895.
205. W. Lv, R. Zhang, P. Gao and L. Lei, *J. Power Sources*, 2014, **253**, 276-281.
206. W. Lv, J. Zhou, F. Kong, H. Fang and W. Wang, *Int. J. Hydrogen Energy*, 2016, **41**, 1585-1591.
207. F. Cai, D. Gao, H. Zhou, G. Wang, T. He, H. Gong, S. Miao, F. Yang, J. Wang and X. Bao, *Chem. Sci.*, 2017, **8**, 2569-2573.
208. A. L. Kohl, R. Nielsen and A. L. Kohl, *Gas purification*, Houston, Tex.: Gulf Pub., 5th ed., 1997.
209. H. Yoshio, K. Katsube, M. Akira and S. Shin, *Chem. Lett.*, 1986, **15**, 897-898.
210. K. Hara, A. Kudo and T. Sakata, *J. Electroanal. Chem.*, 1995, **391**, 141-147.
211. M. Jitaru, D. A. Lowy, M. Toma, B. C. Toma and L. Oniciu, *J. Appl. Electrochem.*, 1997, **27**, 875-889.
212. M. Todoroki, K. Hara, A. Kudo and T. Sakata, *J. Electroanal. Chem.*, 1995, **394**, 199-203.
213. D. Ren, Y. Deng, A. D. Handoko, C. S. Chen, S. Malkhandi and B. S. Yeo, *ACS Catal.*, 2015, **5**, 2814-2821.
214. D. Raciti, K. J. Livi and C. Wang, *Nano Lett.*, 2015, **15**, 6829-6835.
215. A. Bandi, M. Specht, T. Weimer and K. Schaber, *Energy Convers. Manage.*, 1995, **36**, 899-902.
216. M. Gattrell, N. Gupta and A. Co, *Energy Convers. Manage.*, 2007, **48**, 1255-1265.
217. S. Stucki, A. Schuler and M. Constantinescu, *Int. J. Hydrogen Energy*, 1995, **20**, 653-663.
218. K. Hara, A. Tsuneto, A. Kudo and T. Sakata, *J. Electroanal. Chem.*, 1997, **434**, 239-243.
219. P. Dubé and G. M. Brisard, *J. Electroanal. Chem.*, 2005, **582**, 230-240.
220. K. Ogura, *J. CO<sub>2</sub> Util.*, 2013, **1**, 43-49.
221. K. Ogura and M. D. Salazar-Villalpando, *JOM*, 2011, **63**, 35-38.
222. M. Ma, K. Djanashvili and W. A. Smith, *Angew. Chem. Int. Ed.*, 2016, **55**, 6680-6684.
223. M. Akira and H. Yoshio, *Bull. Chem. Soc. Jpn.*, 1991, **64**, 123-127.
224. M. R. Thorson, K. I. Siil and P. J. A. Kenis, *J. Electrochem. Soc.*, 2013, **160**, F69-F74.
225. S. Verma, X. Lu, S. Ma, R. I. Masel and P. J. A. Kenis, *Phys. Chem. Chem. Phys.*, 2016, **18**, 7075-7084.
226. W. Paik, T. N. Andersen and H. Eyring, *Electrochim. Acta*, 1969, **14**, 1217-1232.
227. H. Yoshio and S. Shin, *Bull. Chem. Soc. Jpn.*, 1982, **55**, 660-665.
228. S. Ringe, E. L. Clark, J. Resasco, A. Walton, B. Seger, A. T. Bell and K. Chan, *Energy Environ. Sci.*, 2019, DOI: 10.1039/C9EE01341E.
229. Y. Hori, in *Modern Aspects of Electrochemistry*, eds. C. G. Vayenas, R. E. White and M. E. Gamboa-Aldeco, Springer New York, New York, NY, 2008, DOI: 10.1007/978-0-387-49489-0\_3, pp. 89-189.
230. M. E. Essington, *Soil and water chemistry: an integrative approach*, CRC press, 2015.
231. A. N. Frumkin, *Trans. Faraday Soc.*, 1959, **55**, 156-167.
232. H. Kim, H. S. Park, Y. J. Hwang and B. K. Min, *J. Phys. Chem. C*, 2017, **121**, 22637-22643.
233. M. Liu, Y. Pang, B. Zhang, P. De Luna, O. Voznyy, J. Xu, X. Zheng, C. T. Dinh, F. Fan, C. Cao, F. P. G. de Arquer, T. S. Safaei, A. Mepham, A. Klinkova, E. Kumacheva, T. Filleter, D. Sinton, S. O. Kelley and E. H. Sargent, *Nature*, 2016, **537**, 382.
234. J. N. Mills, I. T. McCrum and M. J. Janik, *Phys. Chem. Chem. Phys.*, 2014, **16**, 13699-13707.
235. D. Strmcnik, K. Kodama, D. van der Vliet, J. Greeley, V. R. Stamenkovic and N. M. Marković, *Nature Chem.*, 2009, **1**, 466.
236. E. Pérez-Gallent, G. Marcandalli, M. C. Figueiredo, F. Calle-Vallejo and M. T. M. Koper, *J. Am. Chem. Soc.*, 2017, **139**, 16412-16419.
237. A. Schizodimou and G. Kyriacou, *Electrochim. Acta*, 2012, **78**, 171-176.
238. Y. Hori, A. Murata and R. Takahashi, *J. Chem. Soc., Faraday Trans. 1*, 1989, **85**, 2309-2326.
239. Y. Hori, in *Handbook of Fuel Cells*, John Wiley & Sons, Ltd, 2010, DOI: 10.1002/9780470974001.f207055.
240. J. Resasco, Y. Lum, E. Clark, J. Z. Zeledon and A. T. Bell, *ChemElectroChem*, 2018, **0**.
241. Y. Hori, A. Murata, R. Takahashi and S. Suzuki, *J. Chem. Soc., Chem. Commun.*, 1988, DOI: 10.1039/C39880000017, 17-19.
242. A. Wuttig, Y. Yoon, J. Ryu and Y. Surendranath, *J. Am. Chem. Soc.*, 2017, **139**, 17109-17113.
243. T. Cheng, H. Xiao and W. A. Goddard, *J. Am. Chem. Soc.*, 2016, **138**, 13802-13805.



244. A. Wuttig, M. Yaguchi, K. Motobayashi, M. Osawa and Y. Surendranath, *Proc. Natl. Acad. Sci.*, 2016, **113**, E4585-E4593.
245. H. Yano, T. Tanaka, M. Nakayama and K. Ogura, *J. Electroanal. Chem.*, 2004, **565**, 287-293.
246. K. Ogura, J. R. Ferrell, A. V. Cugini, E. S. Smotkin and M. D. Salazar-Villalpando, *Electrochim. Acta*, 2010, **56**, 381-386.
247. F. S. Roberts, K. P. Kuhl and A. Nilsson, *Angew. Chem. Int. Ed.*, 2015, **54**, 5179-5182.
248. Y. Kwon, Y. Lum, E. L. Clark, J. W. Ager and A. T. Bell, *ChemElectroChem*, 2016, **3**, 1012-1019.
249. S. Lee, D. Kim and J. Lee, *Angew. Chem.*, 2015, **127**, 14914-14918.
250. I. Shoichiro, T. Takehiko and I. Kaname, *Bull. Chem. Soc. Jpn.*, 1987, **60**, 2517-2522.
251. C. Amatore and J. M. Saveant, *J. Am. Chem. Soc.*, 1981, **103**, 5021-5023.
252. Y. B. Vassiliev, V. S. Bagotsky, N. V. Osetrova, O. A. Khazova and N. A. Mayorova, *J. Electroanal. Chem. Interfacial Electrochem.*, 1985, **189**, 271-294.
253. Y. Matsubara, *ACS Energy Lett.*, 2017, **2**, 1886-1891.
254. Y. Tomita, S. Teruya, O. Koga and Y. Hori, *J. Electrochem. Soc.*, 2000, **147**, 4164-4167.
255. O. Aschenbrenner and P. Styring, *Energy Environ. Sci.*, 2010, **3**, 1106-1113.
256. B. P. Sullivan, K. Krist and H. Guard, *Electrochemical and electrocatalytic reactions of carbon dioxide*, Elsevier, 2012.
257. S.-B. Park, C.-S. Shim, H. Lee and K.-H. Lee, *Fluid Phase Equilib.*, 1997, **134**, 141-149.
258. Y. Qiu, H. Zhong, W. Xu, T. Zhang, X. Li and H. Zhang, *J. Mater. Chem. A*, 2019, DOI: 10.1039/C9TA00039A.
259. F.-Y. Jou, A. E. Mather and F. D. Otto, *Can. J. Chem. Eng.*, 1995, **73**, 140-147.
260. L. L. Snuffin, L. W. Whaley and L. Yu, *J. Electrochem. Soc.*, 2011, **158**, F155-F158.
261. S. Kaneco, K. Iiba, H. Katsumata, T. Suzuki and K. Ohta, *Electrochim. Acta*, 2006, **51**, 4880-4885.
262. S. Kaneco, K. Iiba, N.-h. Hiei, K. Ohta, T. Mizuno and T. Suzuki, *Electrochim. Acta*, 1999, **44**, 4701-4706.
263. T. Mizuno, A. Naitoh and K. Ohta, *J. Electroanal. Chem.*, 1995, **391**, 199-201.
264. E. D. Bates, R. D. Mayton, I. Ntai and J. H. Davis, *J. Am. Chem. Soc.*, 2002, **124**, 926-927.
265. J. L. Anderson, J. K. Dixon and J. F. Brennecke, *Acc. Chem. Res.*, 2007, **40**, 1208-1216.
266. J. F. Brennecke and B. E. Gurkan, *J. Phys. Chem. Lett.*, 2010, **1**, 3459-3464.
267. D. R. MacFarlane, N. Tachikawa, M. Forsyth, J. M. Pringle, P. C. Howlett, G. D. Elliott, J. H. Davis, M. Watanabe, P. Simon and C. A. Angell, *Energy Environ. Sci.*, 2014, **7**, 232-250.
268. M. V. Fedorov and A. A. Kornyshev, *Chem. Rev. (Washington, DC, U. S.)*, 2014, **114**, 2978-3036.
269. M. Smiglak, J. Pringle, X. Lu, L. Han, S. Zhang, H. Gao, D. MacFarlane and R. Rogers, *Chem. Commun. (Cambridge, U. K.)*, 2014, **50**, 9228-9250.
270. M. Armand, F. Endres, D. R. MacFarlane, H. Ohno and B. Scrosati, *Nat. Mater.*, 2009, **8**, 621.
271. F. Zhou, S. Liu, B. Yang, P. Wang, A. S. Alshammari and Y. Deng, *Electrochem. Commun.*, 2014, **46**, 103-106.
272. M. Alvarez-Guerra, J. Albo, E. Alvarez-Guerra and A. Irabien, *Energy Environ. Sci.*, 2015, **8**, 2574-2599.
273. B. A. Rosen, J. L. Haan, P. Mukherjee, B. Braunschweig, W. Zhu, A. Salehi-Khojin, D. D. Dlott and R. I. Masel, *J. Phys. Chem. C*, 2012, **116**, 15307-15312.
274. B. A. Rosen, W. Zhu, G. Kaul, A. Salehi-Khojin and R. I. Masel, *J. Electrochem. Soc.*, 2013, **160**, H138-H141.
275. M. Asadi, B. Kumar, A. Behranginia, B. A. Rosen, A. Baskin, N. Reppin, D. Pisasale, P. Phillips, W. Zhu, R. Haasch, R. F. Klie, P. Král, J. Abiade and A. Salehi-Khojin, *Nat. Commun.*, 2014, **5**, 4470.
276. D. Niu, H. Wang, H. Li, Z. Wu and X. Zhang, *Electrochim. Acta*, 2015, **158**, 138-142.
277. L. Sun, G. K. Ramesha, P. V. Kamat and J. F. Brennecke, *Langmuir*, 2014, **30**, 6302-6308.
278. A. Salehi-Khojin, H.-R. M. Jhong, B. A. Rosen, W. Zhu, S. Ma, P. J. A. Kenis and R. I. Masel, *J. Phys. Chem. C*, 2013, **117**, 1627-1632.
279. J. L. DiMeglio and J. Rosenthal, *J. Am. Chem. Soc.*, 2013, **135**, 8798-8801.
280. J. Medina-Ramos, J. L. DiMeglio and J. Rosenthal, *J. Am. Chem. Soc.*, 2014, **136**, 8361-8367.
281. C. Costentin, M. Robert and J.-M. Saveant, *Chem. Soc. Rev.*, 2013, **42**, 2423-2436.
282. G. P. S. Lau, M. Schreier, D. Vasilyev, R. Scopelliti, M. Grätzel and P. J. Dyson, *J. Am. Chem. Soc.*, 2016, **138**, 7820-7823.
283. X. Zhang, Y. Zhao, S. Hu, M. E. Gliege, Y. Liu, R. Liu, L. Scudiero, Y. Hu and S. Ha, *Electrochim. Acta*, 2017, **247**, 281-287.
284. Q. Wang, C. Chen, J. Zhong, B. Zhang and Z. Cheng, *Aust. J. Chem.*, 2017, **70**, 293-300.
285. Q. Zhu, J. Ma, X. Kang, X. Sun, H. Liu, J. Hu, Z. Liu and B. Han, *Angew. Chem. Int. Ed.*, 2016, **55**, 9012-9016.
286. I. Ganesh, *Renewable Sustainable Energy Rev.*, 2014, **31**, 221-257.
287. A. S. Varela, M. Kroschel, T. Reier and P. Strasser, *Catal. Today*, 2016, **260**, 8-13.
288. R. Kas, R. Kortlever, H. Yilmaz, M. T. M. Koper and G. Mul, *ChemElectroChem*, 2015, **2**, 354-358.
289. I. Katsounaros, J. C. Meier, S. O. Klemm, A. A. Topalov, P. U. Biedermann, M. Auinger and K. J. J. Mayrhofer, *Electrochem. Commun.*, 2011, **13**, 634-637.
290. M. R. Singh, E. L. Clark and A. T. Bell, *Phys. Chem. Chem. Phys.*, 2015, **17**, 18924-18936.
291. A. S. Hall, Y. Yoon, A. Wuttig and Y. Surendranath, *J. Am. Chem. Soc.*, 2015, **137**, 14834-14837.
292. H. Hashiba, H. K. Sato, S. Yotsuhashi, K. Fujii, M. Sugiyama and Y. Nakano, *Sustainable Energy Fuels*, 2017, **1**, 1734-1739.
293. M. Gattrell, N. Gupta and A. Co, *J. Electroanal. Chem.*, 2006, **594**, 1-19.
294. L. Wang, S. A. Nitopi, E. Bertheussen, M. Orazov, C. G. Morales-Guio, X. Liu, D. C. Higgins, K. Chan, J. K. Nørskov, C. Hahn and T. F. Jaramillo, *ACS Catal.*, 2018, **8**, 7445-7454.
295. H. Ooka, M. C. Figueiredo and M. T. M. Koper, *Langmuir*, 2017, **33**, 9307-9313.
296. D. Strmcnik, M. Uchimura, C. Wang, R. Subbaraman, N. Danilovic, D. van der Vliet, A. P. Paulikas, V. R. Stamenkovic and N. M. Markovic, *Nature Chem.*, 2013, **5**, 300.
297. J. Zheng, W. Sheng, Z. Zhuang, B. Xu and Y. Yan, *Sci. Adv.*, 2016, **2**.
298. Y. Hori, A. Murata, R. Takahashi and S. Suzuki, *J. Am. Chem. Soc.*, 1987, **109**, 5022-5023.
299. Y. Hori, I. Takahashi, O. Koga and N. Hoshi, *J. Phys. Chem. B*, 2002, **106**, 15-17.
300. J. H. Montoya, C. Shi, K. Chan and J. K. Nørskov, *J. Phys. Chem. Lett.*, 2015, **6**, 2032-2037.
301. K. Jiang, R. B. Sandberg, A. J. Akey, X. Liu, D. C. Bell, J. K. Nørskov, K. Chan and H. Wang, *Nat. Catal.*, 2018, **1**, 111-119.
302. J. D. Goodpaster, A. T. Bell and M. Head-Gordon, *J. Phys. Chem. Lett.*, 2016, **7**, 1471-1477.
303. N. Hidetomo, I. Shoichiro, O. Yoshiyuki and I. Kaname, *Chem. Lett.*, 1989, **18**, 289-292.
304. K. W. Frese Jr, in *Electrochemical and Electrocatalytic Reactions of Carbon Dioxide*, eds. B. P. Sullivan, K. Krist and H. E. Guard, Elsevier, Amsterdam, 1993, DOI: <https://doi.org/10.1016/B978-0-444-88316-2.50010-3>, pp. 145-216.
305. J. J. Kim, D. P. Summers and K. W. Frese, *J. Electroanal. Chem. Interfacial Electrochem.*, 1988, **245**, 223-244.
306. Y. Hori, R. Takahashi, Y. Yoshinami and A. Murata, *J. Phys. Chem. B*, 1997, **101**, 7075-7081.
307. K. J. P. Schouten, Y. Kwon, C. J. M. van der Ham, Z. Qin and M. T. M. Koper, *Chem. Sci.*, 2011, **2**, 1902-1909.
308. K. J. P. Schouten, E. Pérez Gallent and M. T. M. Koper, *J. Electroanal. Chem.*, 2014, **716**, 53-57.

309. F. Calle-Vallejo and M. T. M. Koper, *Angew. Chem. Int. Ed.*, 2013, **52**, 7282-7285.
310. K. J. P. Schouten, Z. Qin, E. Pérez Gallent and M. T. M. Koper, *J. Am. Chem. Soc.*, 2012, **134**, 9864-9867.
311. J. O. M. Bockris and N. Pentland, *Trans. Faraday Soc.*, 1952, **48**, 833-839.
312. M. Jouny, W. Luc and F. Jiao, *Nat. Catal.*, 2018, **1**, 748-755.
313. M. Dunwell, X. Yang, B. P. Setzler, J. Anibal, Y. Yan and B. Xu, *ACS Catal.*, 2018, **8**, 3999-4008.
314. D. Raciti, M. Mao and C. Wang, *Nanotechnology*, 2017, **29**, 044001.
315. A. D. Handoko, C. W. Ong, Y. Huang, Z. G. Lee, L. Lin, G. B. Panetti and B. S. Yeo, *J. Phys. Chem. C*, 2016, **120**, 20058-20067.
316. X. Liu, P. Schlexer, J. Xiao, Y. Ji, L. Wang, R. B. Sandberg, M. Tang, K. S. Brown, H. Peng, S. Ringe, C. Hahn, T. F. Jaramillo, J. K. Nørskov and K. Chan, *Nat. Commun.*, 2019, **10**, 32.
317. Y. Y. Birdja and M. T. M. Koper, *J. Am. Chem. Soc.*, 2017, **139**, 2030-2034.
318. A. J. Garza, A. T. Bell and M. Head-Gordon, *ACS Catal.*, 2018, **8**, 1490-1499.
319. C. F. C. Lim, D. A. Harrington and A. T. Marshall, *Electrochim. Acta*, 2017, **238**, 56-63.
320. J. F. Richardson, J. H. Harker and J. R. Backhurst, *Coulson & Richardson's Chemical Engineering*, Butterworth-Heinemann London, 2002.
321. G. T. Rochelle, *Science*, 2009, **325**, 1652-1654.
322. F. Karadas, B. Köz, J. Jacquemin, E. Deniz, D. Rooney, J. Thompson, C. T. Yavuz, M. Khraisheh, S. Aparicio and M. Atihan, *Fluid Phase Equilib.*, 2013, **351**, 74-86.
323. P. Singh, D. W. F. Brilman and M. J. Groeneweld, *Int. J. Greenhouse Gas Control*, 2011, **5**, 61-68.
324. T. Mizuno, K. Ohta, A. Sasaki, T. Akai, M. Hirano and A. Kawabe, *Energy Sources*, 1995, **17**, 503-508.
325. S. Nakagawa, A. Kudo, M. Azuma and T. Sakata, *J. Electroanal. Chem. Interfacial Electrochem.*, 1991, **308**, 339-343.
326. H. De Jesús-Cardona, C. del Moral and C. R. Cabrera, *J. Electroanal. Chem.*, 2001, **513**, 45-51.
327. K. Hara, A. Kudo and T. Sakata, *J. Electroanal. Chem.*, 1997, **421**, 1-4.
328. K. Hara, A. Kudo and T. Sakata, *J. Electroanal. Chem.*, 1995, **386**, 257-260.
329. N. Sonoyama, M. Kirii and T. Sakata, *Electrochem. Commun.*, 1999, **1**, 213-216.
330. K. Hara, A. Tsuneto, A. Kudo and T. Sakata, *J. Electrochem. Soc.*, 1994, **141**, 2097-2103.
331. A. Kudo, S. Nakagawa, A. Tsuneto and T. Sakata, *J. Electrochem. Soc.*, 1993, **140**, 1541-1545.
332. E. Stránská and D. Neděla, *Journal of Industrial Textiles*, 2018, **48**, 432-447.
333. F. L. Smith and A. H. Harvey, *Chem. Eng. Prog.*, 2007, **103**, 33-39.
334. H. Perry, *Chemical engineers' handbook*, ACS Publications, 1950.
335. M. J. Moran, H. N. Shapiro, D. D. Boettner and M. B. Bailey, *Fundamentals of engineering thermodynamics*, John Wiley & Sons, 2010.
336. J. Ryu, T. N. Andersen and H. Eyring, *J. Phys. Chem.*, 1972, **76**, 3278-3286.
337. J. Kestin, M. Sokolov and W. A. Wakeham, *J. Phys. Chem. Ref. Data*, 1978, **7**, 941-948.
338. E. N. Fuller, P. D. Schettler and J. C. Giddings, *Ind. Eng. Chem.*, 1966, **58**, 18-27.
339. J. J. Carroll, F.-Y. Jou, A. E. Mather and F. D. Otto, *Can. J. Chem. Eng.*, 1998, **76**, 945-951.
340. J. E. Davis and J. J. McKetta, *J. Chem. Eng. Data*, 1960, **5**, 374-375.
341. M. Azuma, K. Hashimoto, M. Hiramoto, M. Watanabe and T. Sakata, *J. Electroanal. Chem. Interfacial Electrochem.*, 1989, **260**, 441-445.
342. M. Azuma, K. Hashimoto, M. Hiramoto, M. Watanabe and T. Sakata, *J. Electrochem. Soc.*, 1990, **137**, 1772-1778.
343. S. T. Ahn, I. Abu-Baker and G. T. R. Palmore, *Catal. Today*, 2017, **288**, 24-29.
344. S. Kaneco, N.-h. Hiei, Y. Xing, H. Katsumata, H. Ohnishi, T. Suzuki and K. Ohta, *Electrochim. Acta*, 2002, **48**, 51-55.
345. J. Hussain, H. Jónsson and E. Skúlason, *ACS Catal.*, 2018, **8**, 5240-5249.
346. W. Luo, X. Nie, M. J. Janik and A. Asthagiri, *ACS Catal.*, 2016, **6**, 219-229.
347. Sustainion® Anion Exchange Membranes, <https://dioxidematerials.com/technology/sustainion-membranes/>, (accessed 15/08/2019, 2019).
348. K. Scott, C. Xu and X. Wu, *Wiley Interdiscip. Rev.: Energy Environ.*, 2014, **3**, 24-41.
349. I. Vincent and D. Bessarabov, *Renewable Sustainable Energy Rev.*, 2018, **81**, 1690-1704.
350. F. Proietto, B. Schiavo, A. Galia and O. Scialdone, *Electrochim. Acta*, 2018, DOI: <https://doi.org/10.1016/j.electacta.2018.04.159>.
351. S. J. Davis, N. S. Lewis, M. Shaner, S. Aggarwal, D. Arent, I. L. Azevedo, S. M. Benson, T. Bradley, J. Brouwer, Y.-M. Chiang, C. T. M. Clack, A. Cohen, S. Doig, J. Edmonds, P. Fennell, C. B. Field, B. Hannegan, B.-M. Hodge, M. I. Hoffert, E. Ingersoll, P. Jaramillo, K. S. Lackner, K. J. Mach, M. Mastrandrea, J. Ogden, P. F. Peterson, D. L. Sanchez, D. Sperling, J. Stagner, J. E. Trancik, C.-J. Yang and K. Caldeira, *Science*, 2018, **360**.
352. J. R. Hudkins, D. G. Wheeler, B. Pena and C. P. Berlinguette, *Energy Environ. Sci.*, 2016, **9**, 3417-3423.
353. S. Sabatino, A. Galia, G. Saracco and O. Scialdone, *ChemElectroChem*, 2017, **4**, 150-159.
354. T. E. Lister and E. J. Dufek, *Energy Fuels*, 2013, **27**, 4244-4249.
355. I. Moussallem, J. Jörissen, U. Kunz, S. Pinnow and T. Turek, *J. Appl. Electrochem.*, 2008, **38**, 1177-1194.